Copyright Warning & Restrictions

The copyright law of the United States (Title 17, United States Code) governs the making of photocopies or other reproductions of copyrighted material.

Under certain conditions specified in the law, libraries and archives are authorized to furnish a photocopy or other reproduction. One of these specified conditions is that the photocopy or reproduction is not to be "used for any purpose other than private study, scholarship, or research." If a, user makes a request for, or later uses, a photocopy or reproduction for purposes in excess of "fair use" that user may be liable for copyright infringement,

This institution reserves the right to refuse to accept a copying order if, in its judgment, fulfillment of the order would involve violation of copyright law.

Please Note: The author retains the copyright while the New Jersey Institute of Technology reserves the right to distribute this thesis or dissertation

Printing note: If you do not wish to print this page, then select "Pages from: first page # to: last page #" on the print dialog screen

ABSTRACT

ORTHOGONAL TRANSMULTIPLEXERS: EXTENSIONS TO DIGITAL SUBSCRIBER LINE (DSL) COMMUNICATIONS

by
Xueming Lin

An orthogonal transmultiplexer which unifies multirate filter bank theory and communications theory is investigated in this dissertation. Various extensions of the orthogonal transmultiplexer techniques have been made for digital subscriber line communication applications.

It is shown that the theoretical performance bounds of single carrier modulation based transceivers and multicarrier modulation based transceivers are the same under the same operational conditions. Single carrier based transceiver systems such as Quadrature Amplitude Modulation (QAM) and Carrierless Amplitude and Phase (CAP) modulation scheme, multicarrier based transceiver systems such as Orthogonal Frequency Division Multiplexing (OFDM) or Discrete Multi Tone (DMT) and Discrete Subband (Wavelet) Multicarrier based transceiver (DSBMT) techniques are considered in this investigation.

The performance of DMT and DSBMT based transceiver systems for a narrow band interference and their robustness are also investigated. It is shown that the performance of a DMT based transceiver system is quite sensitive to the location and strength of a single tone (narrow band) interference. The performance sensitivity is highlighted in this work. It is shown that an adaptive interference exciser can alleviate the sensitivity problem of a DMT based system. The improved spectral properties of DSBMT technique reduces the performance sensitivity for variations of a narrow band interference . It is shown that DSBMT technique outperforms DMT and has a more robust performance than the latter. The superior performance robustness is shown in this work.

Optimal orthogonal basis design using cosine modulated multirate filter bank is discussed. An adaptive linear combiner at the output of analysis filter bank is implemented to eliminate the intersymbol and interchannel interferences. It is shown that DSBMT is the most suitable technique for a narrow band interference environment.

A blind channel identification and optimal MMSE based equalizer employing a nonmaximally decimated filter bank precoder / postequalizer structure is proposed. The performance of blind channel identification scheme is shown not to be sensitive to the characteristics of unknown channel. The performance of the proposed optimal MMSE based equalizer is shown to be superior to the zero-forcing equalizer.

ORTHOGONAL TRANSMULTIPLEXERS: EXTENSIONS TO DIGITAL SUBSCRIBER LINE (DSL) COMMUNICATIONS

by
Xueming Lin

A Dissertation
Submitted to the Faculty of
New Jersey Institute of Technology
in Partial Fulfillment of the Requirements for the Degree of
Doctor of Philosophy

Department of Electrical and Computer Engineering

January 1998

APPROVAL PAGE

ORTHOGONAL TRANSMULTIPLEXERS: EXTENSIONS TO DIGITAL SUBSCRIBER LINE (DSL) COMMUNICATIONS

Xueming Lin

Dr. Ali N. Akansu, Dissertation Advisor — Date
Associate Professor of Electrical and Computer Engineering, NJIT

Dr. Richard A. Haddad, Committee Member — Date
Professor of Electrical and Computer Engineering, NJIT

Dr. Joseph Frank, Committee Member — Date
Associate Professor of Electrical and Computer Engineering, NJIT

Dr. Zoran Siveski, Committee Member — Date
Member of Technical Staff, Lucent Technologies Inc.

Dr. Sirin Tekinay, Committee Member — Date
Assistant Professor of Electrical and Computer Engineering, NJIT

Dr. Bulent Yener, Committee Member — Date
Assistant Professor of Computer and Information Science, NJIT

BIOGRAPHICAL SKETCH

Author: Xueming Lin

Degree: Doctor of Philosophy

Date: January 1998

Undergraduate and Graduate Education:

- Doctor of Philosophy in Electrical Engineering,
  New Jersey Institute of Technology, Newark, New Jersey, USA, January 1998.
- Master of Science in Electrical Engineering,
  Fudan University, Shanghai, PR China, July, 1987.
- Bachelor of Science in Electrical Engineering,
  Fudan University, Shanghai, PR China, July, 1984.

Major: Electrical Engineering

Presentations and Publications:

[1] Ali N. Akansu, K. Hetling, Xueming Lin, and G. Saulnier, " Transmultiplexers: A Unifying Time-Frequency Tool for TDMA, FDMA and CDMA Communications ." A Chapter in *Wavelet, Subband and Block Transforms in Communications and Multimedia*, A.N. Akansu and M. Medley, Eds., Kluwer, to be published in 1998. (in preparation)

[2] Ali N. Akansu, P. Duhamel, Xueming Lin and M. de Courville " Orthogonal Transmultiplexers in Communications: A Review ," *IEEE Trans. on Signal Processing*, Special Issue on theory and Applications of Filter Banks and Wavelets. To appear, February, 1998.

[3] Xueming Lin, and Ali N. Akansu, " Blind Channel Identification and Optimal MMSE Equalization Using Nonmaximally Decimated Filterbank Precoder/Post-equalizer." Submitted to *IEEE Trans. on Signal Processing.*

[4] Xueming Lin, M. Sorbara and Ali N. Akansu " A Performance Analysis of Single Carrier and OFDM Modulation Techniques for Digital Subscriber Line Applications," in *Proc. of 5th NJIT Symposium of Wavelet, Subband and Block Transforms in Communications.* Newark, NJ, March, 1997.

[5] Ali N. Akansu , Xueming Lin and Mehmet V. Tazebay " Spread Spectrum PR-QMF Transmultiplexer Codes for CDMA Communications," in *Proc. of 7th IEEE Digital Signal Processing Workshop*, September 1996.

[6] Xueming Lin and Ali N. Akansu, " A Distortion Analysis and Optimal Design of Orthogonal Basis for DMT Transceivers," in Proc. of the *IEEE International Conference on Acoustics, Speech and Signal Processing*, Vol. 3, pp. 1475-1478, May 7-10, 1996, Atlanta, Georgia.

[7] Xueming Lin and Ali N. Akansu, " A Performance Evaluation of Digital Subscriber Line Techniques in Single and Multitone Interference Environments," Submitted to *IEEE International Conference on Communications*, 1998.

[8] Xueming Lin and Ali N. Akansu, "Nonmaximally Decimated Filterbank Based Precoder / Post-equalizer For Blind Channel Identification and Optimal MMSE Equalization," Submitted to *IEEE International Conference on Acoustics, Speech and Signal Processing*, 1998.

[9] Ali N. Akansu and Xueming Lin, "A Comparative Performance Evaluation of DMT (OFDM) and DWMT(DSBMT) Based DSL Communications Systems for Single and Multitone Interference ," Submitted to *IEEE International Conference on Acoustics, Speech and Signal Processing*, 1998.

[10] A.N. Akansu, Xueming Lin and Xianggeng Xia "Advanced Multirate Signal Processing Techniques for Channel Estimation, Equalization and Precoding" to be submitted to *IEEE Signal Processing Magazine.* (in preparation)

This work is dedicated to
my family

ACKNOWLEDGMENT

First of all, I would like to attribute my sincere gratitude to my advisor, Professor Ali N. Akansu for his encouragement, support and enthusiasm. He introduced me to the research project of new cutting edge Digital Subscriber Line techniques. He always spent time with me and guided me through the problems we encountered. His restless support is the spirit of our work. It is a privilege to work with him. Thanks a lot from my heart.

I would like to thank Prof. Richard A. Haddad, Prof. Joseph Frank, Prof. Sirin Tekinay of Electrical and Computer Engineering Department, Prof. Bulent Yener of Computer and Information Science Department, New Jersey Institute of Technology, for their kindness help serving in my doctoral dissertation committee. Special thanks to Dr. Zoran Siveski of Lucent Technologies Inc., for taking his work time off from company to serve in the committee. Their time and comments are very precious. Thanks a lot.

Many thanks are due to former AT&T Paradyne Corp., now Globespan Semiconductor Inc., especially to George Malek, Ehud Langberg and Massimo Sorbara, and many others. The research project funded by AT&T Paradyne Corp. give us support not only financially but also technically. I benefited a lot from the discussions and presentations in Middletown as well as in Red Bank, New Jersey.

I also would like to express my thanks to Dr. Mehmet Tazebay and Dr. Adil Benyassine, with whom I have been working together. Their encouragement and discussions helped me a lot on many occasions. I enjoyed my friendship with Qingping Zheng, Yongcheng Qiu and many of my old friends from my high school, university and graduate study. Thanks are also due to my fellow Ph.D. candidates, Doctors of the member of New Jersey Center for Multimedia Research and Center for Communications and Signal Processing Research: Ziqiang Xu, Jin Zhou, Huaping Liu, Jianguo Chen, Weichen Ye, Xiaochun Li, Ambalavanar Arulambalam, Nadir

Sezgin, Ayoub Tareq, Anil Bircan, Aykut Bultan, Feihong Chen, Anne McMahon, Lisa Fitton and many others. Thanks to all of you.

The last, the most, I would like to thank my mother and father, my family, my wife and her family for their encouragement, patience and love. This make my study possible and joyful in New Jersey Institute of Technology.

TABLE OF CONTENTS

Chapter Page

Chapter Page

LIST OF TABLES

Table Page

LIST OF FIGURES

Figure Page

Figure Page

Figure Page

CHAPTER 1

INTRODUCTION

1.1 Telecommunication System Design

The first telecommunication systems were developed more than one hundred years ago. Since the first telephone was built to convey voice signal, there has been a dramatic developments in telecommunication systems.

A telecommunication system transfers information from a source to a destination. The source can be a person, a group of people or any information originator. The destination can be a specific person, such as the conventional phone service or broadcasting receivers. A typical telecommunication system is depicted in Figure 1.1.

Although some information originates in continuous time and amplitude, there are great advantages to transmit discrete information symbols in telecommunication systems. The information source is converted to an information data stream by a source encoder, to reduce its redundancy. This source coding process may involve some data compression to remove unnecessary information. The channel coder may try to induce some redundancy such that the transmitted signal can be recovered successfully. In general, this kind of information stream is a discrete binary data sequence. It allows the channel encoder to generate a transmitted symbol. Different types of data symbols can be generated in order to achieve the full utilization of a transmission channel.

The transmitter shaping filter modulates the encoded transmission symbol so that the transmitted signals match the properties of the transmission channel. The signal passes through the channel, which can induce distortion, noise and interference signals.

At the receiver, the signal is demodulated by the receiver filter. In general, it may involve a frequency transfer from a passband to a baseband. The reconstructed

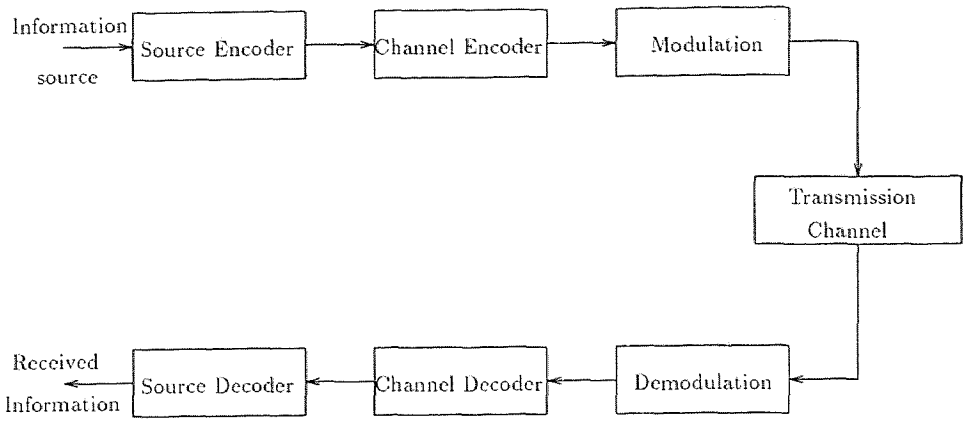

Figure 1.1 A typical digital telecommunication system

discrete symbol is mapped back by the channel and the source decoders. The goal of an optimal communication system is to convey as much information as possible under certain practical constraints.

1.2 Orthogonal Transmultiplexers in Communications

1.2.1 Signal Processing and Communications

Signal processing and communications have been complementary fields of electrical engineering for a long time. Most of the basic processing tools utilized in the design of communication systems come from the signal processing discipline, e.g. Fourier transform, modulation schemes. Others are specifically designed for communication purposes, such as information theory, and error correcting codes. In turn, signal processing experts have been influenced by this cross-fertilization and have expanded their research activities into various communication applications [36].

This mutual influence and interaction, however, has not been as strong in the area of discrete-time multirate signal processing. Highlighting the fundamentals

of orthogonal subband transforms from a time-frequency perspective, this work illustrates how both disciplines would benefit from stronger cooperation on this topic. Several popular communication applications can be described in terms of synthesis/analysis configuration (transmultiplexer) of subband transforms. Code division multiple access (CDMA), frequency division multiple access (FDMA) and time division multiple access (TDMA) communication schemes can be viewed from this perspective. In particular, FDMA (also called orthogonal frequency division multiplexing (OFDM), or discrete multitone (DMT) modulation) based systems have been more widely used than the others.

1.2.2 Time-Frequency and Orthogonality Principles

The orthogonality of multi-carriers was recognized early on as the proper way to pack more sub-channels into the same channel spectrum [28][29][31]. This approach is attractive particularly for the communication scenarios where the channel's power spectrum is unevenly distributed. The subchannels (sub-carriers) with better power levels are treated more favorably than the others. Therefore, this approach provides a vehicle for optimal loading of subchannels where channel dynamics are significant. The sub-carrier orthogonality requirements were contained in a single domain in conventional communication schemes. Namely, they are the orthogonality in frequency (no interference between different carriers or subchannels) and the orthogonality in time (no interference between different subsymbols transmitted on the same carrier at different time slots). If this property is ensured, multichannel communication is achieved naturally.

Originally, the multicarrier modulation technique was proposed by using a bank of analog Nyquist filters, which provide a set of continuous-time orthogonal functions. However, the realization of strictly orthogonal analog filters is impossible. Therefore, the initial formulation was re-worked into a discrete-time model. The steps of this

discrete-time model are summarized as follows. A digital computation first evaluates samples of the continuous signal which are to be transmitted over the channel. Then, these samples drive a digital-to-analog converter (DAC) which generates the actual transmitted signal. This discrete model makes explicit use of a structure which is similar to the orthogonal synthesis/analysis filter bank or transmultiplexer displayed in Figure 4.1[36].

Transmultiplexers were studied in the early seventies by Bellanger et.al.[32] for telephony applications. Their seminal work was one of the first dealing with multirate signal processing, which has matured lately in the signal processing field. Since complexity is an important issue in all of these applications, the discrete Fourier transform (DFT) basis is usually chosen as the set of orthogonal subcarriers [17][30][33]. In addition, it has been shown that the DFT-based transmultiplexers allow efficient channel equalization which make them attractive.

The orthogonality conditions and implementation of discrete-time (digital) function sets are much easier to use than the ones in the continuous-time domain (analog case)[16] [17]. This is the first point where DSP tools can be useful. It is shown that only the Nyquist filter, a rectangular window (time) function, allows the time and frequency orthogonalities when modulated by a DFT. All other modulations using more frequency selective filters can only approximate the orthogonality conditions. On the other hand, more general orthogonality conditions need to be satisfied for other transform bases. This is currently an active research topic in the field [36].

The *time − frequency* and *orthogonality* properties of function sets, or filter banks, are the unifying theme of the topics presented in this thesis. It is shown from a signal processing perspective that these entirely different communications systems are merely variations of the same theoretical concept. The subband transform theory and its extensions provide the theoretical framework which serves all these variations.

This unified treatment of orthogonal multiplexers is expected to improve existing solutions.

1.3 Extensions of Orthogonal Transmultiplexer

Obviously, every part of a telecommunication system is important for the performance of the overall system. In this dissertation, our focus will be on the design and implementation of transmitter filter or modulator and receiver filter (demodulator) using advanced digital signal processing theory. The newly developed theory is applied to design high speed transceiver systems. The orthogonal transmultiplexer constitutes the framework of the theory. Optimal design and analysis of the orthogonal basis functions will be addressed in detail. The optimal time / frequency representation theory makes the design and implementation of high speed telecommunication systems much easier.

The orthogonal transmultiplexer theory is extended to a practical telecommunication application area, the digital subscriber line (DSL) techniques. Hundreds of millions of unshielded twisted pair telephone lines exist around the world. The evolution of telecommunications has made the telephone instrument available everywhere. The low transmission rate of the existing telephone wire creates a bottleneck due to the great demand of high speed data transmission which includes video on demand, Internet service, video conferencing and many other possible services. The digital subscriber line technique provides the high bit rate digital transmission. The bit rate could be up to ten millions bits per second which is several hundred times faster than the current commercially available 28.8 Kbps modem. In the mean time, the conventional plain old telephone service (POTS) is still available. The emerging DSL techniques include high bit rate digital subscriber line (HDSL), asymmetric digital subscriber line (ADSL), very high bit rate digital subscriber line (VDSL) and their variants. They are all called as X-DSL techniques.

In modern digital telecommunication techniques, there are several different modulation (transmitter filter) schemes used. Conventional single carrier modulation techniques use a single broadband transmitted signal to convey a high bit rate stream signal. Quadrature Amplitude Modulation (QAM) modulation and Carrierless Amplitude and Phase (CAP) modulation schemes are single carrier based modulations using bandwidth efficient modulation line code. They are widely used in today's digital communication systems. The newly evolved multicarrier modulation technique utilizes a set of parallel multicarriers or subchannels to convey a high bit rate information signal. Orthogonal Frequency Division Multiplexing (OFDM) or Discrete Multitone transceiver, and discrete wavelet multicarrier transceiver (DWMT) or discrete subband multicarrier transceiver (DSBMT), are the recently proposed techniques for high speed digital telecommunications.

This thesis utilizes the basic multirate filterbank transmultiplexer framework to design and implement advanced modern digital communication systems. This framework can be used in any communication system design problem including wired communication systems (twisted pair, coaxial cable), wireless communication systems (spread spectrum, multi-user communication). In our research, we focus on the wired line, especially on the digital subscriber line applications. But the theory can be used for other communication systems as well.

1.4 Dissertation Organization and Contributions

In chapter 2, we review the basic digital signal processing terminologies and multirate signal processing techniques. We introduce the multirate transmultiplexer framework as a fundamental vehicle to design and implement modern digital communication systems. We provide an in-depth view of transmultiplexers such that the time and frequency relationship, multirate signal decomposition and reconstruction theories are unified.

In chapter 3, we introduce the digital subscriber line (DSL) techniques which are emerging in telecommunication industry in recent years. Different implementation techniques are analyzed and evaluated.

In chapter 4, an orthogonal transmultiplexer framework is extended to DSL applications. An M band cosine modulated synthesis/analysis filter bank structure is implemented in a discrete subband multicarrier transceiver (DSBMT) system. The optimal design criteria are proposed for discrete subband multicarrier modulation schemes. Interchannel interference (ICI) and intersymbol interference (ISI) are theoretically evaluated. Optimal MMSE based linear combiner and an adaptive linear combiner are implemented to eliminate the ICI and ISI in DSBMT transceiver system.

We present a theoretical analysis for a single carrier, broadband, bandwidth efficient modulation and a multicarrier modulation transmission capacity bound in Chapter 5. It is shown that these two different modulation techniques can achieve the same theoretical performance bound with infinite complexity and under the same operational conditions. The performance bound includes the maximal achievable bit rate and maximal achievable signal to noise ratio margin. The performance bounds for different modulation techniques are calculated in various practical digital subscriber line communication scenarios.

In chapter 6, we evaluate the theoretical performance of DMT technique in single tone and narrow band interference environments. It is shown that the performance sensitivity of the DMT transceiver is due to the nature of the discrete Fourier transform which is utilized as the DMT's modulation and demodulation basis functions. The performance degradation is theoretically evaluated. In order to alleviate the sensitivity of the DMT system performance, an adaptive short length FIR single tone exciser is proposed. The interference exciser dramatically improves the overall DMT system performance.

In chapter 7, the performance of discrete subband multicarrier transceiver (DSBMT) in single tone and narrow band interference environments is investigated. It is shown that the DSBMT is much more robust than the discrete Fourier transform based DMT technique for narrow band interference environments. Optimal orthonormal basis functions are designed to implement the DSBMT transceiver. These basis functions have very little side lobes and very good stop band attenuation. The nature of these basis functions will virtually eliminate any interference leakage between subcarriers. All of the subcarriers which are not hit by the narrow band interference work well. The overall system performance is shown to be quite superior to the DMT's. As shown in Chapter 5, DSBMT, DMT, QAM and CAP will eventually approach to the same ultimate transmission bound if the implementation complexity is not of a concern.

In chapter 8, we introduce a new blind channel identification and optimal minimum mean square error equalization using nonmaximally decimated multirate filter bank as precoder and post-equalizer. It is shown theoretically that the blind channel identification and channel equalization works well by the nature of the precoder structure. The proposed MMSE based optimal equalizer recovers the ISI distorted received symbol and suppresses the noise enhancement induced by post-equalization simultaneously. It makes the blind channel identification and equalization work successfully. Using the newly proposed precoder / post-equalization techniques, one can achieve on line blind channel identification and equalization in wireless communications successfully by implementing a single detector transceiver. There is no need to use multi-detector or detector array which the implementation is costly or not feasible in practice.

In chapter 9, we will discuss the related issues and possible future research work and conclude the thesis.

CHAPTER 2
MULTIRATE FILTER BANK TRANSFORMS

In order to set a general framework for multirate filter bank signal processing, we will review the basic material of multirate signal processing and the mathematical terminology which are used in the following chapters. The detailed treatment of fundamentals can be found in the literature [69][74][89].

2.1 Discrete-Time Signal Processing, the Fundamentals

A discrete-time signal is usually denoted as $x(n)$ where n is the time index. This data sequence is sampled from a continuous time signal $x(t)$. The discrete system of primary interest is linear, causal and time invariant throughout this dissertation.

Let's denote the impulse response of a discrete-time system as $h(n)$. The output of such a system corresponding to an input $x(n)$ is defined by the convolution relation as

$$y(n) = \sum_k x(k)h(n-k) = x(n) \otimes h(n), \tag{2.1}$$

where $\otimes$ denotes the linear convolution operation. The two-sided Z-transform of $x(n)$ is defined by

$$X(z) = \sum_{n=-\infty}^{\infty} x(n)z^{-n}. \tag{2.2}$$

The discrete-time Fourier transform (DTFT) of $x(n)$ is defined as

$$X(e^{j\omega}) = \sum_{n=-\infty}^{\infty} x(n)e^{-j\omega n}, \tag{2.3}$$

and the inverse transform is denoted as

$$x(n) = \frac{1}{2\pi}\int_{-\pi}^{\pi} X(e^{j\omega})e^{j\omega n}d\omega. \tag{2.4}$$

When ω is evaluated at the N equally-spaced points on the unit circle of the z plane, Eq. 2.3 becomes the discrete Fourier transform (DFT)

$$X(k) = X(e^{j\omega})\mid_{\omega=\frac{2\pi k}{N}}. \tag{2.5}$$

For finite-length discrete time signals, DFT is defined as

$$X(k) = \sum_{n=0}^{N-1} x(n) e^{-j\frac{2\pi kn}{N}}. \tag{2.6}$$

while the inverse Fourier transform (IDFT) is defined as

$$x(n) = \frac{1}{N} \sum_{k=0}^{N-1} X(k) e^{j\frac{2\pi kn}{N}}. \tag{2.7}$$

The linear convolution relation of Eq. 2.1 can be written in the z-domain as

$$Y(z) = H(z)X(z), \tag{2.8}$$

where $H(z)$ is the z-transform of the discrete-time system. In the frequency domain,

$$Y(e^{j\omega n}) = H(e^{j\omega n})X(e^{j\omega n}). \tag{2.9}$$

2.2 Block Transforms of Discrete-time Signals

In discrete-time signal processing literature, there are many linear transform methodologies that can be used for signal decomposition and composition (reconstruction).

In a conventional block transform processing, the serial input signal is divided into a secession of independent blocks. The block process of size N performs a serial to parallel (S/P) data structuring operation forming a data vector as

$$\underline{x_k}^T = [x_k(0)\ ,\ x_k(1)\ ,\ \ldots\ ,\ x_k(N-1)], \tag{2.10}$$

The multirate equivalent of blocking operation is displayed in Figure 2.1.

The block input discrete-time sequence could be processed or transformed by a block transform B into the frequency (transform) domain. Denote the corresponding spectral vector as $\underline{y_k}$, then,

$$\underline{y_k}^T = [y_k(0)\ ,\ y_k(1)\ ,\ \ldots\ ,\ y_k(N-1)]. \tag{2.11}$$

$$\underline{y_k} = \mathbf{B}\underline{x_k} = \begin{bmatrix} b_{00} & b_{01} & \cdots & b_{0(N-1)} \\ b_{10} & b_{11} & \cdots & b_{1(N-1)} \\ \vdots & \vdots & \ddots & \vdots \\ b_{(N-1)0} & b_{(N-1)1} & \cdots & b_{(N-1)(N-1)} \end{bmatrix} \begin{bmatrix} x_k(0) \\ x_k(1) \\ \vdots \\ x_k(N-1) \end{bmatrix} \tag{2.12}$$

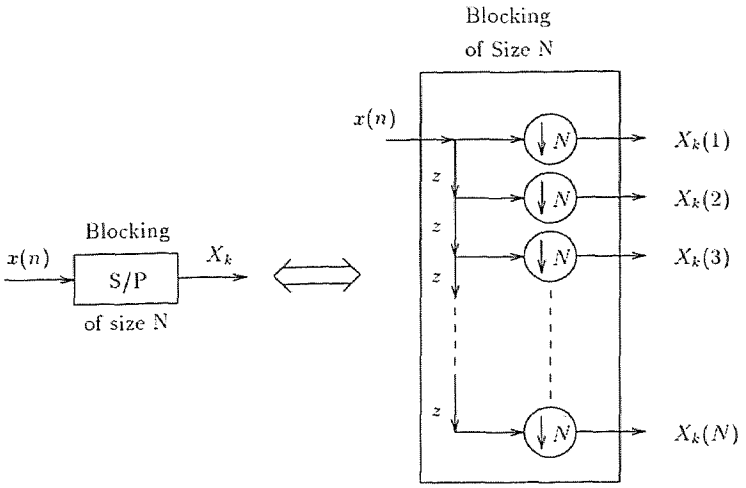

Figure 2.1 Multirate equivalent of Blocking with size N; Serial to Parallel conversion.

The block diagram of the block transform is displayed in Figure 2.2.

The spectral vector $\underline{y_k}$ can be projected back to the time domain as $\underline{\hat{x}_k}$ by

$$\underline{\hat{x}_k} = \mathbf{B}^{-1}\underline{y_k} \ , \tag{2.13}$$

where B^{-1} is the inverse matrix of B. Here we denote the reconstructed signal as $\underline{\hat{x}_k}$ which is the same as original signal if there is no quantization error. Of course, the transform matrix B can be unitary matrix or any other invertible matrix. The unitary matrix is preferred. In this case, Eq.2.13 is rewritten as

$$\underline{\hat{x}_k} = \mathbf{B}^{T}\underline{y_k} \ , \tag{2.14}$$

The inverse of a unitary matrix is the transpose of it, if it is a real-valued matrix.

The unblocking process is a parallel to serial (P/S) data structuring operation forming a serial sequence of discrete time signal $[\hat{x}_k(0)\ ,\ \hat{x}_k(1)\ ,\ldots\ \hat{x}_k(N-1)\ ]$. It is the inverse operation of Blocking with size N. The multirate equivalent of the unblocking operation is displayed in Figure 2.3.

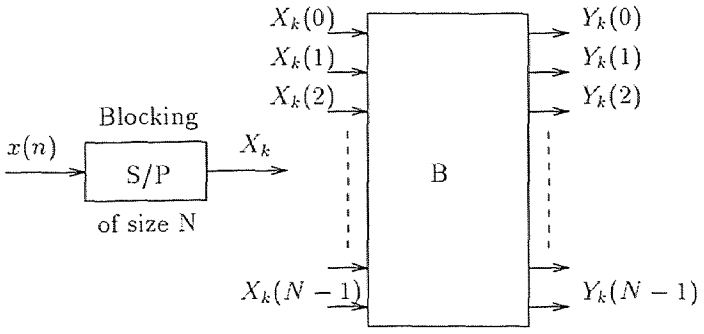

Figure 2.2 Basic structure of a Block transform process.

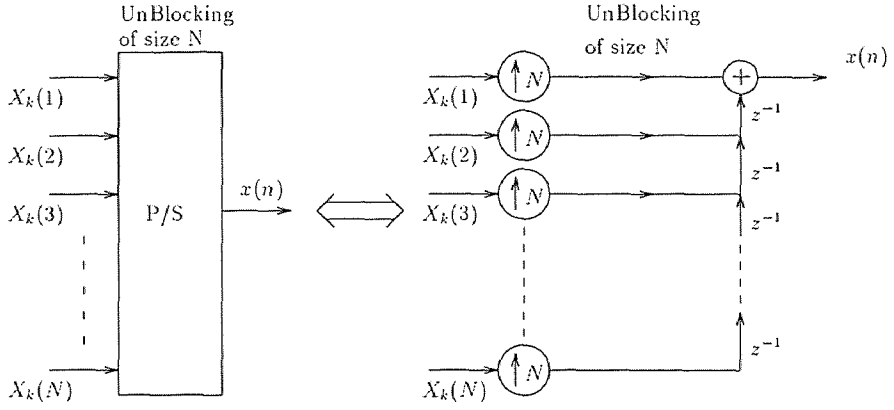

Figure 2.3 Multirate equivalent of Unblocking with size N; Parallel to Serial conversion.

Any $N \times N$ unitary (invertible) matrix can be used in block transform processing. Each column of the unitary matrix forms a transform basis function. These basis functions have a fixed time-frequency properties.

In signal compression applications, the input signal is transformed into spectral coefficients using a block transform such as the discrete cosine transform (DCT). These transform coefficients are then quantized, encoded and transmitted. At the receiver, the inverse block transform operation is performed to reconstruct the signal.

In telecommunication applications, the inverse block transform may serve as a modulation basis at the transmitter, while the forward transform serves as a demodulation basis at the receiver. These orthonormal basis functions have distinct carrier frequencies forming a multicarrier transmission scheme which will be discussed in detail later.

There are several widely used block transforms such as Discrete Fourier Transform (DFT), Discrete Cosine Transform (DCT), and Karhunen-Loeve Transform (KLT) in signal processing and communication applications. In order to increase the flexibility of block transform, the lapped orthogonal transform (LOT) and filter bank theory were proposed. These are revisited in the next section.

2.3 Multirate Filter Banks: Analysis / Synthesis Structure

Multirate filter bank is widely used for signal decomposition. It has been studied extensively for image compression and processing applications. In these applications, the multirate filter bank is implemented as an analysis filterbank followed by a synthesis filterbank. The basic structure of an M band maximally-decimated analysis / synthesis filter bank is displayed in Figure 2.4.

Here a bank of analysis filters $\{h_0(n)\ ,\ h_1(n)\ ,\ \ldots\ ,\ h_{M-1}(n)\}$ decompose (analyze) the input signal $x(n)$ into M different subband spectra $\theta_i(n)$, where $i = 0\ ,1\ ,\ldots\ M$. The symbol $\downarrow M$ represents a down-sampling by a factor of M,

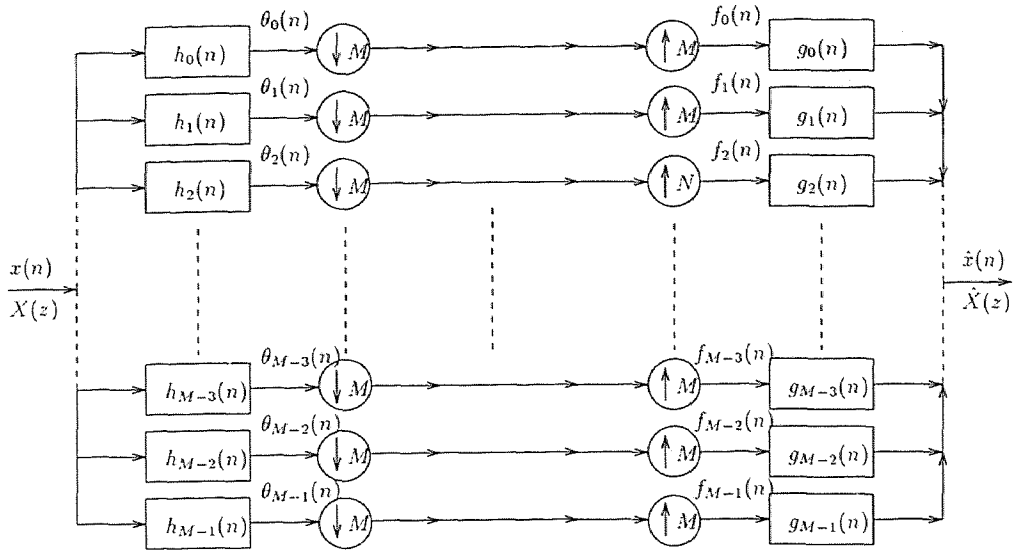

Figure 2.4 M-band maximally-decimated analysis/synthesis filter bank.

which means to get one sample from every M samples. The symbol $\uparrow M$ represents an up-sampling by a factor of M which means to insert $M-1$ zeros between two adjacent input samples. In a maximally decimated analysis / synthesis filter bank, the down-sampling rate is equal to the number of analysis filter banks while the up-sampling rate is equal to the number of synthesis filters. Furthermore, the analysis and synthesis banks have equal number of filters. Each subband filter occupies $\frac{\pi}{M}$ of the full bandwidth and they have an equal bandwidth.

If the up-sampling and down-sampling factors are not equal to the number of filters, the analysis / synthesis filter bank structure is called nonmaximally decimated. We will explore a new application of nonmaximally decimated filter bank later in Chapter 8.

The output of the decimated filterbank can be quantized and processed accordingly. After the processing, they are up-sampled by M and put through an M

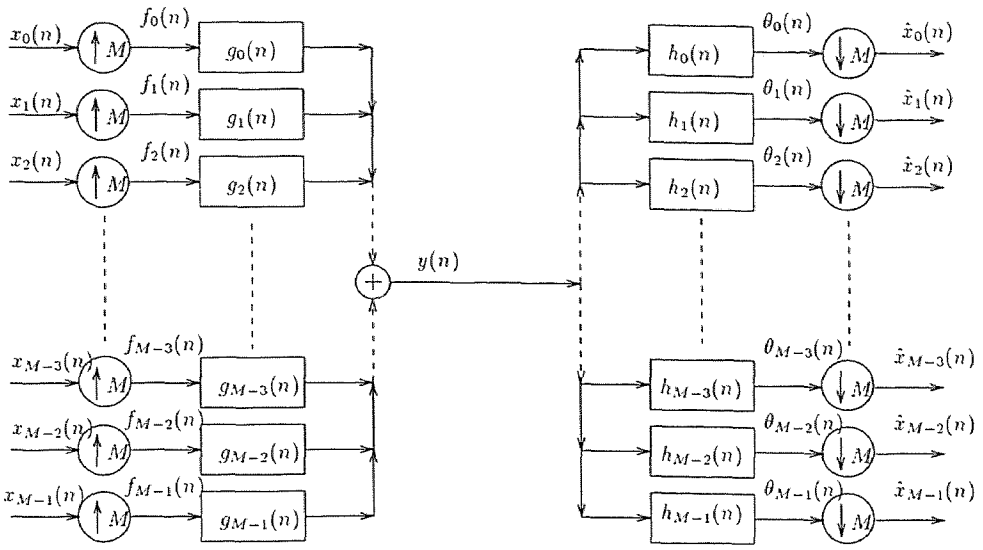

Figure 2.5 M-band maximally decimated synthesis/analysis filter bank.

band synthesis filterbank $\{g_0(n)\ ,\ g_1(n)\ ,\ \ldots\ ,\ g_{M-1}(n)\}$. Then, the interpolated subbands are summed together to obtain the reconstructed signal $\hat{x}(n)$.

If the reconstructed signal $\hat{x}(n)$ is a perfect replica of the original input signal $x(n)$ with only some delay, we call the analysis / synthesis filterbank "Perfect Reconstruction" (PR). Many researchers in the literature have developed the design methodologies for M band perfect reconstruction filter banks [69][87][89].

2.4 Multirate Filter Banks: Synthesis / Analysis Structure

We would like to emphasize another use of multirate filter bank structure where an M band synthesis filter bank is followed by an analysis filter bank. This is of particular interest in this thesis. This filter bank structure is proposed to implement several emerging telecommunication applications.

Figure 2.5 displays a general M band synthesis / analysis filter bank structure. M independent input signals $\{x_0(n)\ ,\ x_1(n)\ \ldots\ x_{M-1}(n)\}$ are up-sampled by a factor of M first. Then, these signals are interpolated by the synthesis filters $\{g_0(n)\ ,\ g_1(n)\ ,\ \ldots\ ,\ g_{M-1}(n)\}$. The outputs synthesis filters are summed together in a composite signal $y(n)$. Using an M band synthesis filter bank, one can multiplex M independent input signals into a synthesized signal. This composite signal $y(n)$ can be transmitted through a communications channel.

At this point, we assume that this transmission channel is ideal so that it does not cause any effect (distortion) on $y(n)$.

The multiplexed signal $y(n)$ is decomposed by an M band analysis filter bank $\{h_0(n)\ ,\ h_1(n)\ ,\ \ldots\ ,\ h_{M-1}(n)\}$ at the receiver. The analysis filters project the received signal $y(n)$ onto their basis functions, and then their spectra are down-sampled by a factor of M. This operation reduces the output signal back to the original transmission rate. The outputs of each analysis filters are denoted as $\{\hat{x}_0(n)\ ,\ \hat{x}_1(n)\ \ldots\ \hat{x}_{M-1}(n)\}$.

The time-frequency interpretation of filter banks and optimal design methodologies are discussed in the next section.

2.5 Time-Frequency Interpretation and Optimal Basis Design for TDMA, FDMA and CDMA Communications

2.5.1 Time - Frequency Interpretation of a Discrete-Time Function $\{h_0(n)\}$

The energy concentration of a function in the time and frequency domains has been a classic problem in the signal processing field. The "uncertainty principle" states that no function can simultaneously concentrate in both the time and frequency domains [20]. The time-spread of a discrete-time function $\{h_o(n)\}$ is defined by [21]

$$\sigma_n^2 \ = \ \frac{1}{E}\sum_n (n-\bar{n})^2 |h_0(n)|^2. \tag{2.15}$$

The energy, E, and time center, $\bar{n}$, of the function $\{h_0(n)\}$ are given as

$$E = \sum_n |h_0(n)|^2 = \frac{1}{2\pi}\int_{-\pi}^{\pi} |H_0(e^{j\omega})|^2 d\omega \tag{2.16}$$

$$\bar{n} = \frac{1}{E}\sum_n n|h_0(n)|^2, \tag{2.17}$$

where its Fourier transform is expressed as

$$H_0(e^{j\omega}) = \sum_n h_0(n)e^{-j\omega n}$$

Similarly, the frequency domain spread of a discrete-time function is defined as

$$\sigma_\omega^2 = \frac{1}{2\pi E}\int_{-\pi}^{\pi} (\omega - \bar{\omega})^2 |H_0(e^{j\omega})|^2 d\omega, \tag{2.18}$$

where its frequency center is written as

$$\bar{\omega} = \frac{1}{2\pi E}\int_{-\pi}^{\pi} \omega |H_0(e^{j\omega})|^2 d\omega. \tag{2.19}$$

Figure 2.6 displays time-frequency tile of a discrete-time function where σ_n^2 and σ_w^2 were defined in Eqs. (2.18) and (2.19), respectively. The shape and the location of the tile can be adjusted by properly designing the time and frequency centers and the spreads of the function under construction. This methodology can be further extended for a basis design [21].

In addition to shaping time-frequency tiles, the orthogonality or completeness requirements are also imposed on the design of a basis (function set).

The engineering challenge is to design the most suitable basis functions for the application at hand [67] [69][71]. Hierarchical filter bank structures lend themselves to more flexibility and can be helpful in achieving design targets more easily. There have been studies on the selection of best basis and the optimality measures for different applications. In this context, note that the block transforms like DFT belong to a subset of subband transforms with the minimum possible duration of basis functions. Subband transforms, however, allow a higher degrees of freedom than

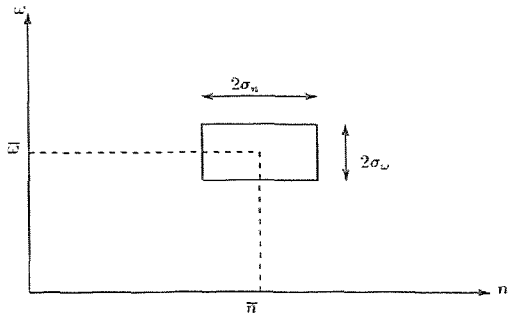

Figure 2.6 Time-Frequency tile of a discrete time function.

block transforms to be utilized for optimal basis design at the expense of additional computational cost[36].

2.5.2 Orthogonal Transmultiplexer Applications

The orthogonal synthesis/analysis filter bank configuration provides a solid theoretical foundation for the single and multiuser communication scenarios. In their most popular version, orthogonal discrete-time transmultiplexers are of the frequency division multiple access (FDMA) type. This implies that the synthesis and analysis filters $\{g_i(n)\}$ and $\{h_i(n)\}$, respectively are frequency selective and brick-wall shaped in their ideal cases. Therefore, ideally, the communication channel is divided into independent frequency subchannels. These subchannels are allocated among the users of multiuser communications or the terrestrial digital audio broadcasting (T-DAB) stations. This type has been the most popular version of orthogonal transmultiplexers.

More recently, the subchannel (multicarrier modulation) concept has also been applied for single user communication scenarios like ADSL applications. In addition, OFDM modulation is currently being pursued by several research groups for the third generation of personal communication systems (PCS) applications [64].

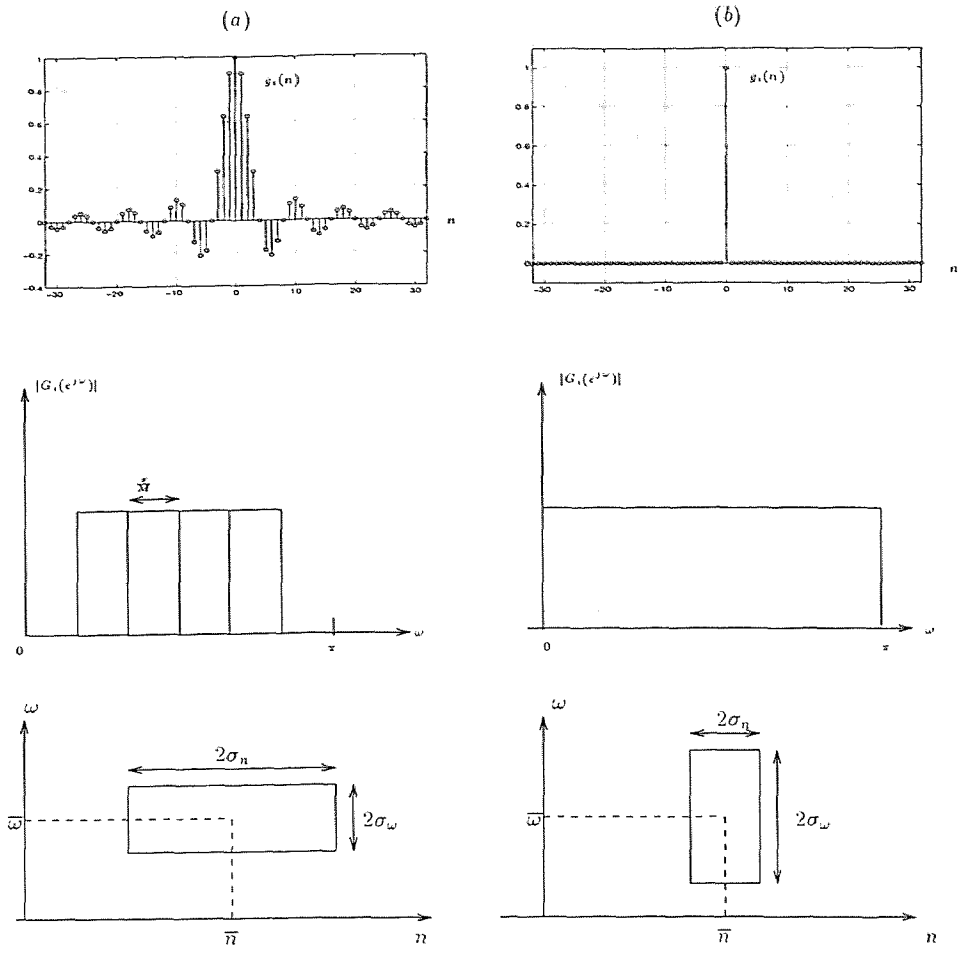

Figure 2.7 Time and Frequency Relationship for FDMA and TDMA type Transmultiplexer.

In contrast to FDMA, a time division multiple access (TDMA) communication scheme allocates a dedicated time slot for each user. A user is allowed to use the full frequency band only during a given time slot. Time slot allocation is a simple delay, with a transform $G_k(e^{j\omega}) = e^{-jk\omega}$. This can be interpreted as the all-pass-like (spectrally spread) user codes or synthesis filters, i.e. $|G_i(e^{jw})| = 1, 0 \leq w \leq \pi$ for i=0, ... , M-1 for the ideal case, used in the orthogonal transmultiplexer shown in Figure 2.5. Figure 2.7 displays the corresponding time and frequency relationships for FDMA and TDMA type transmultiplexers[24].

The emerging code division multiple access (CDMA) communication techniques employ user codes (filters) which are simultaneously spread in both the time and frequency domains. More recently, the filter bank design problem was extended for this purpose and spread spectrum PR-QMFs were proposed as an alternative to the existing codes, e.g. Gold codes, Walsh codes or other pseudo-random codes. These orthogonal transmultiplexers utilize the user codes $\{g_i(n)\}$ which are all-pass-like in the frequency as well as spread in the time domain [24]. It is shown that the popular pseudo-random noise (PN) and Gold codes are binary valued and near orthogonal special subset of general spread spectrum PR-QMF bank framework [25][26][65].

CHAPTER 3

DIGITAL SUBSCRIBER LINE TECHNIQUES: MODULATION AND DEMODULATION SCHEMES

3.1 Digital Subscriber Line Techniques

Digital subscriber line technique provides high speed communications over unshielded twisted pair (UTP) telephone line. It can provide high bit rate digital signal transmission along with the conventional plain old telephone service (POTS). It utilizes higher frequency range of the telephone wire which is not used by the conventional POTS. The unshielded twisted copper pair (UTP) is universally present in the telephone loop plant and within buildings around the world. It has its own unique advantage over other transmission media such as cable and optical fiber. It is very easy to splice, interconnect and terminate. They are always cabled together with many twisted pairs. Due to the nature of bundling, UTP is subject to crosstalk which includes near-end crosstalk (NEXT) and far-end cross talk (FEXT) in a practical scenario. High speed data communications over UTP using DSL techniques allows access for T1/E1, digital video and interactive data applications. There are several types of DSL techniques emerging in industry. Figure 3.1 displays a basic configuration of DSL communications.

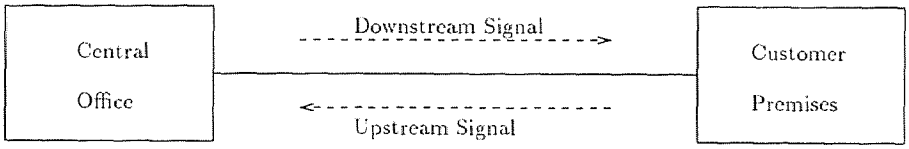

Figure 3.1 A basic block diagram of DSL communications.

High bit rate digital subscriber line (HDSL) defines a bi-directional transmission of T1 (1.544 Mb/s) [9] or E1 (2.048 Mb/s) [10] services on one or more twisted

wire pairs. The symmetric nature of HDSL applications will cause self-NEXT and self-FEXT. Since the self-NEXT interference is much stronger than self-FEXT interference, the transmission throughput is greatly limited by the presence of self-NEXT interference.

Asymmetric digital subscriber line (ADSL) provides higher speed data transmission from Central Office (CO) to the end subscriber in a customer premise (CP) (Downstream) and a lower speed from the end subscriber to the network CO (Upstream). Target applications for ADSL include high speed Internet access and Video on Demand services. Due to a great demand for high-speed Internet access, ADSL technique is up to fly in the coming years. The asymmetric nature of ADSL eliminates the presence of self-NEXT interference, which in return, increases the transmission throughput in ADSL. ADSL communication techniques provide the means for high speed digital transmission up to 8 - 10 Mbps over the POTS on a typical DSL loop plant. The transmission rate is several hundred times higher than current 28.8 Kbps modems. Similarly, Digital Subscriber Line transmission speed is also much higher than Integrated Services Digital Network (ISDN) speed which has become available recently.

Figure 3.2 displays a typical carrier serving area (CSA) test loop configuration from ANSI standard. An ADSL service area range satisfies carrier serving area (CSA) loop requirements. In particular, up to 12 Kft of 24 American gauge wire (AWG) (CSA loop #8) and 9 Kft of 26 American gauge wire (AWG) (CSA loop #6) are often used as test loop channel in the field.

The NEXT interference transfer function is modeled as [3]

$$H_{NEXT}(f) = \frac{1}{1.13 * 10^{13}} * \{\frac{N_{NEXT}}{49}\}^{0.6} * f^{1.5} \tag{3.1}$$

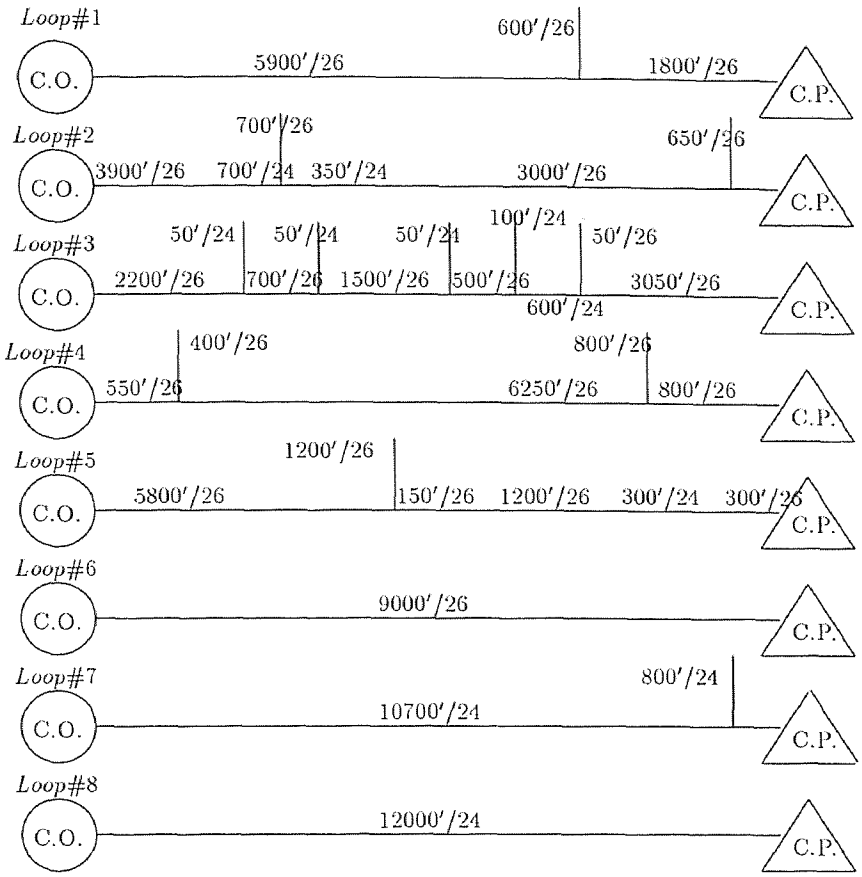

Figure 3.2 ANSI Carrier Serving Area (CSA) Test Loop Configurations [11].

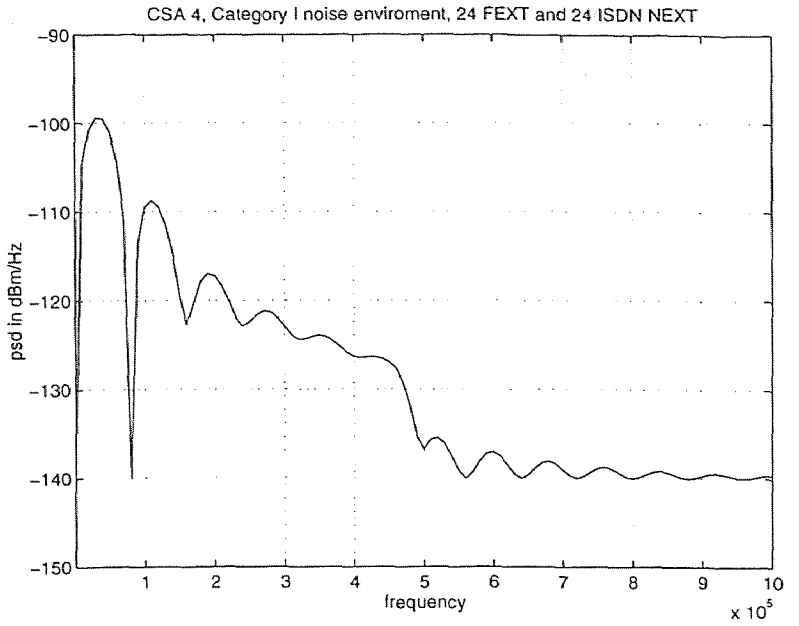

Figure 3.3 ANSI Carrier Serving Area (CSA) Loop # 4 Test Noise Spectrum [11].

where N_{NEXT} is the number of NEXT interferes and f is the frequency in Hertz. Similarly, the FEXT interference transfer function is modeled as [3]

$$H_{FEXT}(f) = 8 * 10^{-20}\{\frac{N_{FEXT}}{49}\}^{0.6} * d * f^2 \tag{3.2}$$

where N_{FEXT} is the number of FEXT interferers, f is the frequency in Hertz and d is the loop length in Kft.

ANSI ADSL standard specifies several test environments in detail. Figure 3.3 displays the noise spectrum of ANSI standard for ADSL test environment for carrier serving area (CSA) Loop # 4 in category I. There are 24 ISDN NEXT and 24 FEXT noise injected into the test loop. Figure 3.4 displays the noise spectrum of ANSI standard for ADSL test environment for CSA Loop # 6 (AWG 26 with 9 Kft loop) in category I. In that test scenario, there are 20 HDSL NEXT noise injected into the test loop. Similarly, Figure 3.5 displays the noise spectrum of ANSI standard for ADSL test environment for mid-CSA in category I. There are 10 T1 NEXT noise injected into the test loop in this case.

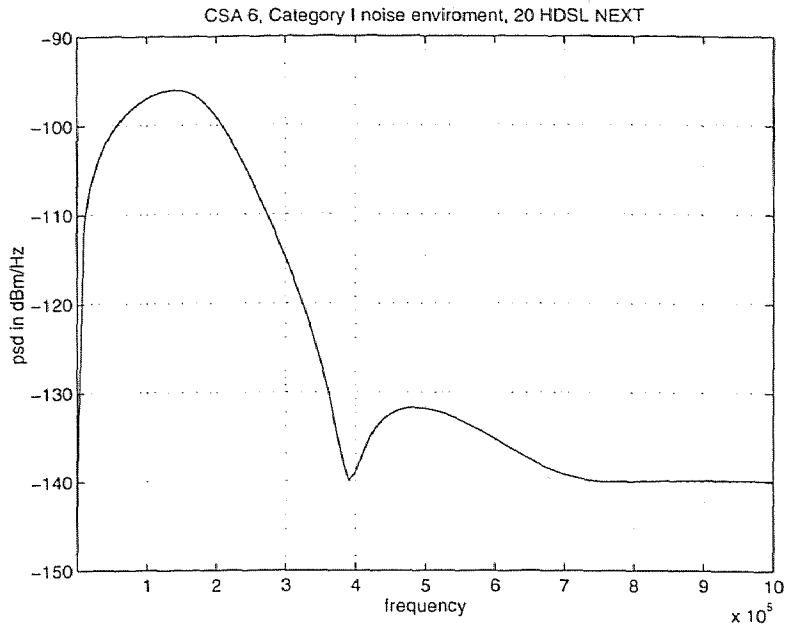

Figure 3.4 ANSI Carrier Serving Area (CSA) Loop # 6 Test Noise Spectrum [11].

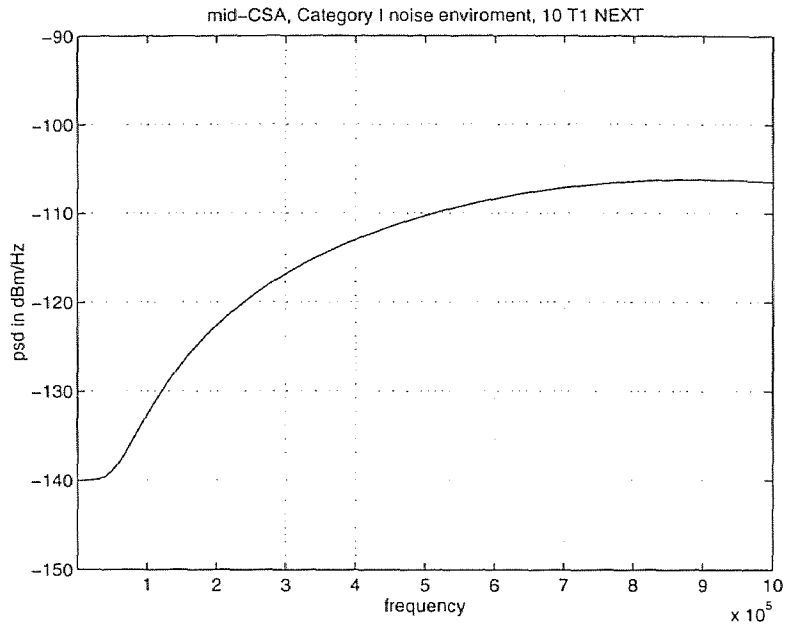

Figure 3.5 ANSI Mid-CSA Loop Plant Test Noise Spectrum [11].

Very high bit rate digital subscriber line (VDSL) provides a vehicle to distribute 25 Mb/s to 50 Mb/s for the last stage of transmission to the customer premises. The service range will be less than several hundred meters for VDSL. It will fit well for fiber to the curb applications. VDSL technique is still in its early stage. It is going to emerge in the very near future. There are many new issues arising as the transmission frequency approaches to several MHz.

In the field of DSL, there are two competing modulation techniques under consideration. The first one is the single carrier broadband modulation systems such as Pulse Amplitude Modulation (4-PAM, 2B1Q for example), Quadrature Amplitude Modulation (QAM) or its variation Carrierless Amplitude Phase (CAP) modulation. Second, multicarrier modulation systems such as Orthogonal Frequency Division Multiplexing techniques namely Discrete Multi-Tone (DMT) and Discrete Wavelet Multitone Transceiver (DWMT) or Discrete Subband Multitone Transceiver (DSBMT). There are various implementations of these modulation techniques in the emerging industry. It is shown in this thesis that these techniques can theoretically approach to the same performance bound (they have the same maximum achievable bit rate and Signal to Noise Ratio margin under the same operational conditions) [35]. We will discuss these techniques in detail in the next several sections.

3.2 Single Carrier Modulation: Quadrature Amplitude Modulation and Carrierless Amplitude and Phase Modulation

The conventional bandwidth efficient digital modulation line code such as Quadrature Amplitude Modulation (QAM) technique has been widely used in digital communications systems. The Carrierless Amplitude Phase (CAP) signaling for DSL applications was proposed in [3][5][8]. CAP modulation is a variant of QAM technique. CAP modulation line code has been implemented in various DSL high speed modem design. It is the most widely deployed DSL technique in today's market.

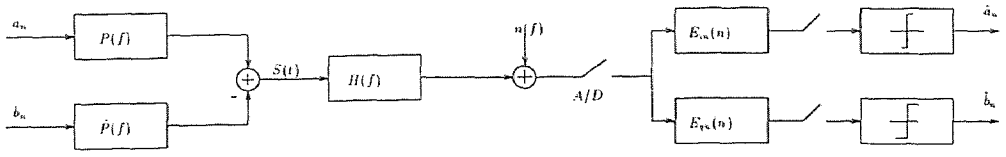

Figure 3.6 A simplified structure of a Carrierless Amplitude and Phase Modulation based transceiver system.

The simplified structure of a CAP based transceiver is displayed in Figure 3.6. The transmitted CAP signal can be modeled as

$$S(t) = \sum_{-\infty}^{\infty} a_n p(t - nT) - \sum_{-\infty}^{\infty} b_n \tilde{p}(t - nT) \tag{3.3}$$

where a_n, b_n are the information bearing symbols. They are the in-phase and quadrature components in the constellation, respectively. It is similar to conventional QAM modulation. $p(t)$ and $\tilde{p}(t)$ are of a Hilbert pair. Both of them are transmitter passband spectral shaping filters. Raised-Cosine signal or Square Root Raised-Cosine signal can be used as shaping filters. Figure 3.7 displays the in-phase and quadrature CAP shaping filters using Raised Cosine Nyquist filter [3].

In the implementation of a CAP based transceiver system, CAP modulation signal is generated digitally by passing transmitted bitstream through the in-phase shaping filter $p(t)$ and quadrature shaping filters $\tilde{p}(t)$. The incoming symbols are up-sampled (oversampled) by a factor of K such that the CAP shaping filters are $\frac{T}{K}$ fractionally spaced. Here T is the symbol period. K is selected as 4 or 5 in general. The in-phase and quadrature shaping filters may have time span of 10 - 20 periods. For the case of $K = 5$ and shaping filters having a time span of 10, in-phase and

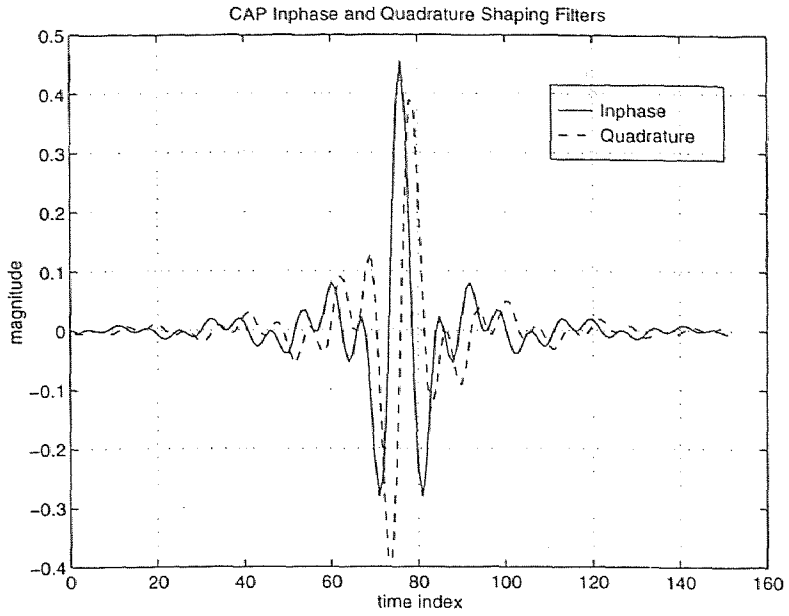

Figure 3.7 The coefficient of In-phase and Quadrature Shaping Filter of a CAP based system [3].

quadrature shaping filters have 50 coefficients. At the transmitter side, the discrete output samples of the shaping filter are converted to an analog signal using a D/A converter. A low pass analog filter is used before it is put through a wire splitter.

Let us design a CAP based ADSL transceiver with 6.72 Mbps downstream and 250 Kbps upstream. The downstream signal constellation is of size 256 and upstream signal constellation is of 64. Figure 3.8 displays the signal constellation of 256 CAP while Figure 3.9 shows the 64 CAP constellation.

Considering the Trellis coding factor of the signal, the bandwidth of CAP based system is 960 kHz for downstream and is 50 kHz for upstream signal. CAP based DSL signal spectrum starts at 35 kHz so that the POTS service signal will not be effected. Figure 3.12 displays the spectrum of 6.72 Mbps downstream and 250 Kbps upstream CAP signalings. Obviously, it is an FDM type implementation. In this case, there is no self near-end crosstalk (NEXT) interference in the system. The far-end crosstalk (FEXT) interference is any way much lower than NEXT.

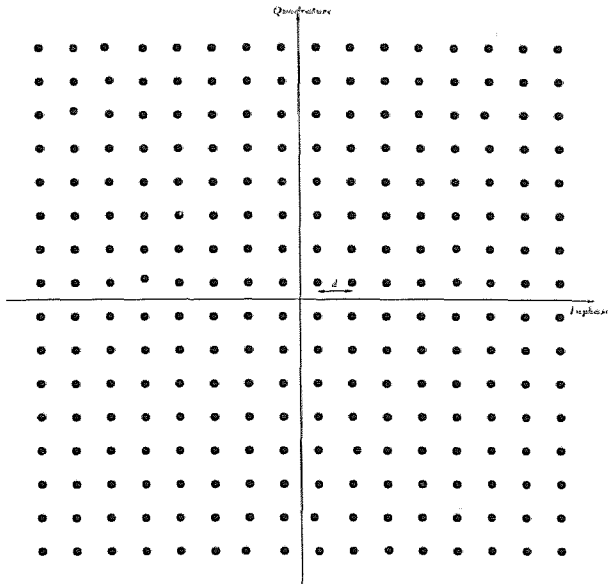

Figure 3.8 Constellation of 256 CAP signaling

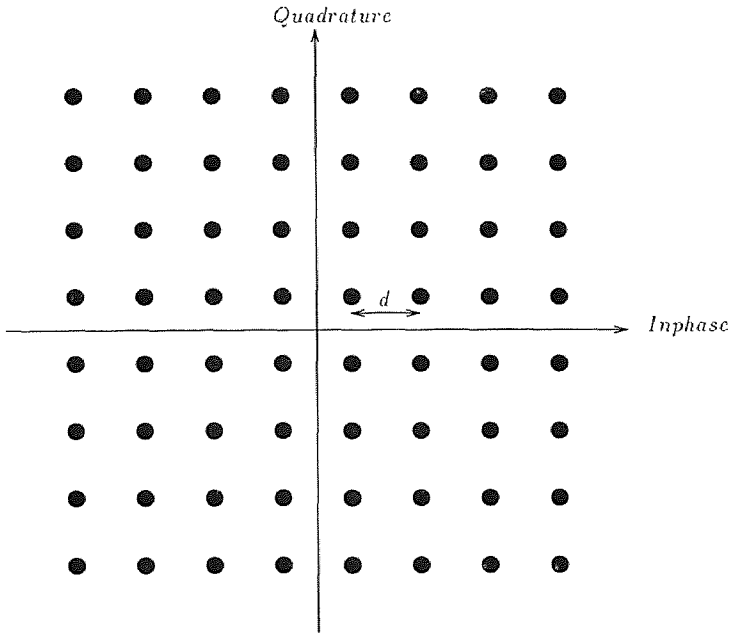

Figure 3.9 Constellation of 64 CAP signaling

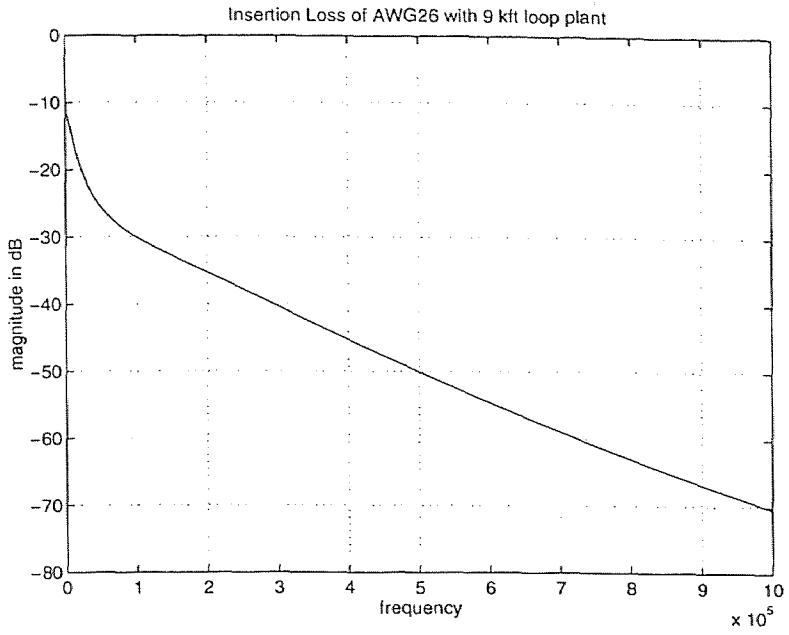

Figure 3.10 The Insertion Loss of AWG 26 with 9 Kft length loop plant.

The transmission loop plant has high attenuation at the high frequency side. Figure 3.10 shows the insertion loss of a typical AWG 26, 9 Kft loop plant. Obviously, there is about 55 dB loss for the signal frequency at 600 kHz. The impulse response of this loop plant is displayed in Figure 3.11.

As we know, there will be significant signal distortion, namely, intersymbol interference introduced by this transmission channel. At the receiver, a well-known adaptive fractionally spaced linear feed-forward filter and symbol spaced decision feedback equalizer (DFE) transceiver structure is implemented. It will effectively cancel the intersymbol interference. In a CAP based system, Noise Predictive (NP), Hybrid or conventional DFE structure may be used. Figure 3.13 is the structure of Noise Predictive DFE used in a CAP based system. The equalized symbol is sliced to make a decision.

In order to prevent error propagation due to the nature of DFE structure, the Tomlinson precoder needs to be implemented in a CAP based system. For different

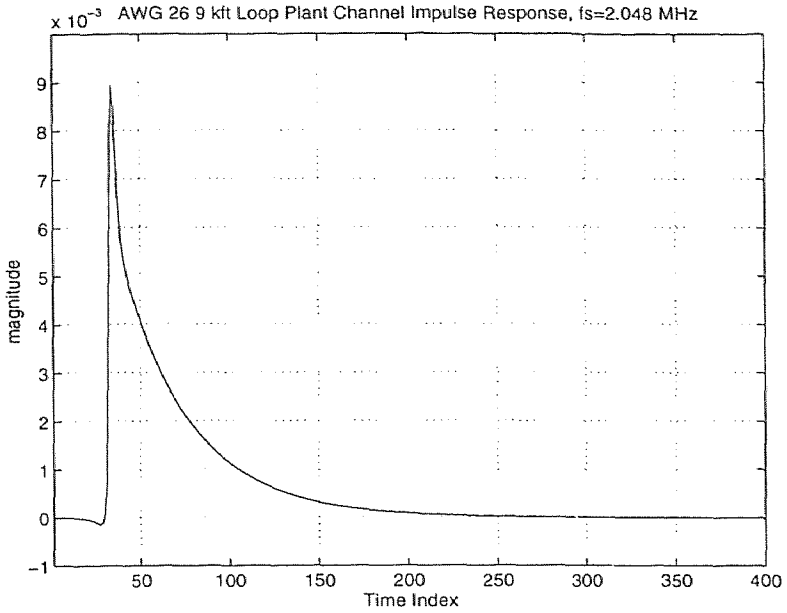

Figure 3.11 The impulse response of AWG 26 with 9 Kft length loop plant.

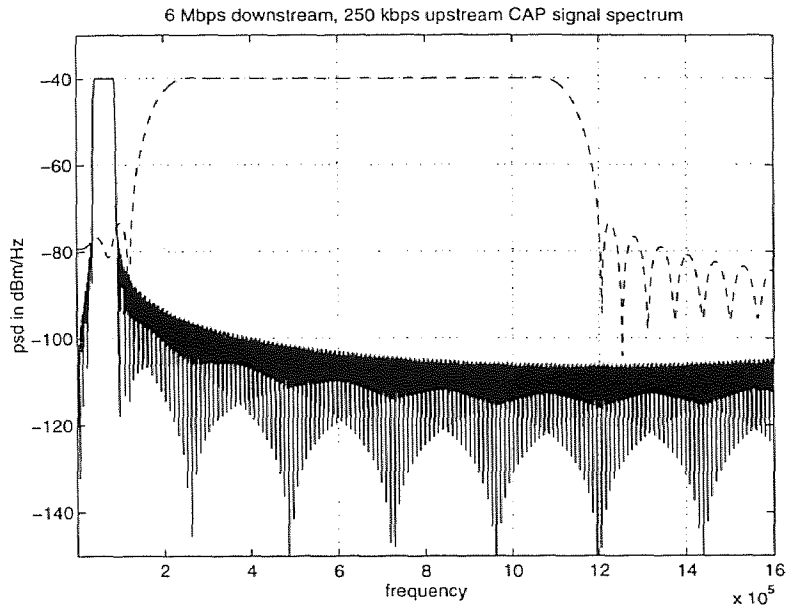

Figure 3.12 Signal Power Spectral Density of ADSL 6.72 Mbps 256-coded CAP Downstream and 250 Kbps 64-coded CAP Upstream.

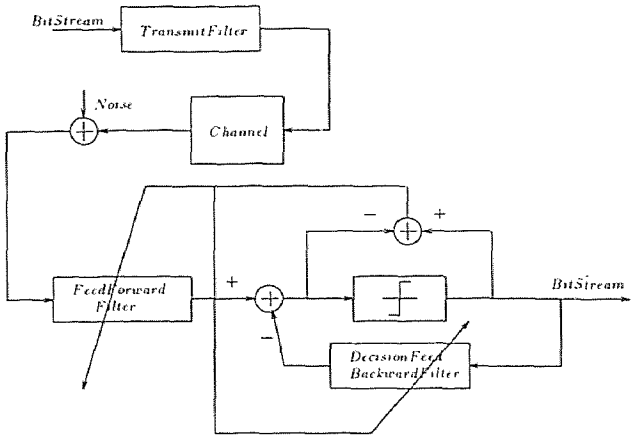

Figure 3.13 Noise Predictive DFE structure implemented in CAP transceiver.

loop plants under different field noise conditions, different transmission rates can be realized. The CAP based rate adaptive ADSL (RADSL) transceiver has been used in a field trial and commercially deployed around the world. It is currently the De Facto standard in ADSL applications.

3.3 Multicarrier Modulation: OFDM (DMT)

Multicarrier modulation techniques utilize a set of modulation line codes for digital communications. Ideally, these modulation line codes divide the transmission channel into a number of independent subchannels. The transmultiplexed digital signals can be transmitted independently in different subchannels. We can model this channel into many parallel brick wall subchannels. As the number of subchannels increases, the brick wall model becomes more accurate. There is no need to consider any inter-symbol interference in any subchannel. A one-tap complex equalizer can be implemented in subchannels to recover the transmitted (multiplexed) signal. Naturally, Multicarrier modulation is of a frequency division type multiplexer.

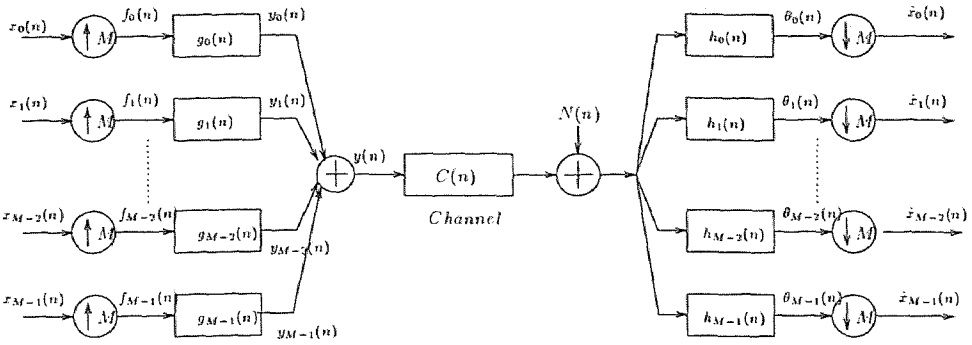

Figure 3.14 Basic structure of a multicarrier modulation based digital transceiver.

The basic structure of a multicarrier modulation based transceiver is displayed in Figure 3.14. It is shown as a multirate M-band synthesis/analysis filter bank transmultiplexer.

In a multicarrier modulation system, a set of M frequency selective orthogonal functions $\{g_i(n)\}$ are used. The subsymbols $\{x_0(n), x_1(n), ..., x_{M-1}(n)\}$ are formed by grouping blocks of an incoming bit stream via a constellation scheme like QAM or PAM. The dynamic parsing of the incoming bit stream to the subsymbol is determined by the achievable signal to noise ratio in all subchannels. The subchannels that suffer less attenuation or less interference will carry more bits of information [2][4].

The modulation filters of the transceiver form an orthogonal function set. The design methodologies of synthesis/analysis filter banks are applicable for this application [69] [89] [74].

3.3.1 OFDM or Discrete Multitone Transceiver Technique for DSL Communications

Discrete Multitone Transceiver (DMT) uses discrete Fourier transform (DFT) as its modulation/demodulation basis function set. Each subcarrier modulation function is indeed one of the DFT basis functions. Since there are fast Fourier

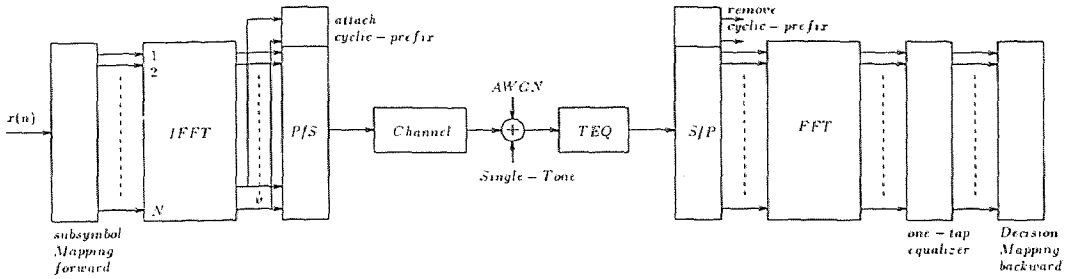

Figure 3.15 An implementation of DFT based DMT Transceiver.

transform algorithms which make the computation complexity very low, DMT is very attractive to industry. Many companies are working on DMT based techniques for digital subscriber line applications. As a matter of fact, ANSI has adopted Discrete Multitone as its standard in ADSL application [11].

The current DMT based ADSL communication systems utilize 512-size DFT basis functions as their orthogonal subcarriers in a synthesis/analysis (transmultiplexer) transform configuration. These subcarriers spectrally overlap although they are orthogonal. The orthogonality of DMT comes from implementation of the guard interval (cyclic prefix) in the transmitter. The idea of cyclic prefix is first proposed by Peled and Ruiz [28]. There is its more detailed derivation in [36]. Figure 3.15 displays an implementation of Discrete Fourier Transform based DMT transceiver system.

The transmission channel has a high dynamic range due to the transmission loss at the higher frequency range. Therefore, it generates severe distortion at the transmitted signal. In order to eliminate the intersymbol interference as well as the interchannel interference, a cyclic prefix is used. Its length of ν should be larger than the duration of impulse response of the transmission channel.

At the transmitter side, the transmitted subsymbols can use QAM constellation in each subchannel. The size of QAM constellation depends on the noise condition of subchannel. This turns into an optimal bit allocation problem (water pouring). The parsed subsymbols are arranged in symmetric Hermitian pairs such that the Inverse Discrete Fourier Transform (IDFT) transformed sequence is real valued. The cyclic prefix is attached to the IDFT modulated supersymbol (block) sequence. Assume that the length of cyclic prefix is ν, we copy the last ν samples of IDFT transformed data samples to the beginning of supersymbol. Then, the composite supersymbol is of size 512+ν. The composite supersymbol is converted from Parallel to Serial and passed through a D/A converter. The modulated signal is then transmitted to the splitter of DSL loop plant. The cyclic prefix makes the linear convolution the same as circular convolution. It will render very simple receiver structure. The addition of cyclic prefix operation will naturally reduce the effective transmission rate by $\frac{N}{N+\nu}$. Here N is the size of IDFT/DFT transform. The reduction of transmission by $\frac{N}{N+\nu}$ is the penalty paid to utilize an efficient modulation and demodulation algorithm. Therefore, ν should not be too big compared to N, the size of IDFT/DFT. In ANSI ADSL standard, N is 512 and the length of cyclic prefix ν is chosen as 32.

As it is displayed in Figure 3.11, the practical loop impulse response has a much longer duration compared to v when the sampling rate is high. If we keep the cyclic prefix length longer than channel impulse response, the throughput is reduced. In order to increase the throughput, a pre-equalizer, called a time domain equalizer (TEQ), is designed. It reduces the duration of composite channel impulse response.

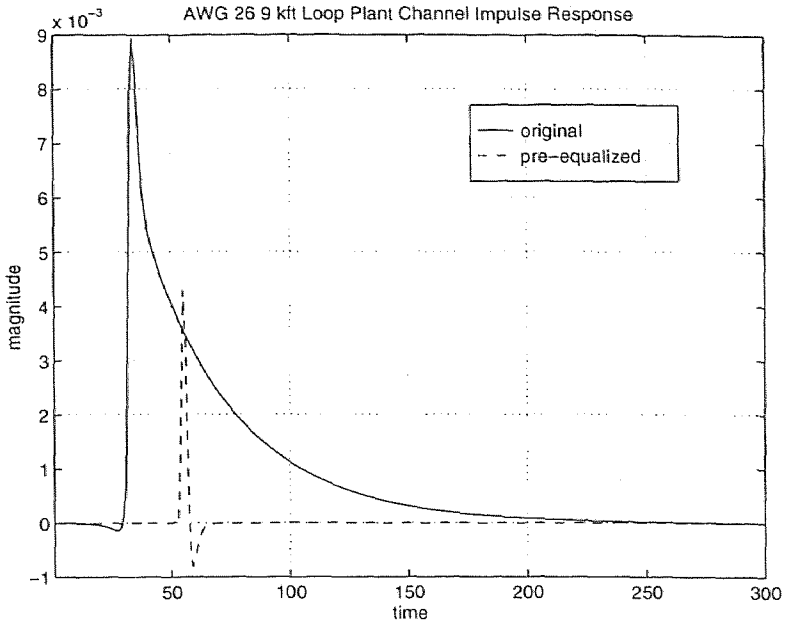

Figure 3.16 Original channel impulse response and TEQ pre-equalized channel impulse response in a DMT transceiver system.

Figure 3.16 shows the original impulse response of AWG 26 wire with length of 9 Kft with a sampling frequency of 2.048 MHz. Obviously, the duration of the channel is long compared to N = 512. Using a TEQ, the channel impulse response is reduced to be less than ν, where ν is set as 32 by ANSI ADSL standard. The TEQ pre-equalized channel impulse response is also displayed in Figure 3.16.

At the receiver side, the received signal is sampled by an A/D converter with the same sampling frequency. The cyclic prefix part of received signal is discarded first. Then the size N Discrete Fourier Transform (FFT) demodulation is performed. Due to the presence of cyclic prefix, all the subchannels are independent. In order to recover a transmitted subsymbol, one tap complex equalizer is used at the DFT output. The one tap complex equalizer for each subchannel is obtained from the inverse of the DFT transform for the composite channel impulse response.

The decision is made after one tap complex equalizer. The sliced subsymbols are mapped back accordingly and form the composite data stream.

According to ANSI standard, Trellis coding, Reed-Solomon coding and proper interleaving technique can be applied to DMT based transceiver system. It will generate 4 - 5 dB coding gain.

CHAPTER 4

DISCRETE SUBBAND MULTICARRIER TRANSCEIVER DESIGN

4.1 Discrete Wavelet Multicarrier Transceiver or Discrete Subband Multitone Transceiver for DSL

Discrete Wavelet Multitone Transceiver was proposed for digital subscriber line application by Sandberg and Tzannes [14]. We observe that the DMT modulation basis functions are spectrally overlapped. The orthogonality of these subchannel is satisfied only when the cyclic prefix length is shorter than the TEQ pre-equalized composite channel impulse response and channel characteristics are estimated accurately. If the TEQ cannot reduce the composite channel impulse response to be shorter than the length of cyclic prefix or there is some sort of mismatch between practical channel and the estimation, the overall system performance will degrade severely. It is reported by in [14] that DWMT is more robust than DMT. It is shown later in this thesis that if there is a single tone or narrow band interference in the environment of a DMT based system, the system performance will degrade severely. The spectral nature of discrete Fourier transform basis functions causes a performance sensitivity to the location of interference.

4.2 Optimal Orthogonal Multicarrier Basis Design

Multicarrier modulation makes use of a set of orthonormal basis functions as its modulation and demodulation line codes. Discrete Multitone Transceiver (DMT) based system utilizes IDFT/DFT basis functions as its modulation and demodulation line code. The length of these basis function is the same as the number of subcarriers. Their subcarriers have spectral overlap in frequency domain. Discrete Wavelet Multicarrier Transceiver or Discrete Subband Multitone Transceiver tries to increase the length of modulation basis functions in order to decrease the spectral overlaps of its subcarriers. Of course, these modulation functions are still orthogonal. In practice,

DWMT and DSBMT use cosine modulated maximally decimated multirate synthesis / analysis filterbank transmultiplexer structure to implement the modulation and demodulation process. These modulation line codes must have good bandpass like spectra. The side lobes of the basis function should be very small compared to the magnitude of band pass spectra. In other words, the spectral overlapping of these basis functions must be very small. This is the fundamental principle for a meritful DSBMT basis function design.

There are a number of subchannels in a multicarrier modulation system. Different subchannels suffer different attenuation (or insertion loss). Many subchannels, especially those at high frequency, suffer larger insertion loss. The equalizers at these subchannels try to compensate attenuation by using higher gain. In this case, small amount of spectral leakage (side lobes) from lower frequency will effect the performance of subchannels at high frequency. In a full-duplex systems, there is near-end crosstalk and far-end crosstalk. The large side lobes will severely degrade the performance of subchannels with high attenuation. The interchannel interference of these basis functions should be well addressed. From the design point of view, it is always desirable to get high side lobe attenuation to alleviate the burden of interchannel interference and intersymbol interference cancellation.

4.2.1 Perfect Reconstruction or Quasi Perfect Reconstruction Filterbank Design for DSL

Figure 4.1 displays the maximally decimated M band synthesis / analysis filterbank structure. The transmission channel is assumed to be ideal. In multirate filterbank literature, perfect reconstruction puts orthogonality and shift orthogonality constraints on the coefficients of filterbank as follows [17][69][89][90]:

$$(a) \quad \sum_k h_i(k)h_i(k+Mn) = 0, \quad n \neq 0, \tag{4.1}$$

$$(b) \quad \sum_k h_i(k)h_j(k+Mn) = 0, \quad \forall n, \tag{4.2}$$

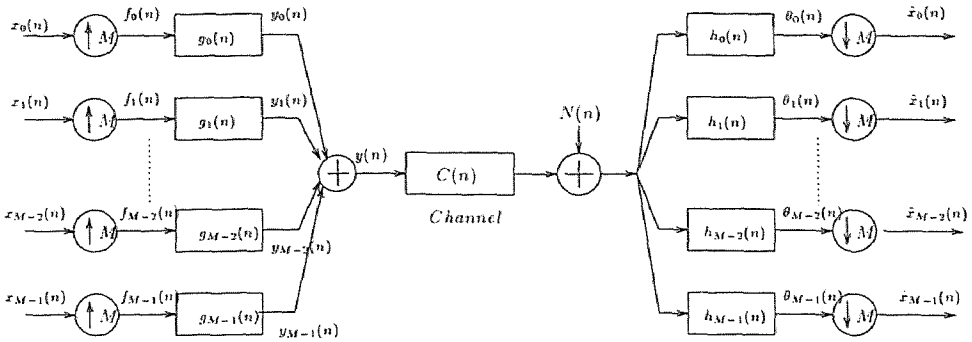

Figure 4.1 M-band maximally decimated synthesis/analysis filter bank.

with the normalization as

$$(c) \quad \sum_k |h_i(k)|^2 = 1. \tag{4.3}$$

where $\{h_i\}$ are analysis filters and $\{g_i\}$ are synthesis filters, which are simply time-reversals of analysis filters.

Under the PR constraints, the optimal two band filterbank design falls into the optimization criterion of **Stopband Minimization**.

An objective function of stopband minimization for a two-band PR-QMF bank is expressed as

$$\phi_s = \int_{\frac{\pi}{2}+\epsilon}^{\pi} |H_0(e^{j\omega})|^2 d\omega + \int_0^{\frac{\pi}{2}-\epsilon} |H_1(e^{j\omega})|^2 d\omega, \tag{4.4}$$

where ϵ is some non-ideal transition bandwidth factor.

For the general case of an M-band PR-QMF,

$$\bar{\phi}_s = \sum_{l=0}^{M-1} \int_{l^{th} stop-band} |H_l(e^{j\omega})|^2 d\omega. \tag{4.5}$$

Figure 4.2 displays the frequency response of a two-band perfect reconstruction filterbank. The impulse response of a two-band PR-QMF filterbank is shown in Figure 4.3. The filters have 60 taps in this filter bank design example.

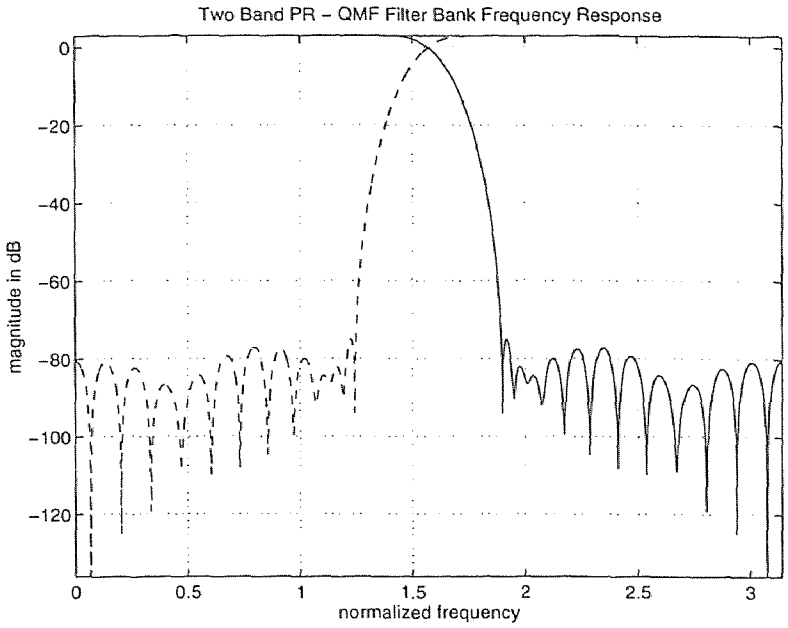

Figure 4.2 Frequency Response of the Two Band PR-QMF Filter Bank.

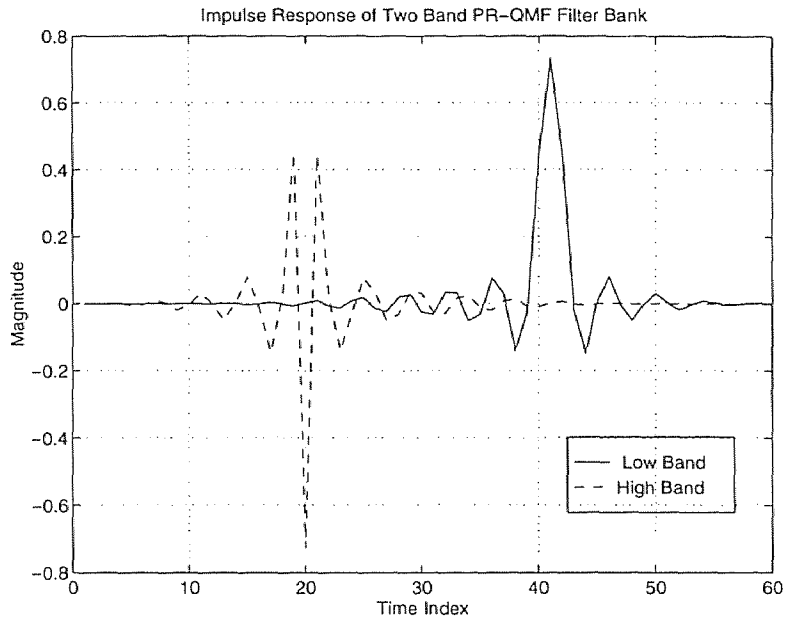

Figure 4.3 The Impulse Response of a Two Band PR-QMF Filter Bank.

As the number of taps of orthonormal basis functions and the number of subcarriers increase, M band synthesis / analysis filter bank design problem becomes computationally involved. It is not very easy to get an optimal solution.

The cosine modulated filter bank fits well into digital subscriber line applications. One needs to design only one prototype low pass filter with $\frac{\pi}{M}$ bandwidth. The other filters can be obtained as the cosine modulated prototype filter with different shift frequencies. In this method, the number of coefficients to be designed is reduced to the number of taps of the prototype filter. The optimization problem is much easier.

In practice, the transmission channel suffers a large dynamic range of attenuation. Although the transmitted signal is composed of Perfect Reconstruction orthogonal transmultiplexer, the received signal will be distorted severely. The demodulation analysis filter bank alone could not recover the transmitted digital signal. Some extra post processing is required. In this sense, perfect reconstruction condition will not be that critical. Any quasi (near) perfect reconstruction basis with small interchannel interference and small intersymbol interference can be used in multicarrier modulation transceiver system. We will investigate the post processing part in next section.

There are fairly extensive cosine modulated filter bank design studies in the literature[89][69]. There are also research activities on quasi perfect reconstruction cosine modulated filter bank design problem[93][94].

In this work, several optimal design criteria are considered.

(a) Minimal stopband .

(b) Minimal first side lobe attenuation.

In the synthesis/analysis cosine modulated multirate filter bank structure, the desired spectral overlap occurs only with the adjacent subcarrier. The side lobe must be highly attenuated. Also, It is desired that the side lobe should be attenuated

further as the frequency goes away from the passband. The equal ripple type of cosine modulated filter bank is not desirable since all subcarriers will generate a same level of interchannel interference. The side lobe or equal ripple attenuation will limit the performance of the transceiver. Based on these analyses, the optimal cosine modulated filterbank basis is desirable such that there is only interchannel interference coming from two adjacent subchannels for most of subchannels while only one adjacent subchannel for subchannel 1 and subchannel M.

In order to get a good stop band performance for a prototype filter, the length of filter will be increased to several times of the number of filters. This ratio is called as the span of the filters. If the number of filters is M, the span of the filter is g, then the length of filters will be gM. This is called overlapped filter bank in the multirate filterbank literature. The value of span g is critical for the achievable side lobe attenuation. When span g is equal to 1, the filter bank becomes a block transform. With an increase of span g, the length of analysis and synthesis filter bank increases, Therefore, one can achieve a better stopband attenuation. In the mean time, larger the span g is, the longer the possible interframe interference will be. This problem will be addressed in the next section.

The PR cosine modulated filter bank basis and quasi PR cosine modulated filter bank basis functions are designed in this section using the methodologies of [89][69] [93][94].

Let's design a 16 band synthesis / analysis filter bank. The overlap span g is set to be 8. It means that the number of filter taps is 128. There are 128 coefficients to be optimally designed. Figure 4.4 displays frequency spectra of a 16 band cosine modulated filter bank with 128 taps in each basis function. The basis functions have equal ripple in the stop band. Figure 4.5 shows the frequency responses of a 16 band cosine modulated filter bank with the same length, 128 taps, but with an unequal ripple. In this case, the first side lobe is about -40 dB. But the stop band attenuation

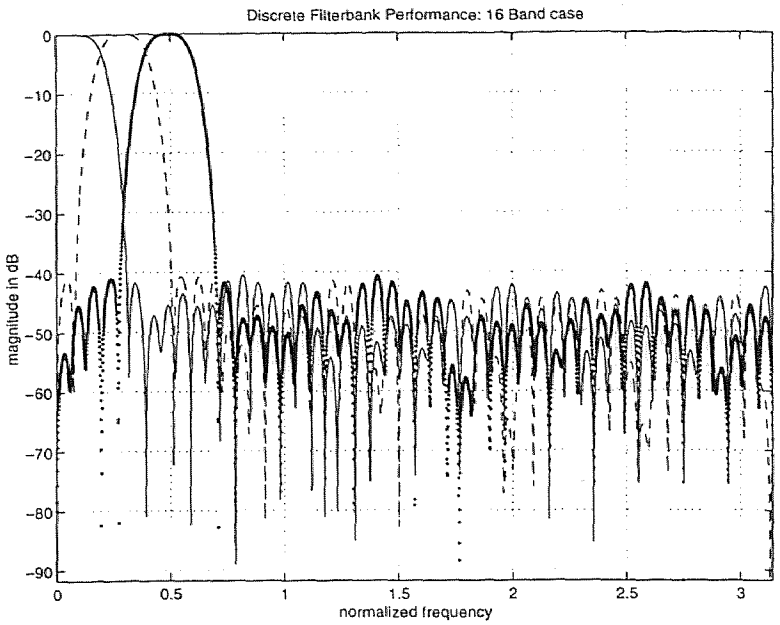

Figure 4.4 Frequency Response of the 16 Band Cosine Modulated Filter Bank with Span g of 8.

increases as frequency increases. There is much less spectral overlap if subcarrier is not adjacent. Each subcarrier occupies $\frac{\pi}{16}$ bandwidth. Figure 4.6 displays the time response of the first 3 subcarriers of this basis. Figure 4.7 shows the time response of the last (No. 16) subcarrier basis function.

When span g is set to be 16, Figure 4.8 shows the spectra of a 16 band cosine modulated filter bank with 256 taps in analysis and synthesis filter banks. It is observed that basis functions with $g = 16$ have much better side lobe attenuation. The first side lobe attenuation for $g = 16$ overlapped filter bank is about -78 dB while $g = 8$ overlapped filter bank is -40 dB.

When the number of subcarriers increases, the length of analysis and synthesis filters increases using the same span g. The computational complexity increases. According to the transmission channel, different number of subchannels are used. If the digital signal processing power is available, higher number of subcarriers may be

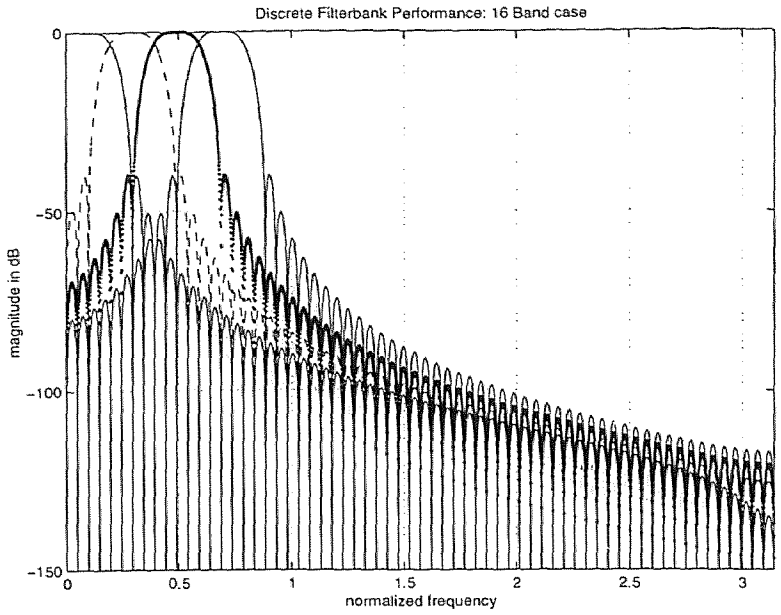

Figure 4.5 Frequency Response of the 16 Band Cosine Modulated Filter Bank with Span g of 8.

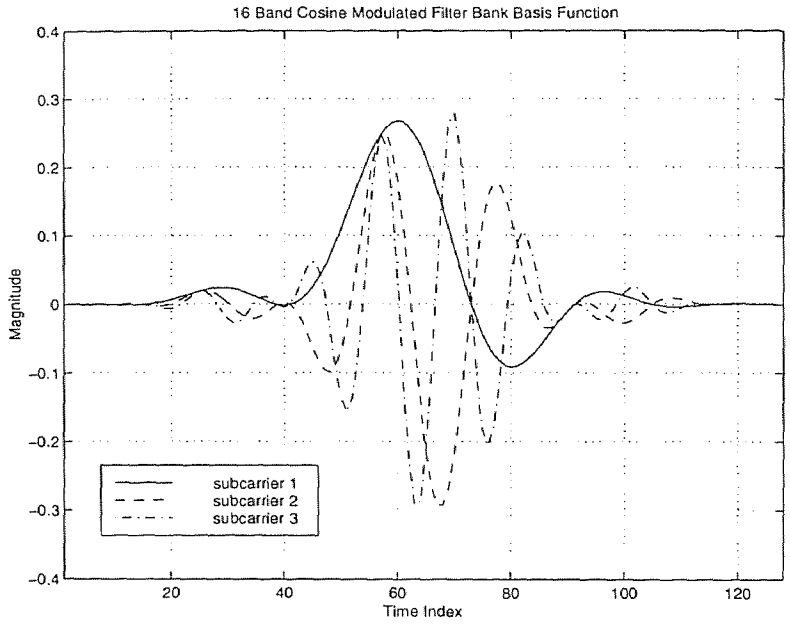

Figure 4.6 Basis Function of the 16 Band Cosine Modulated Filter Bank with Span g of 8.

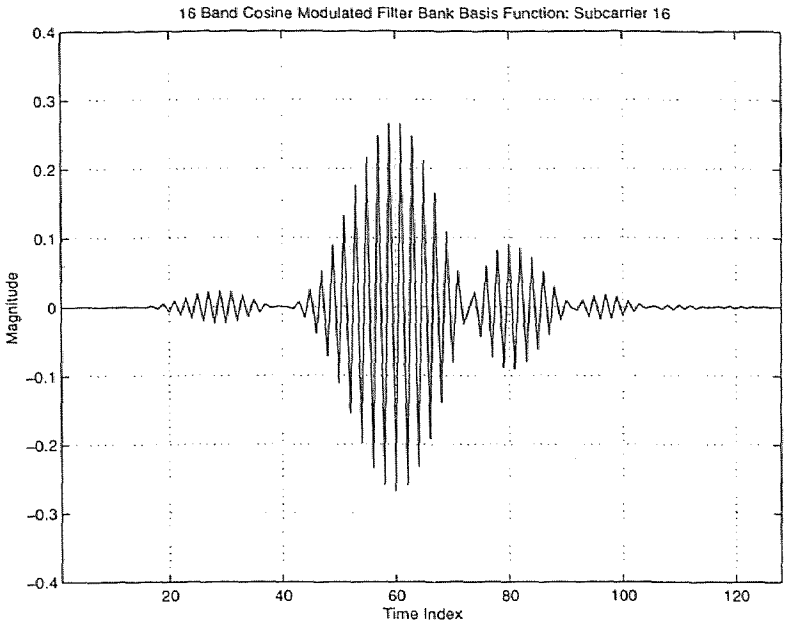

Figure 4.7 Basis Function of the 16 Band Cosine Modulated Filter Bank with Span g of 8.

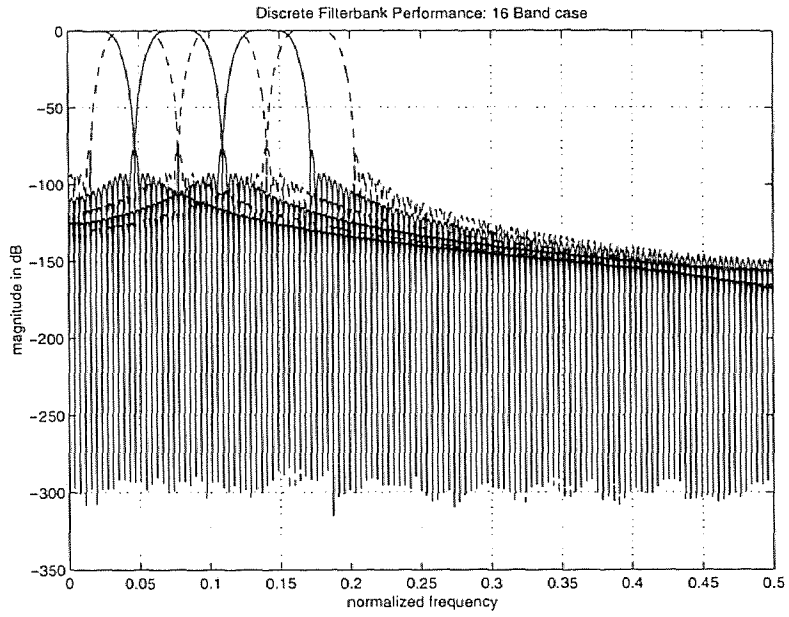

Figure 4.8 Frequency Response of the 16 Band Cosine Modulated Filter Bank with Span g of 16.

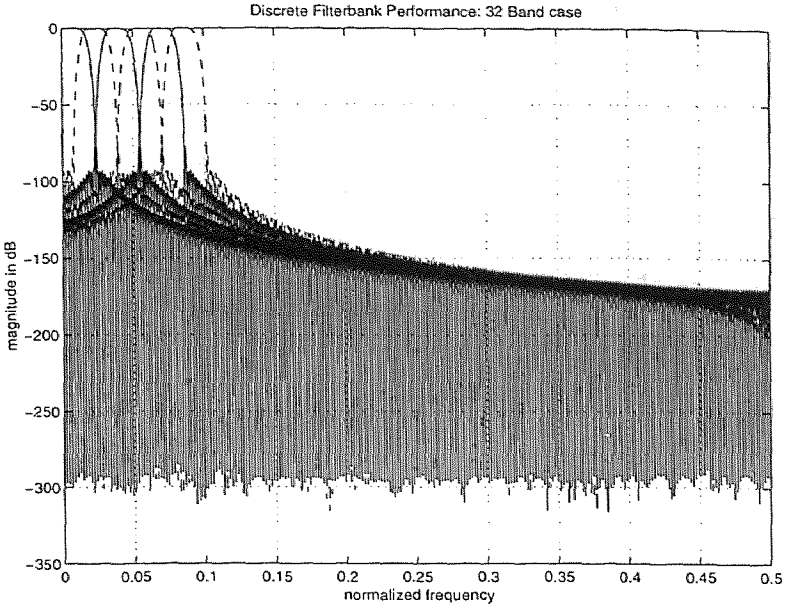

Figure 4.9 Frequency Response of a 32 Band Cosine Modulated Filter Bank with Span g of 16.

implemented. We will see it later that larger number of subcarriers is desirable when there is a narrow band interference in the environment.

$M = 32, 64, 128$ band cosine modulated filter bank design problems have been investigated. As the number of taps increases, it is much more difficult to get good basis functions in general. The optimal design problem has much more computational power involved. Figure 4.9 displays frequency response of a 32 band cosine modulated filter bank with 512 taps in each basis function. In this case, span g is set to be 16. Figure 4.10 shows the spectra of a 64 band cosine modulated filter bank with 1024 taps in analysis and synthesis filters. It is clear that each basis function has $\frac{\pi}{M}$ bandwidth. They have very good side lobe attenuation which is about -75 dB. The spectra are not equally rippled.

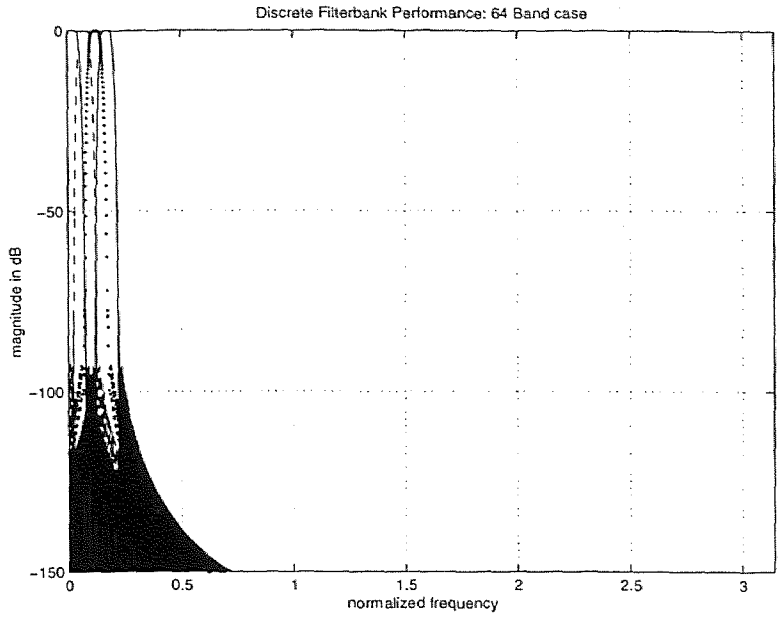

Figure 4.10 Frequency Response of a 64 Band Cosine Modulated Filter Bank with Span g of 16.

4.3 Intersymbol Interference and Interchannel Interference Analysis

Using overlapped discrete synthesis / analysis multirate filter bank transmultiplexer structure, the perfect reconstruction or quasi perfect reconstruction can be achieved if the transmission channel is ideal. In a practical communications scenario, the transmission channel could suffer some dynamic insertion loss. The M band synthesis filterbank modulated signal is transmitted through a practical channel. At the receiver, the received signal is demodulated by an M band analysis filterbank. Due to the imperfectness of channel, overall system will not be PR. There will be intersymbol interference (ISI) as well as interchannel interference (ICI). A theoretical analysis of these ISI and ICI was reported in [35].

An M - band realization of a multicarrier transceiver is basically a transmultiplexer structure with frequency selective orthogonal carrier functions (See Figure 4.1 for detail). Real-world multicarrier transceivers suffer from two types of distortions. The first one is the interchannel (inter-carrier) interference (ICI). It is caused by

non-ideal frequency responses of the finite-length orthogonal carrier filters. In other words, the spectral overlap of orthogonal basis functions introduces ICI directly. Therefore, interchannel interference immunity is not possible in a practical multicarrier transceiver. The second kind of distortion is the intersymbol interference (ISI) caused by the dispersive nature of the channel. Therefore, ISI arises since the channel does not have a brick wall frequency response. We review below a quantitative assessment of the ICI and ISI impairment which are inherent in a real digital communication scenario. For a detailed derivation, check the reference [35].

4.4 ISI and ICI cancellation – Optimal Minimum Mean Square Error Based Linear Combiner Design

In order to recover the transmitted signal, intersymbol interference and interchannel interference must be cancelled. It means that there must be an equalizer at each subchannel output. As we discussed in the previous subsection, ICI comes from other subcarriers. We can not design brickwall like basis functions. There will be some spectral overlap between adjacent subcarriers. The ICI coming from adjacent subchannels might not be negligible. The existing ICI between adjacent subchannels will generate ISI in return. Due to very good side lobe and stop band attenuation performance of an M band synthesis / analysis filter bank, the ISI and ICI cancellation is limited to adjacent subchannels only. It will greatly reduce the complexity of a multicarrier transceiver system.

Let's assume that the transmitted symbols in each subchannel are $\{x_i(n)\}$ where i is the index of subchannel and n is the time index of transmitted symbol. The synthesis filterbank $\{g_i(n)\}$ and analysis filterbank $\{h_i(n)\}$ are designed as in section 4.1. Therefore, the modulated signal can be expressed as

$$y(n) = \sum_{k=-\infty}^{\infty} \sum_{i=1}^{M} x_i(k) g_i(n - kM) \tag{4.6}$$

Let's denote $\tilde{h}_i(n)$ as the convolution of channel $c(n)$ with the i^{th} analysis filter bank basis function as

$$\tilde{h}_i(n) = \sum_{k=-\infty}^{\infty} c(k)h_i(n-k) \tag{4.7}$$

In this case, the output at the i^{th} analysis filter bank, $\hat{x}_i(n)$, at symbol n becomes

$$\hat{x}_i(n) = \sum_{k=-\infty}^{\infty} y(k)\tilde{h}_i(n-kM) + \sum_{k=-\infty}^{\infty} v(k)h(n-kM) \tag{4.8}$$

where $\{v(k)\}$ is the noise and interference sequence in the received signal.

In order to cancel the ISI and ICI, a linear adaptive combiner is proposed to obtain the transmitted signal[14]. Fig. 4.11 displays an adaptive linear combiner block is implemented at the output of analysis filterbank. Figure 4.12 shows the detailed structure of an adaptive linear combiner for subchannel i when $\rho = 1$. Here ρ is the number of subcarriers to be considered to have ICI and ISI.

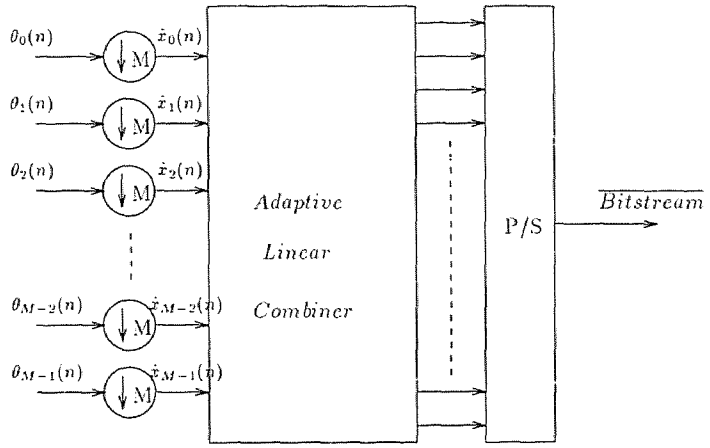

Figure 4.11 Adaptive linear combiner after the analysis filter bank at the receiver of DSBMT.

The outputs from $\pm\rho$ adjacent subchannels are linearly combined with a weight vector W_i. If the intersymbol interference is caused by $\pm\Omega$ symbols, we denote W_i

as the coefficient matrix of $(2\rho + 1) \times \Omega$. The linear combiner will cancel the ISI as well as ICI. The output at the i^{th} combiner becomes

$$\begin{aligned} \tilde{x}_i(n) &= \sum_{j=-\Omega}^{\Omega} \sum_{l=i-\rho}^{i+\rho} w_l(j)\hat{x}_l(n+j) \\ &= a_i(n)x_i(n) + \sum_{i1,n1} a_{i1}(n1)x_{i1}(n1) + noise \end{aligned} \tag{4.9}$$

In Eq. (4.9), the first part is the desired reconstructed symbol. The second part is the contribution from ISI and ICI which comes from different symbol $n1$ and different subchannel $i1$. The third part is the weighted noise component. The optimal weight vector should make $a_i(n)$ to approach 1. In the mean time, it should cancel the second part of Eq. (4.9) and suppress the third part simultaneously. This is the minimum mean square error solution. The equalized signal to noise ratio is defined as

$$SNR_i = \frac{a_i(n)^2}{\sum_{i1,n1}(a_{i1}(n1))^2 + (E_{noise})^2} \tag{4.10}$$

The optimal weight is defined as the one that makes SNR_i maximum. Sandberg, et.al. proposed to use an optimal combiner to cancel the ICI and ISI in an overlapped multicarrier transceiver system. It is claimed that the performance of discrete multirate filterbank based transceiver is much more robust than DMT's.

After some algebraic operations, Eq. (4.10) can be rewritten as

$$SNR_i = \frac{W_i^t A_i^t A_i W_i}{W_i^t B_{ici,isi} W_i + W_i^t C_{noise} W_i} \tag{4.11}$$

where $B_{ici,isi}$ is the covariance matrix of ISI and ICI interference and C_{noise} is the covariance matrix of noise component. The received noise may include AWGN and other coloured noise (interference) in DSL application such as near-end crosstalk, far-end crosstalk and the echo when a multitone transceiver system is full duplex.

The optimal weight vector can be derived as

$$W_i^{opt} = \frac{(B_{ici,isi} + C_{noise})^{-1} A_i}{A_i^t (B_{ici,isi} + C_{noise})^{-1} A_i} \tag{4.12}$$

Using the optimal weight vector in the linear combiner, the ISI and ICI will be cancelled successfully.

4.5 Adaptive RLS Linear Combiner and Optimal Combiner Performance Comparison

In a practical implementation scenario, the exact channel loop coefficients are unknown. The initialization of the start-up process can utilize the known pilot training sequence. In our DSBMT implementation, an adaptive Recursive Least Square algorithm is realized. The RSL adaptive algorithm can converge very fast in the training process. The converged adaptive weight vector matches very well with the theoretical optimal weight vector. Similarly, the RLS adaptive SNR performance matches well with the optimal SNR estimation.

Figure 4.13 shows the theoretical optimal weight and adaptive RLS weight for subchannel 2 of a 64 band multicarrier transceiver system. Figure 4.14 displays the SNR performance for the adaptive RLS combiner and theoretical optimal combiner.

4.6 Simulations and Performance Comparisons

The discrete multicarrier transceiver, more specifically, discrete wavelet multicarrier (DWMT) or discrete subband multicarrier transceiver (DSBMT) has been proposed for digital subscriber line application. In our DSBMT DSL transceiver system, we design a 64 band synthesis / analysis transmultiplexer with spans of 8 and 16. The multicarrier basis function design problem was discussed in section 4.2. These basis function with spans of 16 have about -78 dB first side lobe and the stop band attenuation increases.

The transmission channels used in the simulation are AWG 26, 9 Kft loop plant and AWG 26, 6 Kft loop plants. They are typical CSA loops. The sampling rate is

2.048 MHz. The channel impulse response will be about 200 samples long shown in Figure 3.11 for AWG 26 loop plant of length 9 Kft.

It is necessary to cancel the ISI and ICI from the adjacent subcarriers only. Therefore, ρ is set to be 1. Since our basis function has a span of 16, Ω is also set to be 16.

Using an adaptive linear combiner at the analysis filterbank output, the ISI and ICI are cancelled successfully.

Figure 4.15 displays the signal to noise ratio for each subchannel when there is ISI and ICI and AWGN noise (SNR is 80 dB). The ideal, infinite complexity, multicarrier SNR bound is also plotted in the figure. It is clear that the optimal linear combiner performs well.

It is interesting to see the shape of this SNR curve. Compared to the insertion loss of AWG 26, 9 Kft channel, the shape matches well. Since there is only AWGN noise in the channel, there is no any NEXT and FEXT interference noise except ISI and ICI. SNR in each subchannel has just put the same level of insertion to recover the transmitted signal. No ISI and ICI is left. The theoretical analysis and the simulation results match well.

Figure 4.16 shows the signal to noise ratio performance for each subchannel when the channel is AWG 26 with 6 Kft loop plant. It is clear that shorter the loop length, the smaller the insertion loss. Then, the better the signal to noise ratio in each subchannel which results in higher transmission bit rate and larger the signal to noise ratio margin.

In order to decrease the computational complexity of the transceiver system, we need to decrease the span or the length of modulation basis functions. Using a 64 band cosine modulated filter bank with a span of 8, we performed a simulation on test loop of AWG 26, length 9 Kft. As we know that the first side lobe of these modulation basis function have -45 dB attenuation, one must consider the

interchannel interference from two adjacent subchannels in both direction. In this case, ρ is set to be 2. The Ω is set to be 16 as before.

Figure 4.17 displays the signal to noise ratio performance in each subchannel for the optimal combiner in AWG 26, 9 Kft loop plant. SNR is 80 dB for AWGN noise. The SNR performance of DSBMT and ideal multicarrier match well. Figure 4.18 displays the signal to noise ratio performance in each subchannel for adaptive RLS linear combiner and the optimal combiner in AWG 26, 9 Kft loop plant. SNR is 80 dB. The SNR performance of optimal combiner and adaptive combiner for DSBMT match well.

Comparing with the SNR performance of DSBMT with a span of 8 and a span of 16, it is observed that both of DSBMT implementations have the same performance as the theoretical bound. It means that although the first side lobe of span 8 is -45 dB, we can still achieve the optimal performance bound. The non-equal ripple stop band attenuation of modulation basis function attributes this simulation result.

Figure 4.19 displays the weight vector of the optimal and adaptive combiners for subchannel 3 of 64 Band Cosine Modulated filter bank with a span of 8. We see that these two weights match well. Adaptive linear combiner approaches to the optimal combiner weights.

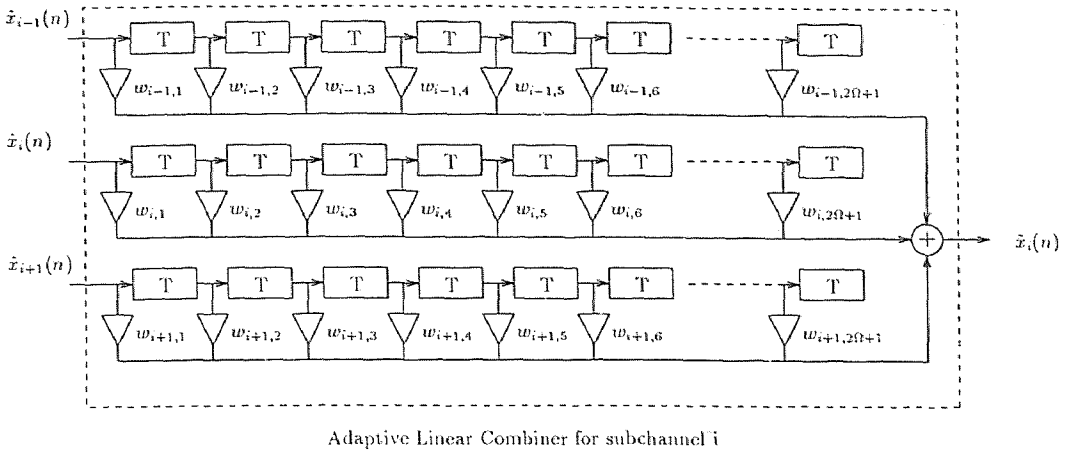

Figure 4.12 Detailed adaptive linear combiner after the analysis filter bank at the receiver of DSBMT for subchannel i when $\rho = 1$.

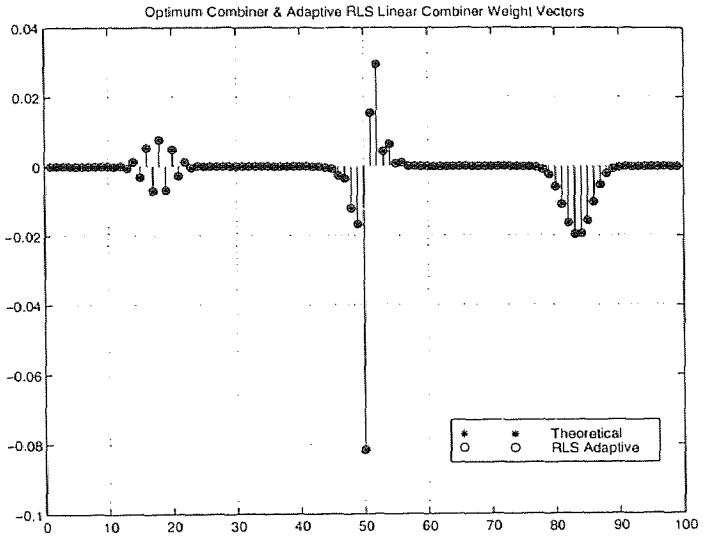

Figure 4.13 Optimal and Adaptive RLS linear combiner weight vector for subchannel 2 of a 64 Band Cosine Modulated Filter Bank with Span g of 16 for AWG 26, 9 Kft loop plant, SNR_{in} is 80 dB.

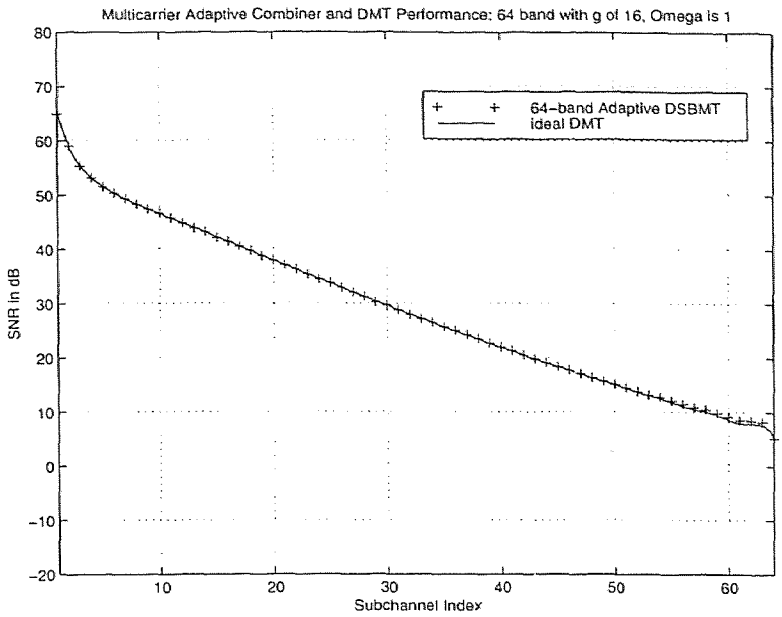

Figure 4.14 Adaptive RLS linear combiner performance of a 64 Band Cosine Modulated Filter Bank with Span g of 16 and Ideal infinite band multicarrier modulation performance for AWG 26, 9 Kft loop plant, SNR_{in} is 80 dB.

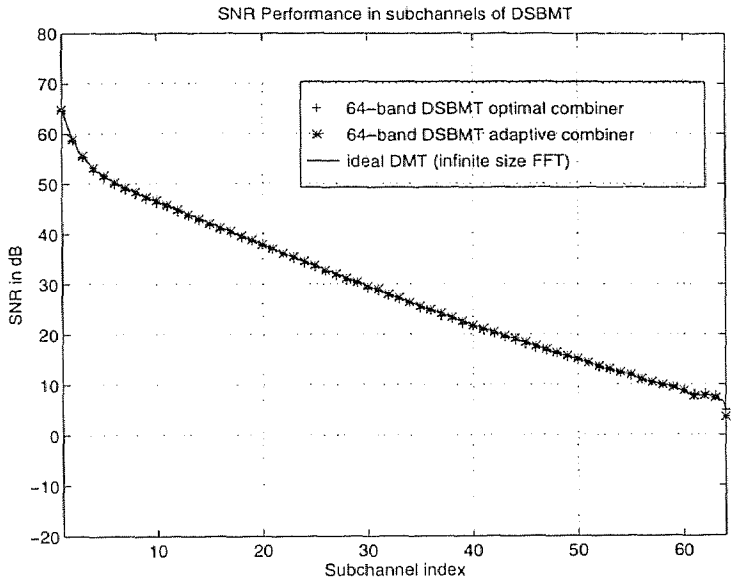

Figure 4.15 Optimal linear combiner performance of a 64 Band Cosine Modulated Filter Bank with Span g of 16 for AWG 26, 9 Kft loop plant, SNR_{in} is 80 dB.

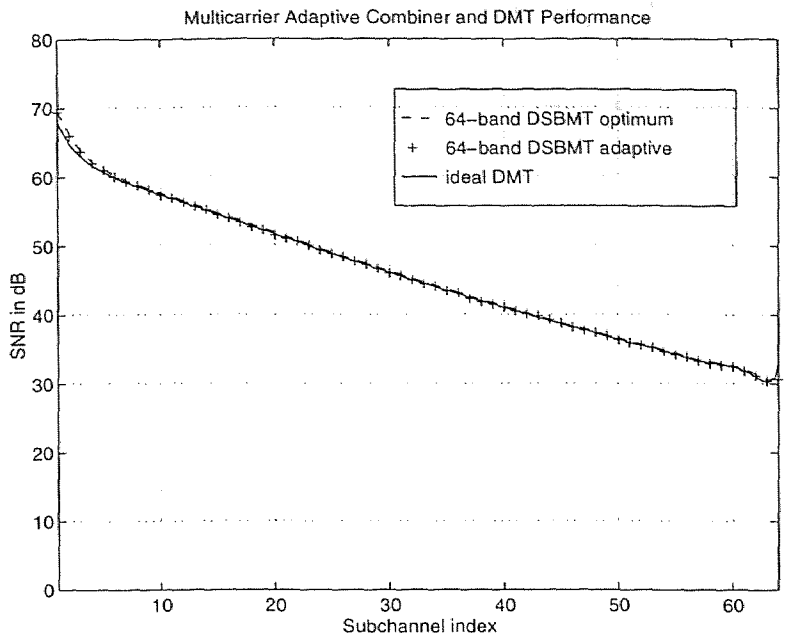

Figure 4.16 Optimal linear combiner performance of a 64 Band Cosine Modulated Filter Bank with Span g of 16 for AWG 26, 6 Kft loop plant, SNR_{in} is 80 dB.

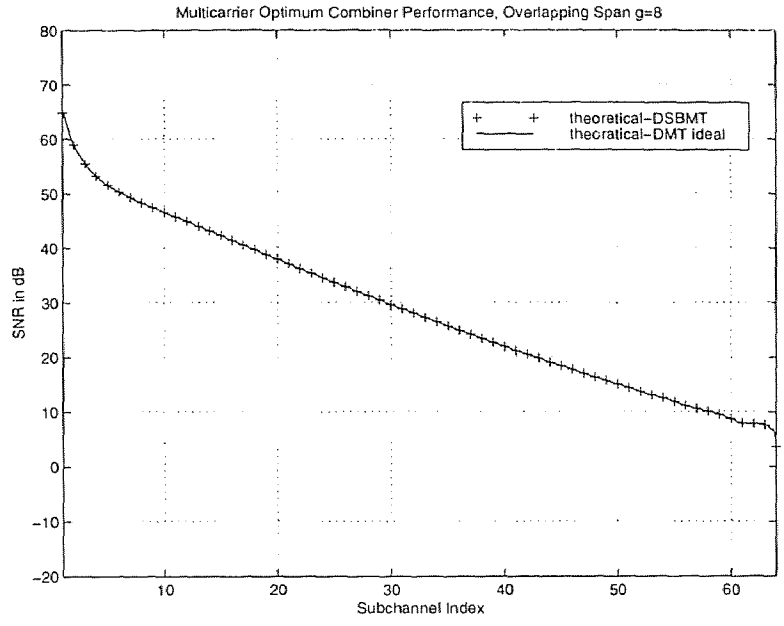

Figure 4.17 Optimal linear combiner performance of a 64 Band Cosine Modulated Filter Bank with Span g of 8 for AWG 26, 9 Kft loop plant, SNR_{in} is 80 dB.

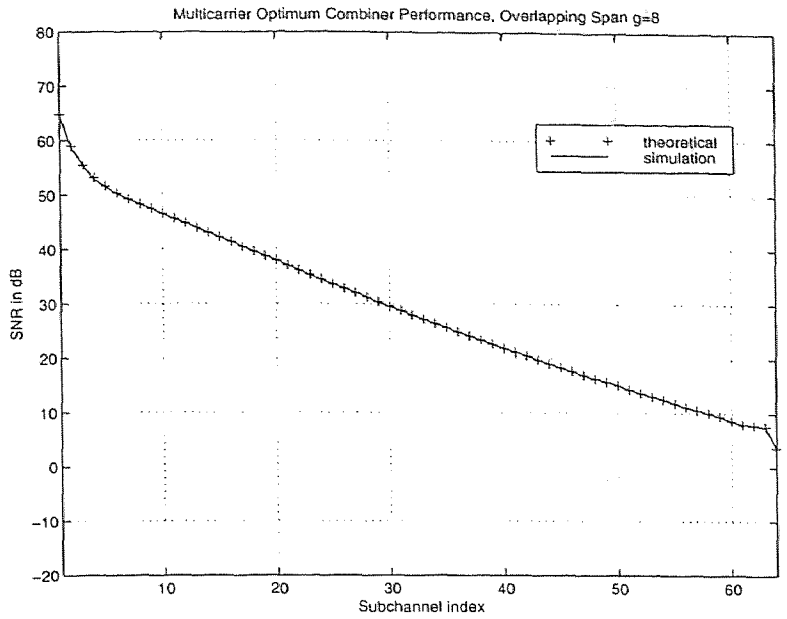

Figure 4.18 Optimal and Adaptive RLS linear combiner performance of a 64 Band Cosine Modulated Filter Bank with a Span g of 8 for AWG 26, 9 Kft loop plant, SNR_{in} is 80 dB.

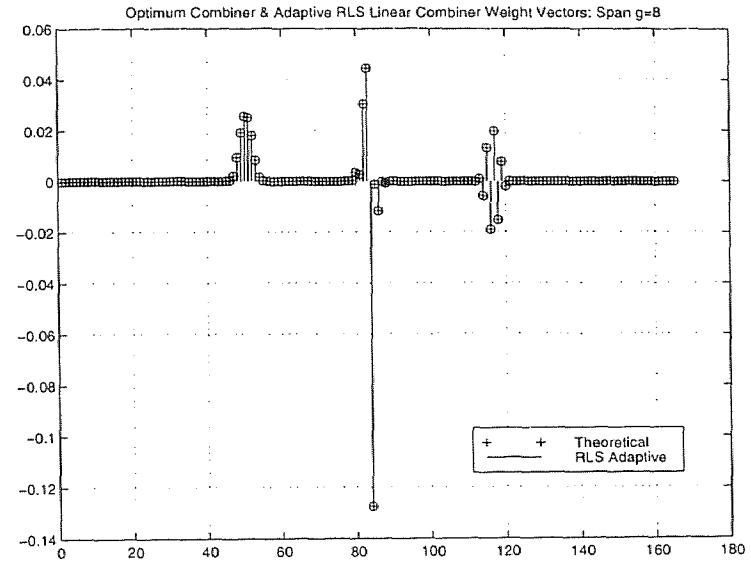

Figure 4.19 Optimal and Adaptive RLS linear combiner weight vectors for subchannel 3 of a 64 Band Cosine Modulated Filter Bank with Span g of 8 for AWG 26, 9 Kft loop plant, SNR_{in} is 80 dB.

CHAPTER 5

A PERFORMANCE ANALYSIS OF SINGLE CARRIER MODULATION AND MULTICARRIER MODULATION TECHNIQUES FOR DIGITAL SUBSCRIBER LINE APPLICATIONS

5.1 Introduction

In the field of ADSL, there are two competing transmission methods under consideration: single carrier systems such as Quadrature Amplitude Modulation (QAM) or its variation Carrierless Amplitude Phase (CAP) modulation and Orthogonal Frequency Division Multiplexing techniques such as Discrete Multi-Tone (DMT). DMT uses Discrete Fourier Transform as its modulation basis. In the industry, DMT has been adopted as ANSI standard for ADSL application while CAP is widely used as a De Facto standard. There has been much interest in performance comparison of single carrier DFE based systems, such as CAP or QAM, with DMT. The performance parameters investigated for the CAP and DMT systems are the achievable transmission capacity and SNR margin. This chapter provides a performance comparison of CAP and DMT transmission methods under numerous DSL scenarios. We evaluate the performance of these technologies on selected CSA loops. We emphasize that the implementation issues of any technique are beyond the focus of this study. Therefore, the results represent ideal cases for both schemes.

From a signal processing point of view, DMT divides the channel into N subchannels while CAP uses only one channel. These two different signaling techniques come up with the same theoretical performance bounds. It will be shown later in this chapter.

5.2 A Theoretical Transmission Capacity Bound for DMT Transceiver

The bandlimited channel has the frequency transfer function $H(f)$. Figure 5.1 displays a typical DSL loop plant: AWG 24 with 12 Kft length frequency response.

DMT technique is an orthogonal frequency division multiplexing scheme. It consists of a large number of independent subcarriers. Suppose that the well known QAM modulation technique is used for each of these subchannels in DMT transceivers. For demonstration purpose, we assume that N independent subchannels are divided from the practical loop plant. If we assume that each subchannel is ideal brick wall like channel, each subchannel use individual QAM modulation, The multicarrier modulation based transceiver system can be modeled as N parallel subchannels transmitting bit stream in these independent subchannels. After transmission, the bit stream can be multiplexed into one high bit rate data stream. The overall achievable bit rate is the summation of bit rate in all the subchannels.

At this moment, It is also assumed that the complexity is not of our concern.

For the i^{th} subchannel, we have the corresponding subchannel magnitude transfer function $|H_i(f)|$. The power spectral density function of additive white Gaussian noise is $\frac{N_0}{2}$. We assume that the probability of symbol error P_e is the same for all subchannels of the DMT transceivers. Assume the transmitted signal power in the i^{th} subchannel is P_i and the bandwidth of the i^{th} subchannel is W_i. Using two-dimensional symbol QAM modulation, the number of bits assigned to the i^{th} subchannel becomes [8]

$$n_i = \log_2 \left[1 + \frac{3P_i}{N_0 W_i \left[Q^{-1} \left(\frac{P_e}{N_e} \right) \right]^2} \right] \tag{5.1}$$

where N_e is the number of adjacent constellation. $N_e = 4\left(1 - \frac{1}{\sqrt{2^{n_i}}}\right) \simeq 4$ for large n_i.

SNR gap is defined as $\Gamma = \frac{\gamma_m}{3\gamma_{code}} \left[Q^{-1} \left(\frac{P_e}{N_e} \right) \right]^2$ where γ_m is the system design target SNR margin and γ_{code} is the coding gain [2][4]. For an un-coded QAM in each subchannel, $\gamma_{code} = 1(0dB)$. We also assume the target SNR margin $\gamma_m = 1(0dB)$ for clear demonstration purpose.

One can rewrite Eq. (5.1) using SNR gap definition as

$$n_i = \log_2\left[1 + \frac{P_i}{N_0 W_i \Gamma}\right] \tag{5.2}$$

If we increase the number of subcarriers N in the modulation, eventually there are N subchannel in this bandlimited loop. Whenever N approaches to infinity, we can model subchannel using index of frequency f. Let's denote $S_{psd}(f)$ as the power spectral density function of transmitted signal in subchannel index of f. The received signal power spectral density at the receiver input is $S_{psd}(f)|H(f)|^2$, then the number of bits assigned for the subchannel at tone f is obtained as

$$n(f) = \log_2\left[1 + \frac{S_{psd}(f)|H(f)|^2}{N_0\Gamma}\right] \tag{5.3}$$

The total achievable bit rate is therefore obtained as [2] [8]

$$R_{DMT} = \int_0^W \log_2\left[1 + \frac{S_{psd}(f)|H(f)|^2}{N_0\Gamma}\right] df \tag{5.4}$$

If there is some crosstalk interference in the bandlimited channel, then the total achievable bit rate is similarly calculated as

$$R_{DMT} = \int_0^W \log_2\left[1 + \frac{S_{psd}(f)|H(f)|^2}{(N_0 + |X(f)|^2 S_{xt}(f))\,\Gamma}\right] df \tag{5.5}$$

where $S_{xt}(f)$ is the crosstalk interference signal power spectrum and $|X(f)|$ is the crosstalk coupling filter.

5.3 Transmission Capacity Bound for DFE-based Single Carrier Based System

The probability of symbol error for single carrier broadband QAM or CAP Minimum Mean Square Error Decision Feedback Equalization (MMSE-DFE) based transceiver system can be found as [5][7]

$$P_e = N_e Q\left(\sqrt{\frac{d_{min}^2}{4\sigma_{DFE}^2}}\right) \tag{5.6}$$

where σ^2_{DFE} is the variance of DFE mean squared error. d_{min} is the minimum distance between any two points in a constellation (See Figure 3.8 and Figure 3.9 for detail). For individual dimension of M-ary QAM modulation technique, we assume that the transmitted signal power is S_x where

$$S_x = \frac{d^2_{min}}{12}(M^2 - 1) = \frac{d^2_{min}}{12}(2^{R_{bitrate}T_{symbol}} - 1). \tag{5.7}$$

where $R_{bitrate}$ is the transmission bit rate and T_{symbol} is the symbol duration. Denote the signal to noise ratio of this MMSE-DFE based transceiver system as $SNR_{DFE} = \frac{S_x}{\sigma^2_{DFE}}$.

There are various types of decision feedback equalization techniques such as Zero-Forcing DFE and Minimum Mean Square Error-DFE [5][7]. MMSE-DFE based transceiver system performance is investigated in the thesis work. Then, the channel maximum achievable rate $R_{MMSE-DFE}$ becomes

$$R_{MMSE-DFE} = \frac{1}{T}\log_2\left(1 + \frac{SNR_{MMSE-DFE}}{\Gamma}\right) \tag{5.8}$$

where

$$SNR_{MMSE-DFE} = \exp\left(\frac{1}{W}\int_0^W \ln\left(1 + \sum \frac{S_{psd}(f)|H(f)|^2}{N_0}\right) df\right) - 1 \tag{5.9}$$

The last term -1 in Eq. (5.9) comes from the unbiased version of MMSE-DFE derived from [7]. This SNR is defined for the additive Gaussian noise environment.

In general, the symbol rate is approximately same as the bandwidth ($\frac{1}{T} \simeq W$) and then the maximum achievable bit rate can be expressed as

$$R_{MMSE-DFE} = W\log_2\left(1 + \frac{SNR_{MMSE-DFE}}{\Gamma}\right) \tag{5.10}$$

If there are some crosstalk such as near-end crosstalk (NEXT) and far-end crosstalk (FEXT) in the bandwidth efficient single carrier broadband transceiver system, the channel capacity bound is calculated as

$$C = \int_0^W \log_2\left[1 + \frac{S_{psd}(f)|H(f)|^2}{(N_0 + |X(f)|^2 S_{psd}(f))\,\Gamma}\right] df \tag{5.11}$$

All of these calculations are based on the well known Shannon capacity theorem. We assume that any real number QAM for each subchannel is realizable and the crosstalk noise is of a Gaussian type. The background AWGN at the receiver input is assumed to have a spectral density N_0 of -140 dBm/Hz. The power spectrum density of transmitted signal is -40 dBm/Hz within transmission band. Square root raised cosine shaping filter can be used. We also assume that the targeted $BER = 10^{-7}$ for the transceiver system.

Using CAP signal power spectral density function $S_{psd}(f)$ (See Figure 3.12 in detail) for Eq. (5.11), we can obtain the channel capacity bound by numerical integration.

5.4 Performance Comparison of Infinite Complexity Multicarrier Modulation based Systems and DFE-based Single Carrier Modulation Based Systems

5.4.1 Maximum Achievable Bit Rate Performance

It can be shown that when the complexity is not of a concern and SNR is high in a Gaussian noise environment, the performance of multicarrier modulation based system and MMSE-DFE based single carrier modulation based system are the same [35]. It is assumed that the roll-off factor of single carrier broadband transmission shaping filter α is zero for a fair comparison. In this case, we use the unfolded spectrum in the derivation. The MMSE-DFE based CAP system has the maximum achievable bit rate as

$$\begin{aligned} R_{DFE-MMSE} &= R_{symbol}\log_2\left(1+\frac{SNR_{DFE-MMSE}}{\Gamma}\right) \\ &= W_{DFE}\log_2\left(1+\frac{\exp\left(\frac{1}{W_{DFE}}\int_0^{W_{DFE}}\ln\left(1+\frac{S(f)|H(f)|^2}{N_0}\right)df\right)-1}{\Gamma}\right) \end{aligned}$$

Whenever $\frac{SNR_{DFE}}{\Gamma} \gg 1$ or $\frac{S(f)|H(f)|^2}{N_0\Gamma} \gg 1$, we can omit 1 and -1 in the equation and rewrite the above formula as

$$\begin{aligned}
R_{DFE} &\simeq W_{DFE}\log_2\left(\frac{\exp\left(\frac{1}{W_{DFE}}\int_0^{W_{DFE}}\ln\left(\frac{S(f)|H(f)|^2}{N_0}\right)df\right)}{\Gamma}\right) \\
&= W_{DFE}\log_2 2^{\log_2\frac{1}{\Gamma N_0}\exp\frac{1}{W_{DFE}}\int_0^{W_{DFE}}\ln S(f)|H(f)|^2 df} \\
&= W_{DFE}\log_2 2^{\log_2\frac{1}{\Gamma N_0}+\log_2\exp\frac{1}{W_{DFE}}\int_0^{W_{DFE}}\ln S(f)|H(f)|^2 df} \\
&= W_{DFE}\log_2 2^{\log_2\frac{1}{N_0\Gamma}+\frac{1}{W_{DFE}}\int_0^{W_{DFE}}\log_2 S(f)|H(f)|^2 df} \\
&= W_{DFE}\log_2 2^{\frac{1}{W_{DFE}}\int_0^{W_{DFE}}\log_2\frac{S(f)|H(f)|^2}{N_0\Gamma}df} \\
&= \int_0^{W_{DFE}}\log_2\frac{S(f)|H(f)|^2}{N_0\Gamma}df
\end{aligned} \tag{5.12}$$

Similar to Eq. (5.12), the achievable bit rate for DMT can be written as [4][5]

$$\begin{aligned}
R_{DMT} &= \int_0^{W_{DMT}}\log_2\left(1+\frac{S(f)|H(f)|^2}{N_0\Gamma}\right)df \\
&\simeq \int_0^{W_{DMT}}\log_2\frac{S(f)|H(f)|^2}{N_0\Gamma}df
\end{aligned} \tag{5.13}$$

Where W_{DFE} and W_{DMT} are bandwidths of the transmitted signals. If we assume that $W_{DFE} = W_{DMT}$, then $R_{DMT} = R_{DFE}$ for high SNR case.

It was reported by Kalet and Zervos that the maximum achievable bit rate is the same in the NEXT environment[5]. Under certain conditions, this claim is correct. In [8], the condition for the equivalence is mentioned as the integrand of Eq. (5.11) is larger than 1. In other words, the number of bits for each subchannel should be larger than one. In a practical implementation, this condition always holds for DMT. It is necessary to note that the frequency bandwidth or operation symbol rate of DFE-based single carrier transceiver system should be chosen properly. If the symbol rate is not properly selected, the achievable bit rate may be lower than DMT's. If the optimum bandwidth is chosen, the achievable bit rate is nearly the same for DMT as MMSE-DFE based QAM or CAP system.

In the self-NEXT only scenario, the DFE based CAP system has the achievable bit rate

$$\begin{aligned} R_{DFE-MMSE} &= R_{symbol}\log_2\left(1+\frac{SNR_{DFE-MMSE}}{\Gamma}\right) \\ &= W_{DFE}\log_2\left(1+\frac{\exp\left(\frac{1}{W_{DFE}}\int_0^{W_{DFE}}\ln\left(1+\frac{|H_c(f)|^2}{|H_x(f)|^2}\right)df\right)-1}{\Gamma}\right) \end{aligned}$$

Whenever $\frac{SNR_{DFE}}{\Gamma} \gg 1$, we can omit 1 and -1 and rewrite the above equation as

$$\begin{aligned} R_{DFE} &\simeq W_{DFE}\log_2\left(\frac{\exp\left(\frac{1}{W_{DFE}}\int_0^{W_{DFE}}\ln\left(1+\frac{|H_c(f)|^2}{|H_x(f)|^2}\right)df\right)}{\Gamma}\right) \\ &= \int_0^{W_{DFE}}\log_2\frac{1+\frac{|H(f)|^2}{|H_x(f)|^2}}{\Gamma}df \\ &\simeq \int_0^{W_{DFE}}\log_2\frac{|H(f)|^2}{|H_x(f)|^2\Gamma}df \end{aligned} \tag{5.14}$$

this approximation holds if $\frac{|H(f)|^2}{|H_x(f)|^2} \gg 1$.

Similar to AWGN only scenario, the R_{DMT} for the self-NEXT case can be written as

$$\begin{aligned} R_{DMT} &= \int_0^{W_{DMT}}\log_2\left(1+\frac{|H_c(f)|^2}{|H_x(f)|^2\Gamma}\right)df \\ &\simeq \int_0^{W_{DMT}}\log_2\frac{|H_c(f)|^2}{|H_x(f)|^2\Gamma}df \end{aligned} \tag{5.15}$$

This approximation also holds if $\frac{|H(f)|^2}{|H_x(f)|^2\Gamma} \gg 1$. We can say that $R_{MMSE-DFE} = R_{DMT}$ under this condition.

This conclusion is valid for any kind of Gaussian noise environment.

5.4.2 SNR Margin Performance

SNR margin is the measure used to evaluate the performance of HDSL and ADSL systems. In ANSI T1E1 technical subcommittee discussions, a variety of SNR margin results were forwarded as contributions. But they have different calculations in many cases.

However, the fair comparison should be performed under the same test conditions.

SNR margin is defined as the difference of achievable SNR with the SNR required for the specified target transmission bit rate and the transmission error rate. In ADSL applications, the transmission error rate is set to be less than 10^{-7}. From system design point of view, one must design the transceiver system SNR as high as possible, approach the theoretical bound. But we should evaluate the attainable SNR to make sure that certain level of SNR margin can be achieved. There is 6 dB SNR margin requirement for ADSL applications.

In single carrier modulation techniques based transceiver system, let's say a CAP based transceiver system is implemented. Assume that Minimum Mean Square Error Decision Feedback Equalization (MMSE-DFE) technique is utilized. The required SNR to achieve the transmission error rate of 10^{-7} using different constellation size modulation are listed in Table 5.1. Considering the coding gain of 4 dB, we need to increase the constellation size by 1 bit. The required SNR are also listed Table 5.1.

Table 5.1 Required Signal to Noise Ratio to achieve 10^{-7} error rate using MMSE-DFE technique for different constellation size in single carrier modulation schemes with and without 4 dB coding gain.

Constellation	4	8	16	32	64	128	256
SNR w/o coding (dB)	14.5	18.0	21.5	24.5	27.7	30.6	33.8
Constellation		8	16	32	64	128	256
SNR w coding (dB)		14.0	17.5	20.5	23.7	26.6	29.8

For the multicarrier modulation based transceiver system such as DMT technique, the theoretical SNR margin is calculated as the difference of achievable average SNR of all subcarrier and the required SNR for target transmission error

rate. It is defined Average SNR as by [2]

$$\begin{aligned}\overline{SNR} &= \Gamma\{[\prod_{i}^{\overline{N}}(1+\frac{SNR_i}{\Gamma_i})]^{\frac{1}{\overline{N}}}-1\} \\ &= \Gamma\{[\prod_{i}^{\overline{N}}(1+\frac{SNR_i}{\Gamma_i})^{\frac{1}{\overline{N}}}]-1\} \end{aligned} \tag{5.16}$$

Where Γ is the overall SNR gap and Γ_i implies the SNR gap of the i^{th} subchannel. It is assumed that $\Gamma = \Gamma_i$. $\overline{N}$ is the total number of subchannels used in a DMT transceiver. The subchannels in which $b_i > 1$ bit are defined as usable subchannels. Denote the total number of bits transmitted per symbol (super-block) b as

$$b = \sum_{i=1}^{\overline{N}} b_i \tag{5.17}$$

In a high SNR environment, we can ignore +1 and -1s. Then,

$$\begin{aligned}\overline{SNR} &= [\prod_{i}^{\overline{N}} SNR_i]^{\frac{1}{\overline{N}}} \\ &= [\prod_{i}^{\overline{N}} SNR(f_i)]^{\frac{1}{\overline{N}}} \end{aligned} \tag{5.18}$$

Now, the SNR margin is defined as [2]

$$\begin{aligned} SNR_{margin} &= 10log_{10}[\frac{\overline{SNR}}{2^{\frac{b}{\overline{N}}}}] + \gamma_{code} - \Gamma_{gap} \\ &= 10log_{10}\overline{SNR} - 10log_{10}2^{\frac{b}{\overline{N}}} + \gamma_{code} - \Gamma_{gap} \\ &= 10\{\sum_{i=1}^{\overline{N}} \frac{1}{\overline{N}} log_{10}SNR(f_i) - \frac{b}{\overline{N}}log_{10}2\} + \gamma_{code} - \Gamma_{gap} \\ &= 10\{\frac{df}{W_{DMT}}\sum_{i=1}^{\overline{N}} log_{10}SNR(f) - \frac{b}{\overline{N}}log_{10}2\} + \gamma_{code} - \Gamma_{gap} \\ &= \frac{10}{W_{DMT}}\int_{f_{start}}^{f_{end}} log_{10}SNR(f)df - \frac{10b}{\overline{N}}log_{10}2 + \gamma_{code} - \Gamma_{gap} \end{aligned} \tag{5.19}$$

Where W_{DMT} is the bandwidth used for DMT system. Assume that b_{DMT} is the transmission bit rate of DMT and T_{symbol} is the duration of DMT supersymbol. Then, b must be equal to $b_{DMT}T_{symbol}$;

$$\frac{b}{\overline{N}} = \frac{b_{DMT}T_{symbol}}{\overline{N}} = \frac{b_{DMT}}{\frac{\overline{N}}{T_{symbol}}} = \frac{b_{DMT}}{W_{DMT}} \tag{5.20}$$

Then, one can rewrite Eq. 5.20 as

$$SNR_{margin}^{DMT} = \frac{10}{W_{DMT}} \int_{f_{start}}^{f_{end}} log_{10} SNR(f) df - 10 \frac{b_{DMT}}{W_{DMT}} log_{10} 2 + \gamma_{code} - \Gamma_{gap} \quad (5.21)$$

In MMSE DFE-based CAP system, we calculate $SNR_{ref-cap}$ for each CAP signaling corresponding to symbol error rate $Pe = 10^{-7}$. Assume b_{CAP} is the transmission bit rate and m is the number of bits per symbol for CAP signaling. For 256 CAP signaling, $SNR_{ref-cap}$ is about 30.8 dB. Then, we can write

$$\begin{aligned} SNR_{ref-cap} &= 10 log_{10} \frac{Q^{-1}(\frac{P_e}{2})}{3} + 10 log_{10}(2^m - 1) \\ &= \Gamma_{gap} + 10 \frac{b_{CAP}}{W_{CAP}} log_{10} 2 \end{aligned} \quad (5.22)$$

$$SNR_{DFE} = 10 log_{10} \{ exp\{ \frac{1}{W_{CAP}} \int_{f_{start}}^{f_{end}} log_e (1 + SNR(f)) df \} - 1 \} \quad (5.23)$$

Therefore,

$$\begin{aligned} SNR_{margin}^{CAP} &= SNR_{DFE} - SNR_{ref-cap} + \gamma_{code} \\ &= \frac{10}{W_{CAP}} \int_{f_{start}}^{f_{end}} log_{10}(1 + SNR(f)) df - SNR_{ref-cap} + \gamma_{code} \\ &= \frac{10}{W_{CAP}} \int_{f_{start}}^{f_{end}} log_{10}(1 + SNR(f)) df - 10 \frac{b_{CAP}}{W_{CAP}} log_{10} 2 - \Gamma_{gap} + \gamma_{code} \end{aligned} \quad (5.24)$$

From Eq. (5.22) and Eq. (5.24), we see that if both CAP and DMT systems transmit the same digital bit rate, and use the same transmitted signal power spectral density and the same frequency range with the same noise condition, SNR_{margin} performance bounds of both techniques are the same. In the derivation, +1 and -1s are ignored. It means that high SNR case is assumed. In ADSL and HDSL practical application scenarios, $SNR(f)$ is much larger than 1.

5.5 Performance Simulation Results and Discussions

We evaluated the theoretical bounds for the achievable bit rate as well as the SNR margin for HDSL and ADSL applications. It is shown that these performance bounds

are the same for both DMT and CAP modulation line codes under the same test conditions. Numerical performance results are in accord with the theoretical analysis.

In the simulation, ADSL Category I Test Platform is used according to ADSL standard [9]. The FDM types of downstream and upstream signaling are implemented. The starting point of upstream signal is 20 KHz such that the POTS is available in the low 4 KHz band. The downstream signal power spectrum starts at 165 KHz. There is some separate gap between upstream and downstream signal (See Figure 3.12 for detail).

In maximum achievable bitrate calculation, the SNR margin and coding gain are assumed to be 0 dB. In SNR margin calculation for both DMT and CAP-DFE scenario, 5 dB coding gain is assumed.

Figure 5.2 and Figure 5.3 display the maximum achievable bitrate for DMT and CAP on CSA 6 and CSA 7 under ADSL Category I noise scenario, respectively.

SNR margins are listed in Table 5.2.

Table 5.2 ADSL standard, Category I, SNR margin in dB for DMT and CAP DFE: 256 coded CAP 6.72 Mbps downstream, 64 coded CAP 250 Kbps upstream.

Loop Number	SNR_{margin} down, DMT	SNR_{margin} down, CAP	SNR_{margin} up, DMT	SNR_{margin} up, CAP
T1.601(7)	8.8	8.9	8.7	8.7
T1.601(13)	12.1	12.1	9.3	9.4
CSA (4)	10.7	10.7	22.6	22.7
CSA (6)	10.6	10.6	13.1	13.1
CSA (7)	10.8	10.8	25.8	25.7
mid-CSA	7.6	7.5	59.8	59.9

It is found from these results that the single carrier and multicarrier modulation schemes provide the same performance upper bounds for the communication channels considered.

5.6 Conclusions

A comparative performance study of DMT and CAP based systems for DSL communication applications in presented in this Chapter. It is shown that they have the same performance for the communications scenarios considered. This performance bound equivalence pave the solid ground for the implementation of multicarrier modulation. One can use different modulation scheme, the ultimate achievable bounds are the same under the same operational conditions.

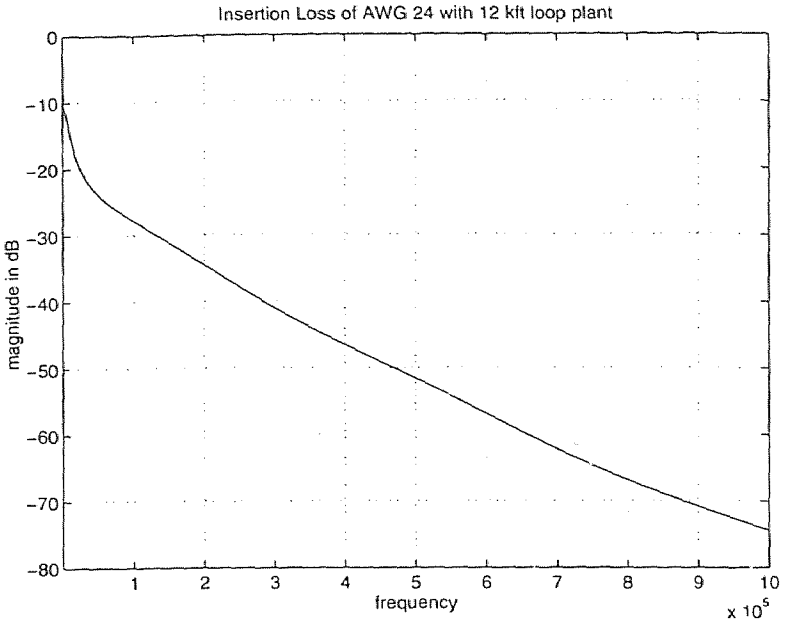

Figure 5.1 Frequency transfer function of a typical DSL loop: AWG 24 loop plant with 12 Kft length.

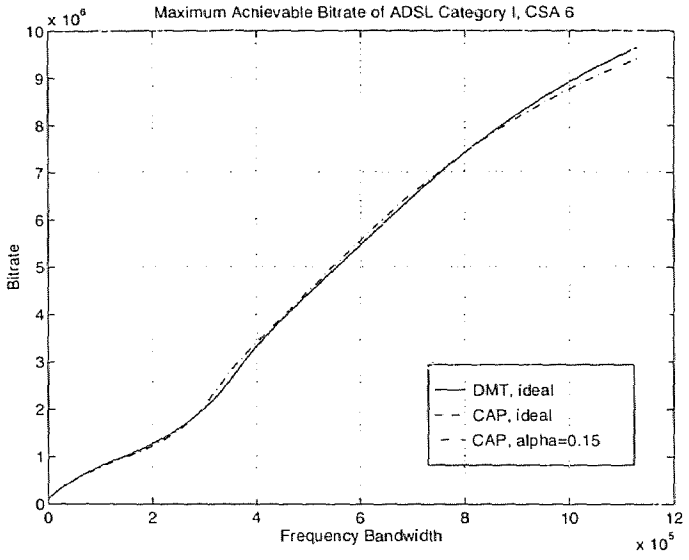

Figure 5.2 Maximum Achievable Bitrate in ADSL, Category I, CSA 6.

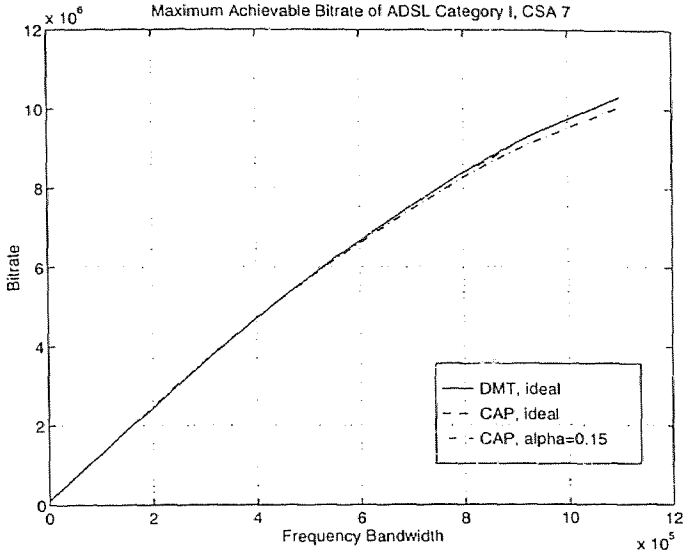

Figure 5.3 Maximum Achievable Bitrate in ADSL, Category I, CSA 7.

CHAPTER 6

PERFORMANCE EVALUATION OF DMT TRANSCEIVER FOR NARROW BAND INTERFERENCE ENVIRONMENTS

6.1 Problem Formation

As we discussed in Chapter 5, Orthogonal Frequency Division Multiplexing (OFDM) or Discrete Multitone Transceiver (DMT) is widely used in digital subscriber line applications. DMT has been adopted as ANSI standard for ADSL technique. DMT uses Discrete Fourier Transform as its orthogonal subcarrier basis. Due to its efficient implementation, DMT is also proposed for VDSL applications.

In ADSL application scenarios, the transmitted signal frequency range may be up to 1 or 2 MHz. There will be some narrow band interference such as AM radio stations and other narrow band interference sources. It is necessary to evaluate the performance of OFDM (DMT) technique in the narrow band interference environments.

The performance robustness of DMT modulation scheme for the cases of single and multitone interference types are studied in this chapter. The theoretical performance analysis presented are supported by computer simulations. It is shown that the spectral overlap of subcarriers is the critical feature for the robustness of a multicarrier modulation technique.

6.2 Performance of DMT Transceiver for Single Tone Interference

It is naturally assumed that a DMT based system can shut down one subchannel corresponding to that narrow band or single tone interference. How much would this technique be effective? This problem is carefully examined in this section.

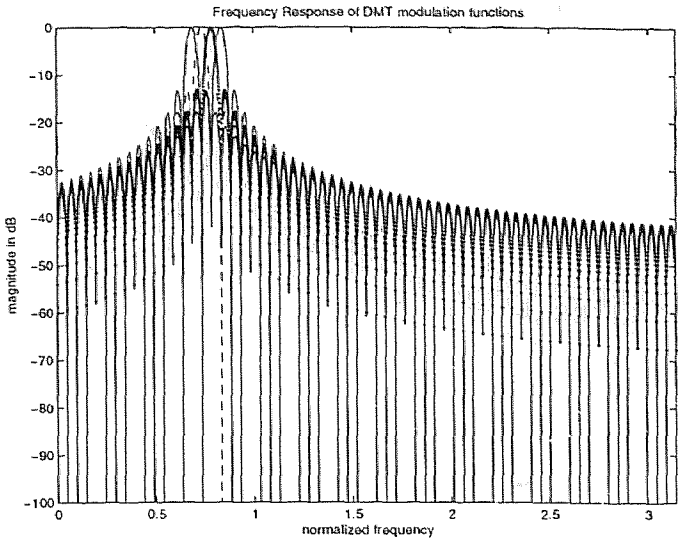

Figure 6.1 Frequency responses of subcarriers 15, 16, 17 and 18 of 128-point DFT basis.

6.2.1 Spectral Overlapping of DMT Subcarriers

Figure 6.1 displays the frequency responses of DFT basis functions $\{g_{15}(n), g_{16}(n), g_{17}(n), g_{18}(n)\}$ which correspond to the frequency range around $\frac{\pi}{4}$ for a 128-point DFT.

If the single-tone interference is perfectly located at one of these N frequency points on the unit circle, then a size N IDFT/FFT would decompose the single tone interference into only one subchannel or DFT bin. That is what one usually assumes. Theoretically speaking, the size of IDFT/DFT can be very large. A typical implementation limits the size of DFT to 512. Whenever the narrow band or single tone interference is not perfectly located at one of these N equal distant frequency points, say a little bit away from a DFT bin, or the sampling frequency is drafting a little bit, then the single tone interference energy spreads into many subchannels. The amount of interference leakage depends on the location and the strength of the single tone and narrow band signals. It is shown that this type of interference will significantly degrade the DMT performance.

6.2.2 Theoretical Evaluation of Single Tone Interference Leakage in DMT

In Figure 3.15, the received signal is a combination of desired signal, additive white Gaussian channel noise and a single or multitone interference. Assume that an N_f+1 tap TEQ preequalizer is used to reduce the duration of channel impulse response. The coefficients of the preequalizer is $W^{TEQ} = [w_0, w_1, ..., w_{N_f}]^t$. Here t denotes the vector transpose operation. Also, we assume that a single-tone interference is located at the frequency ω_{st} with a random phase ϕ_{st} which is uniformly distributed from 0 to 2π. The Signal to Interference Ratio (SIR) is defined as the ratio of transmitted signal energy over a single-tone interference energy, $SIR = \frac{E_{signal}}{E_{st}}$. Let's assume that the magnitude of a single-tone interference is A_{st}, and the transmitted signal energy is normalized to 1. The sampled single-tone interference signal is represented as $A_{st}cos(\omega_{st}i + \phi_{st})$. The sampled AWGN is assumed to have a variance of σ_n^2. Let's denote $\mathbf{v_k} = [v_0, v_1, ..., v_{N-1}]^t$ as the noise sequence. It is independent of interference component. Then, the interference at the output of the preequalizer is expressed as

$$u_k = \sum_i A_{st}cos(\omega_{st}i + \phi_{st})w_{k-i} \tag{6.1}$$

The correlation between the samples u_k and u_{k-l} can be derived as

$$\begin{aligned} \mathbf{E}[u_k u_{k-l}] &= \mathbf{E}[(\sum_i A_{st}cos(\omega_{st}i + \phi_{st})w_{k-i})(\sum_n A_{st}cos(\omega_{st}n + \phi_{st})w_{k-l-n})] \\ &= \frac{A_{st}^2}{2}\sum_m cos(\omega_{st}m)\sum_{\hat{k}} w_{\hat{k}}w_{\hat{k}-(l-m)} \end{aligned} \tag{6.2}$$

where $\mathbf{E}$ stands for the expected value, m and $\hat{k}$ are any integer.

The noise component at the output of the preequalizer is written as

$$\hat{v}_k = \sum_i v_i w_{k-i} \tag{6.3}$$

Then the correlation between $\hat{v}_k$ and $\hat{v}_{k-l}$ is

$$\mathbf{E}[\hat{v}_k\hat{v}_{k-l}] = \sigma_n^2(\sum_i w_i w_{i+l}) \tag{6.4}$$

Let's form a single-tone interference vector $\mathbf{u_{st}}$ as $[u_0, u_1, ..., u_{N-1}]^t$ and a noise component vector $\hat{\mathbf{v}}$ as $[\hat{v}_0, \hat{v}_1, ..., \hat{v}_{N-1}]^t$. Here N is the size of DFT. The interference component after DFT is denoted as

$$[U_0, U_1, ..., U_{N-1}] = DFT(\mathbf{u_{st}}) \tag{6.5}$$

where each component U_m is calculated as

$$U_m = \frac{1}{\sqrt{N}} \sum_{k=0}^{N-1} u_k cos(\frac{2\pi km}{N}) - j \sum_{k=0}^{N-1} u_k sin(\frac{2\pi km}{N}), \qquad 1 \leq m \leq \frac{N}{2} \tag{6.6}$$

The real and imaginary parts of U_m are denoted as U_m^{Re} and U_m^{Im}, respectively. It is easy to see that $\mathbf{E}[U_m^{Re}] = 0$ and $\mathbf{E}[U_m^{Im}] = 0$. Then, the interference energy at subchannel m can be calculated as

$$\begin{aligned} \mathbf{E}[(U_m^{Re})^2] &= \frac{1}{\sqrt{N}} \sum_{i=0}^{N-1} \sum_{k=0}^{N-1} \mathbf{E}[u_k u_{k-i}] cos(\frac{2\pi km}{N}) cos(\frac{2\pi(k-i)m}{N}) \\ \mathbf{E}[(U_m^{Im})^2] &= \frac{1}{\sqrt{N}} \sum_{i=0}^{N-1} \sum_{k=0}^{N-1} \mathbf{E}[u_k u_{k-i}] sin(\frac{2\pi km}{N}) sin(\frac{2\pi(k-i)m}{N}) \end{aligned} \tag{6.7}$$

Using the result of Eq.(6.2), $\mathbf{E}[(U_m^{Re})^2]$ and $\mathbf{E}[(U_m^{Im})^2]$ can be calculated directly.

The noise component at the output of DFT is denoted as

$$[V_0, V_1, ..., V_{N-1}] = FFT(\hat{\mathbf{v}}) \tag{6.8}$$

The real and imaginary parts of V_m are denoted as V_m^{Re} and V_m^{Im}, respectively. It is also clear that $\mathbf{E}[V_m^{Re}] = 0$ and $\mathbf{E}[V_m^{Im}] = 0$. Then the noise energy $\mathbf{E}[(V_m^{Re})^2]$ and $\mathbf{E}[(V_m^{Im})^2]$ at subchannel m can be calculated as

$$\begin{aligned} \mathbf{E}[(V_m^{Re})^2] &= \frac{1}{\sqrt{N}} \sum_{i=0}^{N-1} \sum_{k=0}^{N-1} \mathbf{E}[\hat{v}_k \hat{v}_{k-i}] cos(\frac{2\pi km}{N}) cos(\frac{2\pi(k-i)m}{N}) \\ \mathbf{E}[(V_m^{Im})^2] &= \frac{1}{\sqrt{N}} \sum_{i=0}^{N-1} \sum_{k=0}^{N-1} \mathbf{E}[\hat{v}_k \hat{v}_{k-i}] sin(\frac{2\pi km}{N}) sin(\frac{2\pi(k-i)m}{N}) \end{aligned} \tag{6.9}$$

Note that the noise components in real and imaginary subchannels of a DMT based system are not the same.

Assume that the complex one-tap post-equalizer at subchannel m is in the form of $W_m^{one-tap} = W_m^{Re} + jW_m^{Im}$. Then, interference plus noise components at the output of complex one-tap equalizer can be expressed as $R_m + jI_m$, where R_m is real part and I_m is imaginary part. They can be derived as

$$\begin{aligned} R_m &= [V_m^{Re} + U_m^{Re}]W_m^{Re} - [V_m^{Im} + U_m^{Im}]W_m^{Im} \\ I_m &= [V_m^{Re} + U_m^{Re}]W_m^{Im} + [V_m^{Im} + U_m^{Im}]W_m^{Re} \end{aligned} \tag{6.10}$$

Therefore, the variance of the output single tone interference plus noise can be derived as

$$\begin{aligned} \mathbf{E}[R_m^2] &= \mathbf{E}[R_m^2]_{st} + \mathbf{E}[R_m^2]_{noise} \\ \mathbf{E}[I_m^2] &= \mathbf{E}[I_m^2]_{st} + \mathbf{E}[I_m^2]_{noise} \end{aligned} \tag{6.11}$$

where single tone part is expressed as

$$\begin{aligned} \mathbf{E}[R_m^2]_{st} &= \mathbf{E}[(U_m^{Re})^2](W^{Re})^2 - \mathbf{E}[2U_m^{Re}U_m^{Im}]W_m^{Re}W_m^{Im} + \mathbf{E}[(U_m^{Im})^2](W^{Im})^2 \\ \mathbf{E}[I_m^2]_{st} &= \mathbf{E}[(U_m^{Re})^2](W^{Re})^2 + \mathbf{E}[2U_m^{Re}U_m^{Im}]W_m^{Re}W_m^{Im} + \mathbf{E}[(U_m^{Im})^2](W^{Im})^2 \end{aligned} \tag{6.12}$$

and noise part is expressed as

$$\begin{aligned} \mathbf{E}[R_m^2]_{noise} &= \mathbf{E}[(V_m^{Re})^2](W_m^{Re})^2 - \mathbf{E}[2V_m^{Re}V_m^{Im}]W_m^{Re}W_m^{Im} + \mathbf{E}[(V_m^{Im})^2](W_m^{Im})^2 \\ \mathbf{E}[I_m^2]_{noise} &= \mathbf{E}[(V_m^{Re})^2](W_m^{Re})^2 + \mathbf{E}[2V_m^{Re}V_m^{Im}]W_m^{Re}W_m^{Im} + \mathbf{E}[(V_m^{Im})^2](W_m^{Im})^2 \end{aligned} \tag{6.13}$$

where $\mathbf{E}[V_m^{Re}V_m^{Im}]$ and $\mathbf{E}[U_m^{Re}U_m^{Im}]$ can be calculated as

$$\begin{aligned} \mathbf{E}[V_m^{Re}V_m^{Im}] &= \frac{1}{N}\sum_{i=1}^{N-1}\mathbf{E}[\hat{v}_k\hat{v}_{k-i})]\sum_{n=0}^{N-1-i}cos(\frac{2\pi nm}{N})sin(\frac{2\pi(n+i)m}{N}) \\ \mathbf{E}[U_m^{Re}U_m^{Im}] &= \frac{1}{N}\sum_{i=1}^{N-1}\mathbf{E}[u_ku_{k-i})]\sum_{n=0}^{N-1-i}cos(\frac{2\pi nm}{N})sin(\frac{2\pi(n+i)m}{N}). \end{aligned} \tag{6.14}$$

The signal to noise and interference ratio in each of real and imaginary subchannels can be calculated as $SNIR_m^R = \frac{1}{\mathbf{E}[R_m^2]}$ and $SNIR_m^I = \frac{1}{\mathbf{E}[I_m^2]}$. Let's define $SNIR$ as $[SNIR^R, SNIR^I]$. The theoretical $SNIR$ in a DMT based system for AWG 26 loop

plant with a length of 9 Kft for a signal tone interference and AWGN environment is displayed in Figure 6.2. The simulation result of $SNIR$ is also plotted in the figure. The analysis and simulation results match well. The single tone interference frequency ω_{st} is of $\frac{\pi}{4}$ (the single-tone located exactly at bin 65 of 512 DFT). There is no interference leakage into the adjacent subchannels.

If the single tone interference frequency ω_{st} is shifted around $\frac{\pi}{4}$ even by a small amount as $\mp 10^{-4}$, The interference energy is distributed in many subchannels as seen in Figure 6.2. Hence, it is not sufficient to null subchannel 65 only. The DMT system performance degrades severely. The sensitivity of $SNIR$ for each subchannel of DMT Transceiver is displayed in Figure 6.2.

Similarly, another single tone interference case evaluation for the theoretical $SNIR$ in a DMT based system for AWG 26 loop plant with a length of 9 Kft is displayed in Figure 6.3. The simulation result of $SNIR$ is also plotted in the figure. The analysis and simulation results match well. The single tone interference frequency ω_{st} is of $\frac{\pi}{8}$ (the single-tone located exactly at bin 33 of 512 DFT). There is no interference leakage into the adjacent subchannels.

If the single tone interference frequency ω_{st} is shifted around $\frac{\pi}{8}$ by a small amount as $\mp 10^{-4}$, the interference energy is distributed in many subchannels as seen in Figure 6.3. Hence, it is not sufficient to null subchannel 33 only. The DMT system performance degrades severely. The sensitivity of $SNIR$ for each subchannel of DMT Transceiver is displayed in Figure 6.3.

6.2.3 Performance of DMT in a Narrow Band Interference

Since a narrow band interference is not an ideal single tone in a practical scenario, it is better to consider the received interference with some bandwidth. Let's assume the power spectrum of a narrow band interference is flat with a center frequency ω_{sto} and bandwidth NB_w. In other words, the narrow band interference components

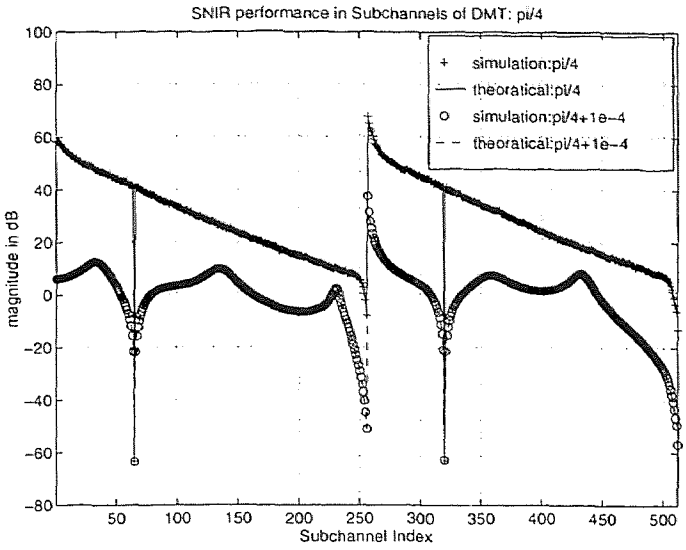

Figure 6.2 The sensitivity of SNIR for each subchannel of DMT based system for a single-tone interference and AWGN scenario with $\omega_{st} = \frac{\pi}{4}$ and $\omega_{st} = \frac{\pi}{4} + 10^{-4}$ on AWG 26, 9 Kft loop plant, $SNIR = 0dB$.

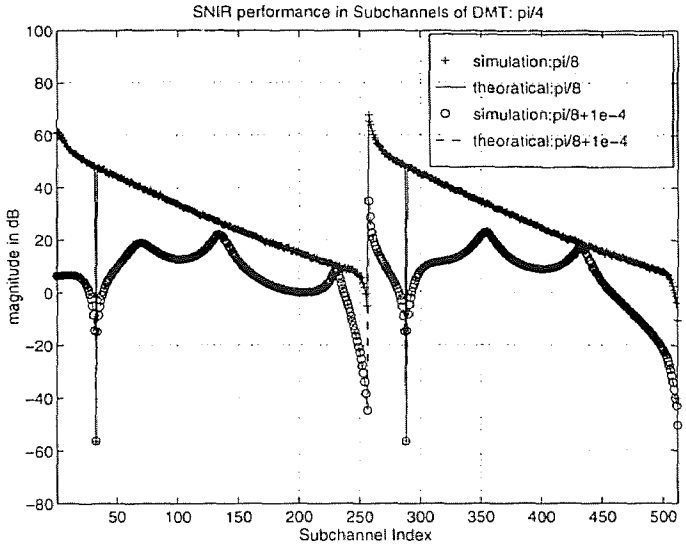

Figure 6.3 The sensitivity of SNIR for each subchannel of DMT based system for a single-tone interference and AWGN scenario with $\omega_{st} = \frac{\pi}{8}$ and $\omega_{st} = \frac{\pi}{8} + 10^{-4}$ on AWG 26, 9 Kft loop plant, $SNIR = 0dB$.

are uniformly distributed in the bandwidth range with the same strength. These interference components at different frequencies are assumed to be independent. The overall interference energy is fixed. In this case, the interference leakage component can be derived as the contribution from all these independent single tone interference with different frequencies. It is not difficult to get the theoretical $SNIR$ performance by using the relationship

$$\begin{aligned} \mathbf{E}[u_k u_{k-l}] &= \mathbf{E}[(\sum_{st}\sum_{i} \hat{A}_{st} cos(\omega_{st} i + \phi_{st}) w_{k-i})(\sum_{st}\sum_{n} \hat{A}_{st} cos(\omega_{st} n + \phi_{st}) w_{k-l-n})] \\ &= \frac{\hat{A}_{st}^2}{2} \sum_{m} cos(\omega_{sto} m) \frac{sin(\frac{NB_w m}{2})}{\frac{NB_w m}{2}} \sum_{k} w_k w_{k-(l-m)} \end{aligned} \tag{6.15}$$

where $\hat{A}_{st}$ is the magnitude of a single tone component, while ω_{sto} is the center frequency of the narrow band interference.

Using Eq.(6.15), we can obtain all the interference components using the same derivation as in a single tone interference case given earlier.

We evaluate the $SNIR$ performance of a DMT based system for the environment of a narrow band interference on an AWG 26 9Kft loop plant. The assumed SIR values are of 40 dB, 60 dB and 80 dB with a center frequency of $\omega_{sto} = \pi/4$ and the bandwidth $NB_w = 0.01\pi$. Figure 6.4 displays the theoretical and simulation results. The simulation results match well with the theoretical ones.

Several different narrow band interference scenarios are evaluated theoretically as well as via simulations. Figure 6.5 displays the sensitivity of performance as a function of interference bandwidth. It is observed that whenever the bandwidth is decreased, the $SNIR$ performance approaches to the ideal single tone case. We observe that although the interference center frequency is at one of DFT bins, a non-ideal single tone will severely degrade the system performance. Figure 6.6 displays the performance of a DMT based system for different SIR environments. Figure 6.7 displays the performance sensitivity for the frequency location of narrow band interference in a DMT based system.

The maximum achievable bit rate for a DMT based system for different center frequency narrow band interference environments are displayed in Figure 6.8.

6.3 Narrow Band Interference Excision in a DMT Based System

We have shown that the performance of a DMT transceiver is very sensitive to the location of interference. The overall system performance will degrade significantly if no special interference cancellation is included. In order to alleviate the sensitivity of $SNIR$ performance to the location of the single-tone interference, a single-tone canceller must be implemented at the receiver side. This is not a very difficult problem. Let's insert a 3-tap adaptive interference exciser which has two zeros at the specific frequency of the interference. The zeros at that frequency put a null in the spectrum. It will effectively cancel most of interference. The most important effect of this 3-tap interference canceller is that it will eventually eliminate the interference leakage which could severely degrade the overall DMT performance. Figure 6.9 displays the signal to noise and interference ratio for the subchannels of DMT when a 3-tap interference canceller is implemented. We observe that a little deviation of single-tone interference location will not cause significant leakage to the others. There will be some $SNIR$ loss around $\omega = \frac{\pi}{4}$ due to the insertion of an extra 3-tap interference canceller. The average $SNIR$ loss is limited to 1 dB in this case.

Of course, the insertion of the 3 - tap adaptive interference exciser will increase the order of composite channel impulse response. It will reduce the overall throughput of DMT based system. It is the penalty coming from the insertion of adaptive interference exciser.

6.4 Remarks

We highlight the performance sensitivity of a DMT transceiver in a single tone and narrow band interference scenarios in this chapter. It is shown that a DMT system

is very sensitive to the location and bandwidth of a narrow band interference. The performance sensitivity of DMT also depends on the strength of a single tone or narrow band interference. If the strength of the interference is not so strong, the interference leakage induced from the spectral overlap will not be severe. In order to eliminate the strong single and multitone interference, a DMT based system needs an interference canceller at the receiver.

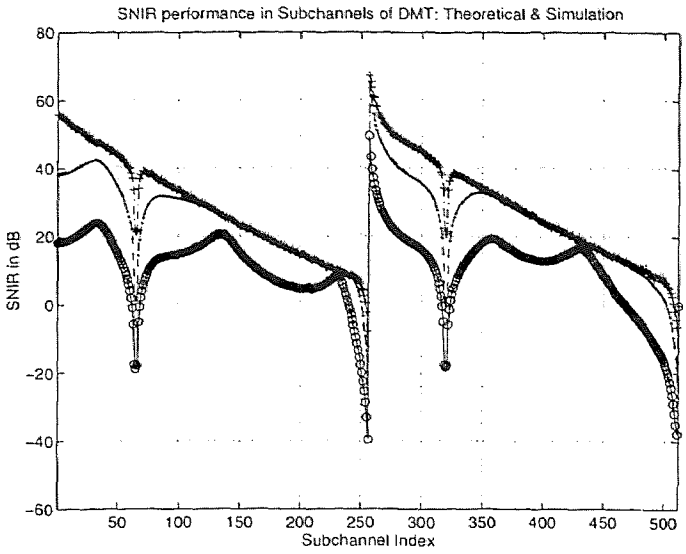

Figure 6.4 The theoretical and simulation SNIR performance of each subchannels of DMT based system in a narrow band interference and AWGN environment for AWG 26, 9 Kft loop plant with a fixed center frequency of $\omega_{sto} = \frac{\pi}{4}$, NB bandwidth is 0.01π,$SIR = 40dB$, $SIR = 60dB$, and $SIR = 80dB$, respectively.

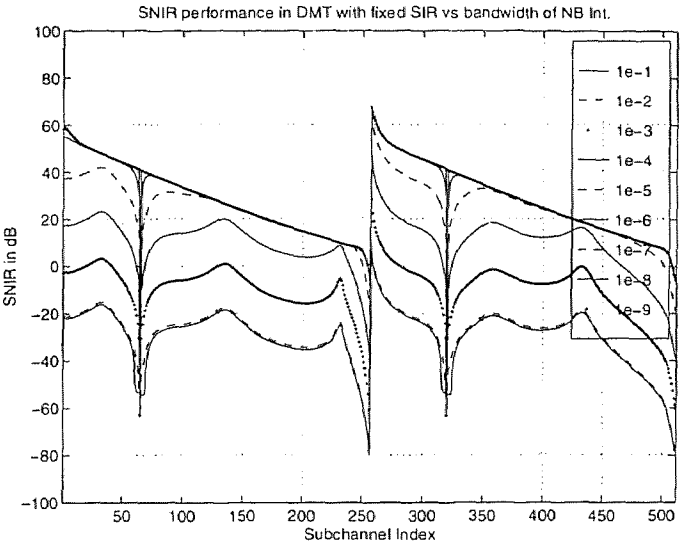

Figure 6.5 The performance of SNIR for each subchannel of a DMT based system in a narrow band interference and AWGN scenario for AWG 26, 9 Kft loop plant for different NB bandwidth with fixed SIR and a center frequency $\omega_{sto} = \frac{\pi}{4}$.

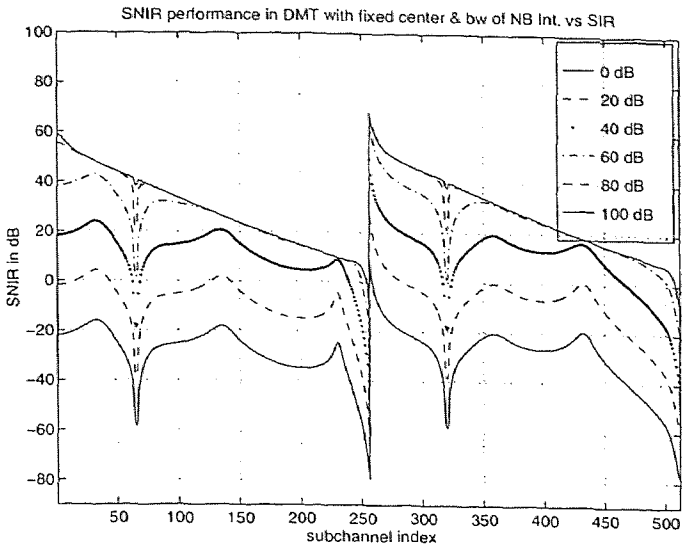

Figure 6.6 The performance of SNIR for each subchannel of a DMT based system in a narrow band interference and AWGN environment for AWG 26, 9 Kft loop plant for different SIR with fixed center frequency of $\omega_{sto} = \frac{\pi}{4}$ and NB bandwidth.

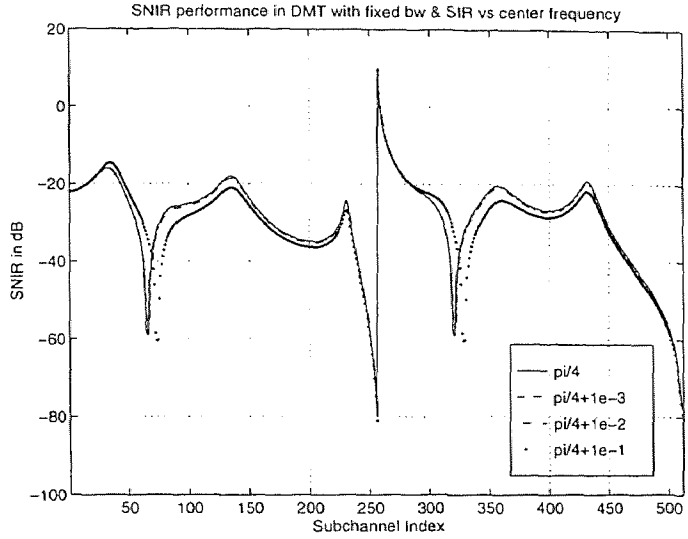

Figure 6.7 The performance of SNIR in each subchannel of a DMT based system in a narrow band interference and AWGN environment for AWG 26, 9 Kft loop plant for different interference center frequencies scenario with fixed SIR and NB bandwidth.

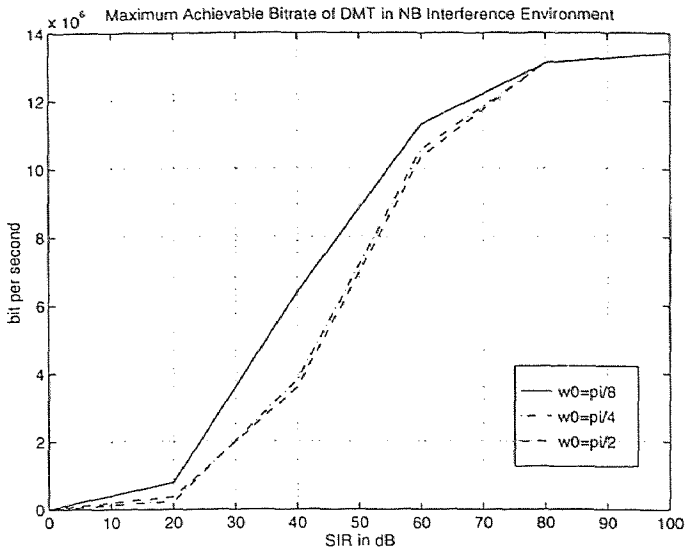

Figure 6.8 The Maximum achievable bitrate of a DMT based system in a narrow band interference and AWGN environment, $NBw = 0.01\pi$, $\omega_{sto} = \frac{\pi}{8}$, $\omega_{sto} = \frac{\pi}{4}$ and $\omega_{sto} = \frac{\pi}{2}$ for AWG 26, 9 Kft loop plant.

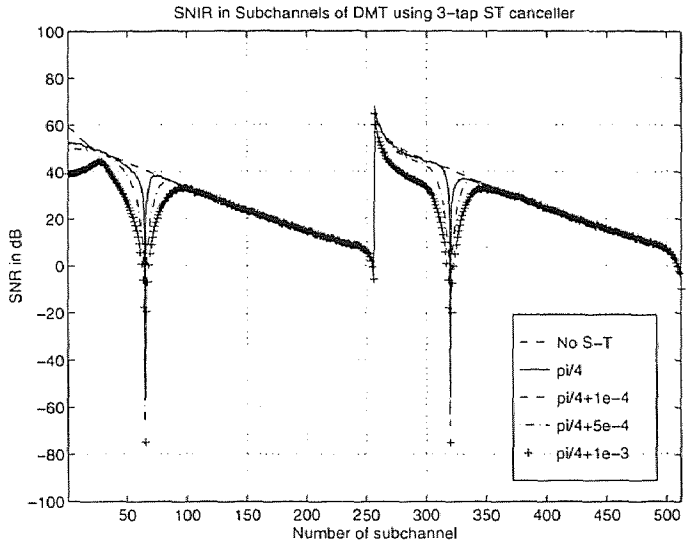

Figure 6.9 SNIR of each subchannels in DMT based system in single-tone interference and AWGN scenario with 3-tap interference canceller.

CHAPTER 7

PERFORMANCE EVALUATION OF DSBMT TRANSCEIVER FOR NARROW BAND INTERFERENCE ENVIRONMENTS

7.1 Introduction

As it is investigated in previous chapter, DMT is sensitive to the location of narrow band interference and the strength of the narrow band interference. Although one can alleviate this problem by inserting an adaptive interference exciser, the overall system performance is degraded. Intuitively, multicarrier modulation should be able to handle single tone or narrow band interference. If there is no interference leakage in the demodulator, shutting down (or null) the subchannel at which the narrow band interference exists will do a very good job. That is the merit of multicarrier modulation technique. The interference leakage of DMT comes from the nature of discrete Fourier transform. The orthogonality of DFT basis function only fit at the N discrete point on the unit circle. Their spectra are overlapping.

In DSBMT technique, Due to very little spectral overlap between subcarriers, single (multi)- tone interference could effect only one or two subchannels which correspond to these interferences. Interference aliasing is free in DSBMT. The performance of DSBMT is much more robust than DMT's in strong single tone or narrow band interference environment.

7.2 Performance of DWMT (DSBMT) Based System in a Single (Multi)-Tone Interference

As we discussed in Chapter 4, Discrete Subband Transceiver (DSBMT) is a superior multicarrier modulation scheme than OFDM (DMT) due to its improved subcarriers. The stopband properties in turn decide the interchannel interference between the subchannels. The narrow band interference leakage is greatly reduced in DSBMT system.

In the narrow band interference environment, the analysis filterbank decomposes the received signal and narrow band interference into a number of subchannels. The adaptive linear combiner will cancel the ISI, ICI and narrow band interference. For these subchannels, in which the narrow band interference does not locate, the ISI and ICI covariance matrice will remain the same as before. This is what we expected, of course.

For the subchannel, in which single tone interference exists, the strong interference will effect the SNR performance. Since we use an adaptive linear combiner to cancel ISI and ICI, if ρ is set to 1, the output from $2\rho + 1$ subchannels are used in the adaptive linear combiner. The subchannel with strong narrow band interference may induce some interference to adjacent subchannels. Fortunately, this kind of interference will not effect the adjacent subchannels severely.

7.3 Simulation Results

In our simulations, an adaptive weight combiner is initialized by a known PN training sequence. As we discussed in Chapter 4, the signal to noise ratio performance of AWG 26 with 9 Kft and AWG 24 with 12 Kft loop plant are investigated. If there is no narrow band interference, the performance of an adaptive linear combiner fits very well as the optimal combiner.

In single and multitone interference cases, only the subchannels where interference exists could decompose the incoming single (multi)-tone interference. There will be no interference aliasing in other subcarriers. These subchannels will get the desired data symbols back. It is the beauty of Discrete Subband Multitone Transceiver. Since there is no cyclic prefix throughput loss, DSBMT will work with the full symbol rate. The cost of DSBMT is that it needs more computational power in both transmitter and receiver side to implement the synthesis and analysis filter banks. Fortunately, there are some fast algorithms to implement it.

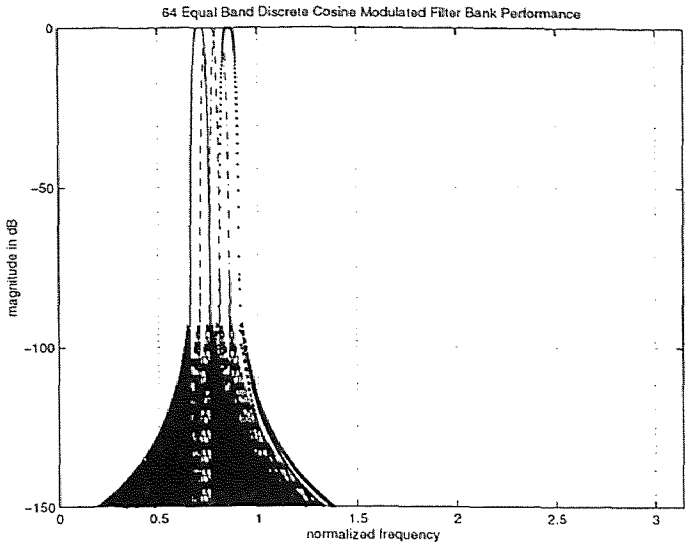

Figure 7.1 Frequency Response of Subcarrier 15, 16, 17 and 18 of a 64 Equal Band Discrete Cosine Modulated Filter Bank.

In our simulations, a 64 equal band synthesis and analysis cosine modulated filter bank is designed. These filter banks have very good stopband properties. Figure 7.1 shows the frequency responses of subcarriers 15, 16, 17 and 18 which correspond to $\frac{\pi}{4}$ in normalized frequency domain.

In the simulations, the single tone interference is at $\omega_0 = \frac{\pi}{4} - 0.02$ and the transmitted signal to interference ratio is 0 dB. After a known PN training sequence, the adaptive linear combiner works fine except subcarrier 16 which is hit by the single tone interference. What we should do is to shut down subchannel 16 or not use this subchannel. All other subchannels work fine. The overall transmission doesn't suffer performance loss even at the presence of a strong single tone interference. Figure 7.2 displays the SNR performance for each subchannel.

In another multitone interference scenario, three tones at $\omega_0 = \frac{\pi}{4} - 0.02$, $\omega_1 = \frac{\pi}{4} - 0.02 + 10^{-3}$ and $\omega_0 = \frac{\pi}{4} - 0.02 - 10^{-3}$ are injected at the receiver, all of them

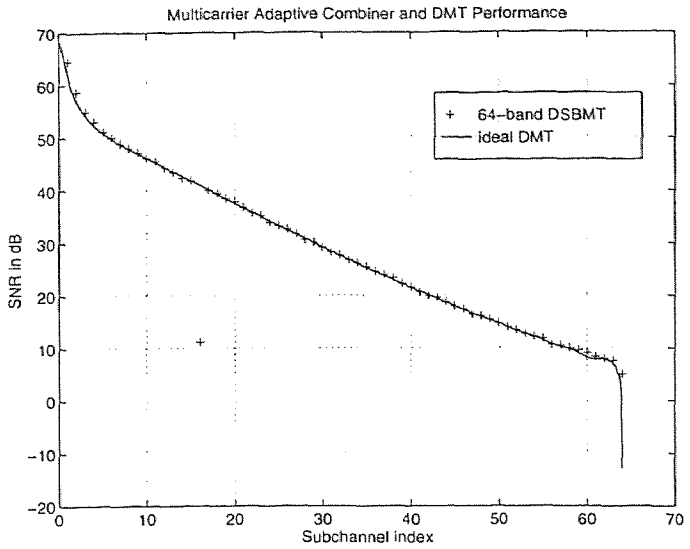

Figure 7.2 Discrete Wavelet (Subband) Multitone Transceiver Performance in Single Tone Interference Environment on AWG 26 9 Kft loop plant.

with an SIR of 0 dB. After the initial training, the signal to noise and interference ratio is displayed in Figure 7.3. We can see that all the subchannels work fine except subchannel 16. The system performs fine despite the presence of a strong multitone interference.

In another simulation, multitone interferences are at $\omega_0 = \frac{\pi}{4}$, $\omega_1 = \frac{\pi}{4} + 10^{-3}$ and $\omega_2 = \frac{\pi}{4} - 10^{-3}$, The system performance is displayed in Figure 7.4. We can see that all the subchannels work fine except subchannel 16 and 17. It results from the fact that these three interference tones hit both subchannels 16 and 17. Multitone interferences are decomposed only into these two subchannels.

When the narrow band interference frequency is changed to $\frac{\pi}{2}$, the performance are displayed in Figure 7.5 and Figure 7.6, respectively.

In order to reduce the transmission subchannel loss, we might design 128 or 256 band synthesis and analysis filter bank. The overall transmission efficiency is higher. Of course, the computational complexity is higher than 64 equal band case.

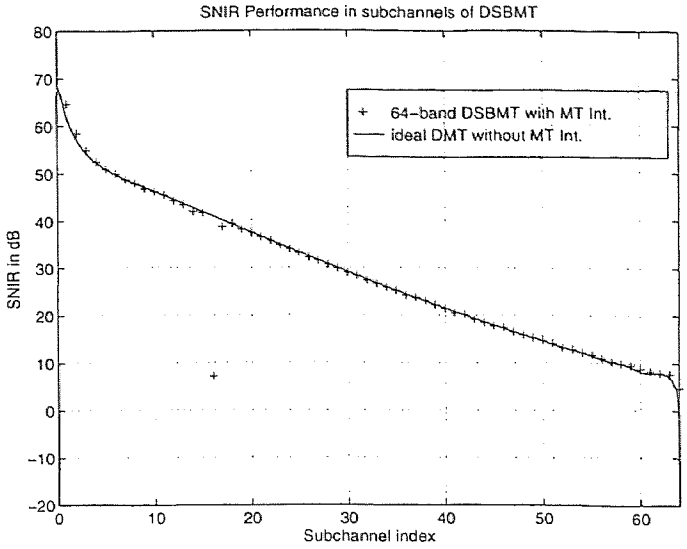

Figure 7.3 Discrete Wavelet (Subband) Multitone Transceiver Performance in Multitone Interference Environment on AWG 26 9 Kft loop plant.

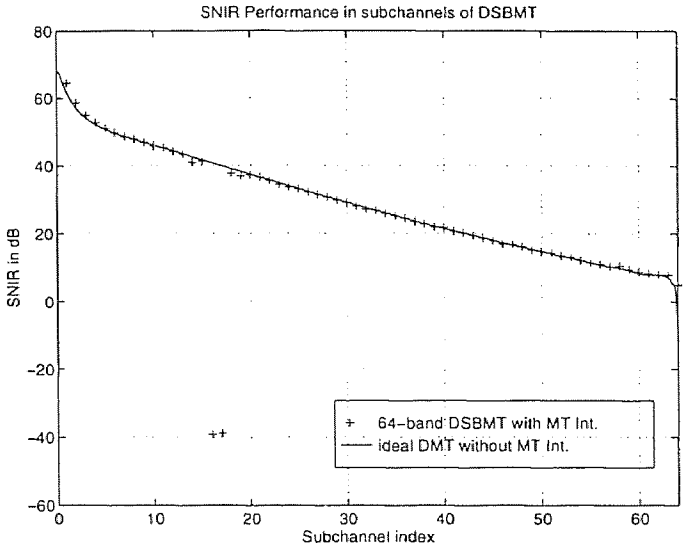

Figure 7.4 Discrete Wavelet (Subband) Multitone Transceiver Performance in Multitone Interference Environment on AWG 26 9 Kft loop plant.

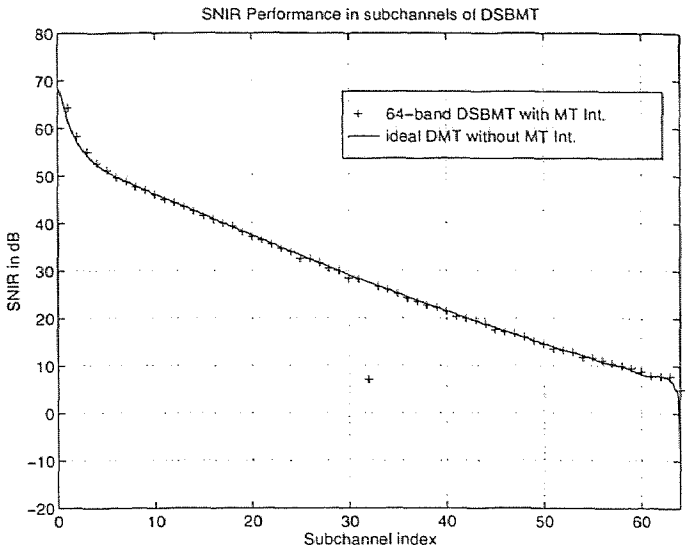

Figure 7.5 Discrete Wavelet (Subband) Multitone Transceiver Performance in Multitone Interference Environment on AWG 26 9 Kft loop plant.

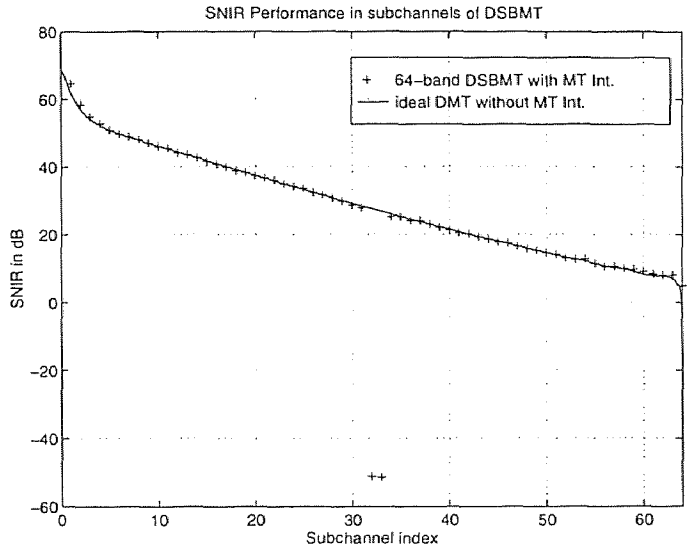

Figure 7.6 Discrete Wavelet (Subband) Multitone Transceiver Performance in Multitone Interference Environment on AWG 26 9 Kft loop plant.

7.4 Remarks

Comparing with DMT, Discrete Wavelet Multitone Transceiver (DWMT) or Discrete Subband Multitone Transceiver (DSBMT) works much better in strong multitone or narrow band interference environments. DSBMT fits well for VDSL applications since there will be some severe narrow band interference in the down link spectrum. Its robustness comes from very good bandpass like cosine modulated synthesis/ analysis filterbank structure.

CHAPTER 8

BLIND CHANNEL IDENTIFICATION AND OPTIMAL MMSE EQUALIZATION USING NONMAXIMALLY DECIMATED MULTIRATE FILTERBANK BASED PRECODER / POST-EQUALIZER

8.1 Introduction and Existing Literature

Telecommunication system performance through a channel with multipath fading or high level of attenuation is severely degraded by intersymbol interference [53]. It is a common problem in many communication systems, including wireless mobile communication applications. In order to reliably recover the transmitted data stream, we must eliminate the impairment of ISI. That is why channel identification and equalization are very important. As the time-variant transmission channel may change in difference environments, the channel equalization must keep track of these variations. The self-recovery of channel estimation is very desirable in the design of a transceiver system. One channel identification and equalization method is to transmit a known pilot training sequence periodically. This will reduce the transmission throughput and increase the system complexity.

The so-called blind channel identification and equalization does not need to send any known pilot training sequence from time to time. It will exploit some characteristics of transmitted signal. The channel properties can be identified directly from the output of the channel. Figure 8.1 shows the basic concept of blind channel identification and equalization. Well performing channel estimations are of significant interest in communications field due to its performance insensitivity to the channel properties.

In the literature of channel identification, conventional blind channel estimation techniques rely on high-order statistics of the stationary channel output. The second-order cyclostationarity based approaches were proposed by Xu and Tong which utilize fractionally spaced oversampling technique[56] [57][58]. Recently, Xia proposed a

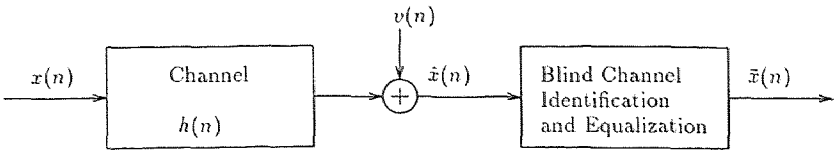

Figure 8.1 The basic schematic of blind channel identification and equalization.

new precoding scheme to overcome ISI using nonmaximally decimated multirate filterbank as an ideal FIR equalizer [61]. Giannakis forwarded a new filterbank precoder for blind channel identification and equalization [62]. In fact, Xia and Giannakis independently came up with the same precoding structure from different perspectives.

Xia suggested the idea of using nonmaximally decimated filterbank as a precoder. He defined some conditions such that there exists an ideal FIR precoder to eliminate the ISI. He considered only the zero-forcing post-equalization solution to handle ISI. Giannakis' scheme utilizes an analysis/synthesis filterbank as a blind channel identification precoder. The post equalization is also a zero-forcing equalization in that scheme, which may greatly enhance the channel noise causing significant SNR degradation. A nonmaximally decimated multirate filterbank precoder / post-equalizer structure is presented in this chapter. It is shown that the proposed approach turns out to be the same as Giannakis' with respect to the problem of blind channel identification. Additionally, we propose an optimal MMSE linear FIR combiner as a post-equalizer. It jointly maximizes the overall signal to noise ratio of blind identification and equalization steps.

8.2 Nonmaximally Decimated Multirate Filterbank Framework as a Precoder/Decoder

Figure 8.2 displays a nonmaximally decimated multirate filterbank precoder structure at the transmitter. Similarly, Figure 8.3 depicts a nonmaximally decimated multirate filterbank decoder / post-equalizer structure. In these two figures, $\downarrow K$ represents a down-sampling by a factor of K and $\uparrow N$ represents an up-sampling by a factor of N.

In Figure 8.2, $x(n)$ is the independent identically distributed (i.i.d.) information sample sequence. $\{G_i(z)\}$ and $\{F_i(z)\}$ are of FIR filters, $1 \leq i \leq N$. Their lengths and filter coefficients will be addressed later. These filters are to be optimally chosen such that the blind identification of the channel is efficient and the Signal to Noise Ratio (SNR_{out}) after blind equalization is maximized. $\tilde{x}(n)$ is the precoded data sequence which is transmitted through the channel. $\hat{x}(n)$ is the received data sequence at the receiver.

In Figure 8.3, the received data samples go through a decoder / post-equalizer step. The decoder consists of a nonmaximally decimated filterbank. $\overline{x}(n)$ are post-equalized / reconstructed data sample. Whenever the transmission system has perfect reconstruction (PR) property, $\overline{x}(n)$ will be the same as input $x(n)$ with some time delay.

The intersymbol interference transmission channel model used is the baseband discrete model which combines the effects of transmitter shaping filter, transmission channel and receiver's anti-aliasing filter. In this bandlimited ISI channel environment, there are ISI and additive white Gaussian noise. It is assumed that the unknown ISI channel is a linear time invariant (LTI) system. Also assume that the impulse response of the transmission channel is of order L, which is known. The channel coefficients are expressed as

$$h = [h_0\,,\, h_1\,,\, h_2\,,\, \ldots\,,\, h_L]$$

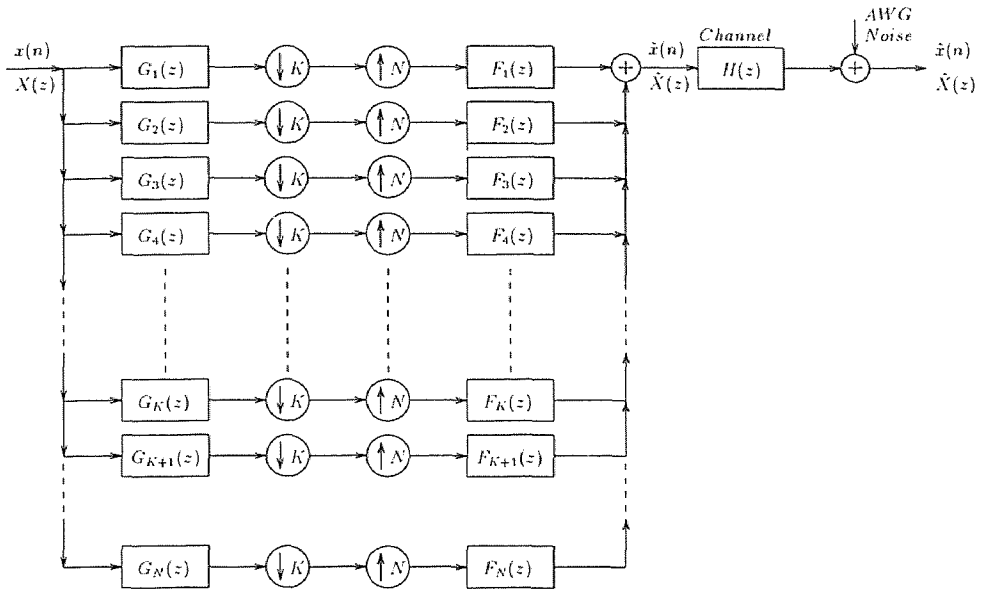

Figure 8.2 Generalized Nonmaximally Decimated Filterbank Precoder / Pre-equalizer Structure.

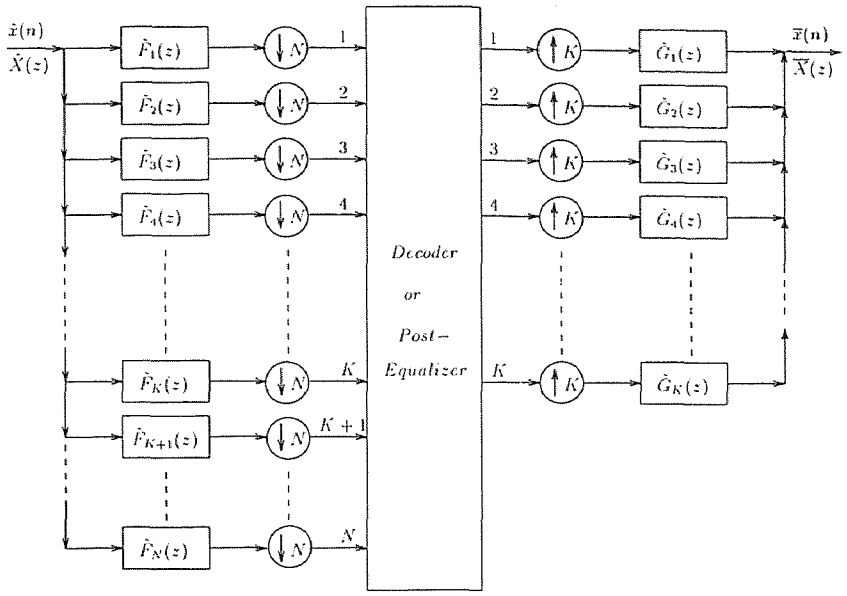

Figure 8.3 Generalized Nonmaximally Decimated Filterbank Decoder / Post-equalizer Structure.

Its Z transform function $H(z)$ is defined as

$$H(z) = \sum_{i=0}^{L} h_i z^{-i}$$

Without any loss of generality, we can assume that $h(0)$ must not be zero. The received samples $\hat{x}(n)$ can be expressed as a function of the transmitted sequence $\tilde{x}(n)$ as

$$\hat{x}(n) = \sum_i \tilde{x}(i) h_{n-i} + v(n) \tag{8.1}$$

where $\{v(n)\}$ are samples of additive white Gaussian noise.

Using multirate filterbank theory [69][89] [74], the channel's transfer function $H(z)$ can be decomposed using polyphase representation as

$$H(z) = \sum_{i=0}^{N-1} H_i(z^N) z^{-i} \tag{8.2}$$

where $H_i(z) = \sum_n h_{Nn+i} z^{-n}$. Let us form blocks of transmitted and received data samples with a size of N for $\tilde{X}_k$ and $\hat{X}_k$, respectively. Then, Eq.(8.1) can be expressed in a blocked form as

$$\hat{X}_k(z) = H(z)\tilde{X}_k(z) + V_k(z). \tag{8.3}$$

$H(z)$ is an $(N \times N)$ pseudo-circulant matrix as

$$H(z) = \begin{bmatrix} H_0(z) & z^{-1}H_{N-1}(z) & z^{-1}H_{N-2}(z) & \cdots & z^{-1}H_1(z) \\ H_1(z) & H_0(z) & z^{-1}H_{N-1}(z) & \cdots & z^{-1}H_2(z) \\ H_2(z) & H_1(z) & H_0(z) & z^{-1}H_{N-1}(z) \cdots & z^{-1}H_3(z) \\ \cdot & \cdot & \cdot & \cdots & \cdot \\ \cdot & \cdot & \cdot & \cdots & \cdot \\ H_{N-1}(z) & H_{N-2}(z) & \cdot & \cdots & H_0(z) \end{bmatrix} \tag{8.4}$$

It is well known in multirate filterbank theory that there can not be any perfect reconstruction (PR) solutions for the case of $K > N$. Therefore, K must be less than N. In order to impose some cyclostationarity to the transmitted symbols, a subset of analysis and synthesis filters of a precoder / pre-equalizer structure are set to be zero as $G_i(z) = 0$ and $F_i(z) = 0$ for $K < i \leq N$. Then, Figure 8.2 is redrawn as Figure 8.4.

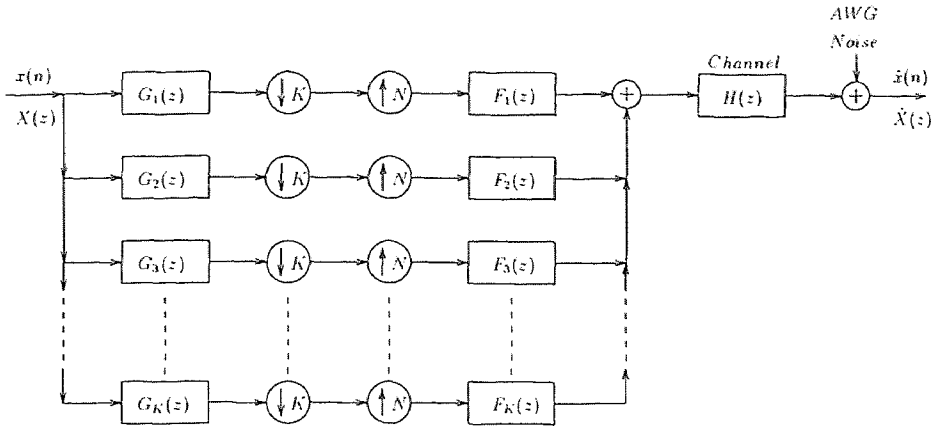

Figure 8.4 The proposed Nonmaximally Decimated Filterbank Precoder / Pre-equalizer structure for Blind Channel Identification and Equalization.

In the proposed precoder structure of Figure 8.2, every block of K information data symbols X_k is precoded / pre-equalized into a block of N transmitted samples $\tilde{X}_k$ by going through a nonmaximally decimated filterbank precoder at the transmitter. This precoding process can be mathematically expressed as a matrix operation as

$$\tilde{X}_k(z) = F(z)G(z)X_k(z) \tag{8.5}$$

where $F(z)$ and $G(z)$ are polyphase matrices of multirate analysis and synthesis filterbank, respectively.

At the receiver side in Figure 8.4, if the received signal samples form a block $\hat{X}_k$ of size N. Then, the output of the channel is expressed in a matrix form as

$$\hat{X}_k(z) = H(z)F(z)G(z)X_k(z) + V_k(z) \tag{8.6}$$

As $G_i(z)$ and $F_i(z)$ for $K < i \leq N$ of the proposed precoder / pre-equalizer structure are set to be zero, a nonmaximally decimated filterbank with $K < N$ puts $(N - K)$ zeros as dummy inputs to the channel. The channel $(N \times N)$ ploy phase

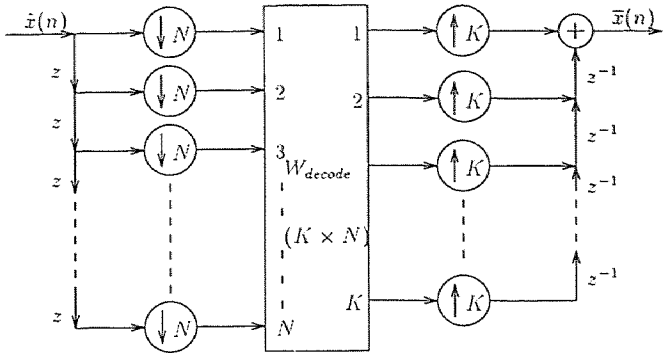

Figure 8.5 The proposed Nonmaximally Decimated Filterbank Decoder / Post-equalizer structure for Blind Channel Identification and Equalization.

matrix $H(z)$ is reduced to $H_{part}(z)_{N\times K}$ where $H_{part}(z)_{N\times K} = H(z)_{(N\times K)}$ as

$$H_{part}(z) = \begin{bmatrix} H_0(z) & z^{-1}H_{N-1}(z) & z^{-1}H_{N-2}(z) & \cdots & z^{-1}H_{N-K+1}(z) \\ H_1(z) & H_0(z) & z^{-1}H_{N-1}(z) & \cdots & z^{-1}H_{N-K+2}(z) \\ H_2(z) & H_1(z) & H_0(z) & \cdots & z^{-1}H_{N-K+3}(z) \\ \cdot & \cdot & \cdot & \cdots & \cdot \\ \cdot & \cdot & \cdot & \cdots & \cdot \\ H_{N-1}(z) & H_{N-2}(z) & \cdots & \cdots & H_{N-K+0}(z) \end{bmatrix} \tag{8.7}$$

Whenever analysis and synthesis filterbanks are set with a proper time delay, $G_i(z) = z^{i-1}$ and $F_i(z) = z^{-i+1}$ for $1 \leq i \leq K$, their polyphase representation matrices $G(z)$ and $F(z)$ become identity matrices of size K and N, respectively. In this case, Eq. 8.6 is derived as

$$\begin{aligned} \hat{X}_k(z) &= H(z)F(z)[G(z); 0_{(N-K)\times K}]^T X_k(z) + V_k(z) \\ &= H_{part}(z)X_k(z) + V_k(z). \end{aligned} \tag{8.8}$$

8.3 The Conditions of Blind Channel Identification

Assume that the channel has an order of L, and the following constraints are set as

$$\begin{aligned} K &< N, \\ K &\geq L+1, \\ N &\geq K+L \end{aligned} \tag{8.9}$$

Then the pseudo-circular matrix $H(z)$ is expressed as

$$H(z)_{(N\times N)} = \begin{bmatrix} h_0 & 0 & 0 & \cdot & \cdot & 0 & z^{-1}h_L & z^{-1}h_{L-1} & \cdot & \cdot & \cdot & z^{-1}h_1 \\ h_1 & h_0 & 0 & \cdot & \cdot & 0 & 0 & z^{-1}h_L & z^{-1}h_{L-1} & \cdot & \cdot & z^{-1}h_2 \\ h_2 & h_1 & h_0 & 0 & \cdot & 0 & 0 & 0 & z^{-1}h_L & \cdot & \cdot & z^{-1}h_3 \\ \cdot & \cdot & \cdot & \cdot & \cdot & \cdot & \cdot & \cdot & \cdot & \cdot & \cdot & \cdot \\ \cdot & \cdot & \cdot & \cdot & \cdot & 0 & \cdot & \cdot & \cdot & \cdot & \cdot & \cdot \\ h_L & h_{L-1} & h_{L-2} & h_{L-3} & \cdot & h_0 & 0 & 0 & 0 & \cdot & \cdot & z^{-1}h_L \\ 0 & h_L & h_{L-1} & \cdot & h_2 & h_1 & h_0 & \cdot & \cdot & \cdot & \cdot & \cdot \\ \cdot & \cdot & \cdot & \cdot & \cdot & \cdot & \cdot & \cdot & \cdot & \cdot & \cdot & \cdot \\ 0 & 0 & 0 & \cdot & 0 & h_L & h_{L-1} & h_{L-2} & \cdot & \cdot & \cdot & h_0 \end{bmatrix} \tag{8.10}$$

Therefore, the matrix $H_{part}(z)$ becomes

$$H_{part}(z)_{(N\times K)} = \begin{bmatrix} h_0 & 0 & 0 & \cdot & \cdot & \cdot & 0 \\ h_1 & h_0 & 0 & \cdot & \cdot & \cdot & 0 \\ h_2 & h_1 & h_0 & 0 & \cdot & \cdot & 0 \\ \cdot & \cdot & \cdot & \cdot & \cdot & \cdot & \cdot \\ \cdot & \cdot & \cdot & \cdot & \cdot & \cdot & 0 \\ h_L & h_{L-1} & h_{L-2} & h_{L-3} & \cdot & \cdot & h_0 \\ 0 & h_L & h_{L-1} & \cdot & \cdot & h_2 & h_1 \\ \cdot & \cdot & \cdot & \cdot & \cdot & \cdot & \cdot \\ 0 & 0 & 0 & \cdot & \cdot & 0 & h_L \\ 0 & 0 & 0 & \cdot & \cdot & 0 & 0 \\ 0 & 0 & 0 & \cdot & \cdot & 0 & 0 \end{bmatrix} \tag{8.11}$$

Obviously, any arbitrary integer values of K , N which satisfy the conditions of Eq.(8.9) will generate a constant $N \times K$ matrix $H_{part}(z)$. The decoder / post-equalizer section of the proposed system becomes a constant $K \times N$ matrix. It is quite simpler than Smith form operation used in [61] which is a $K \times N$ polynomial matrix.

Assume that we pick $K = L+1$ and $N = K+L$ as the critical value of (K, N). Then, $H_{part}(z)$ is a constant matrix as shown

$$H_{part}(z)_{(N\times K)} = \begin{bmatrix} h_0 & 0 & 0 & \cdot & \cdot & \cdot & 0 \\ h_1 & h_0 & 0 & \cdot & \cdot & \cdot & 0 \\ h_2 & h_1 & h_0 & 0 & \cdot & \cdot & 0 \\ \cdot & \cdot & \cdot & \cdot & \cdot & \cdot & \cdot \\ \cdot & \cdot & \cdot & \cdot & \cdot & \cdot & 0 \\ h_L & h_{L-1} & h_{L-2} & h_{L-3} & \cdot & \cdot & h_0 \\ 0 & h_L & h_{L-1} & \cdot & \cdot & h_2 & h_1 \\ \cdot & \cdot & \cdot & \cdot & \cdot & \cdot & \cdot \\ 0 & 0 & 0 & \cdot & \cdot & 0 & h_L \end{bmatrix} \tag{8.12}$$

Now, let us denote the received signal block of size N as $\hat{X}_k(z)$ and assume that AWGN samples have a variance of σ_n^2. The information symbols are assumed to have variance of σ_x^2. The AWGN is assumed to be independent of the information sequence. The autocorrelation matrix $R_{\hat{X}_k(z)}$ for the case of $G(z) = I_{K\times K}$ and $F(z) = I_{N\times N}$ can be derived as

$$\begin{aligned} R_{\hat{X}_k(z)} &= \mathbf{E}[\hat{X}_k(z)\hat{X}_k(z)^{*T}] \\ &= \mathbf{E}[[H(z)F(z)[G(z); 0_{(N-K)\times K}]^T X_k(z) + V_k(z)] \\ &\quad [H(z)F(z)[G(z); 0_{(N-K)\times K}]^T X_k(z) + V_k(z)]^{*T}] \\ &= \mathbf{E}[H_{part}(z)X_k(z)[X_k(z)]^{*T}[H_{part}(z)]^{*T}] + \mathbf{E}[V_k(z)V_k(z)^{*T}] \\ &= \sigma_x^2 H_{part}(z)[H_{part}(z)]^{*T} + \sigma_n^2 I_{N\times N} \end{aligned} \tag{8.13}$$

where $\mathbf{E}$ is the expected value and * denotes the complex conjugate operation. Using the structure of matrix $H_{part}(z)$, $R_{\hat{X}_k(z)}$ can be expressed as

$$R_{\hat{X}_k(z)} = \sigma_x^2 \begin{bmatrix} h_0h_0^* & h_0h_1^* & h_0h_2^* & \cdot & \cdot & h_0h_L^* & 0 & \cdot & 0 \\ h_1h_0^* & h_0^2+h_1^2 & \cdot & \cdot & \cdot & \cdot & \cdot & \cdot & 0 \\ \cdot & \cdot & \cdot & \cdot & \cdot & \cdot & \cdot & \cdot & \cdot \\ \cdot & \cdot & \cdot & \cdot & \cdot & \cdot & \cdot & \cdot & h_L^2 \end{bmatrix} + \sigma_n^2 I_{N\times N} \tag{8.14}$$

If the coefficients are real valued, we can omit the conjugate sign in the equation above. The first raw, $R_{\hat{X}_k}(1)$, of autocorrelation matrix $R_{\hat{X}_k}$ is therefore in the form of

$$R_{\hat{X}_k}(1) = \sigma_x^2 h_0 \left[h_0 + \frac{\sigma_n^2}{\sigma_x^2 h_0} \quad h_1 \quad h_2 \quad \cdot \quad \cdot \quad h_L \quad 0 \quad 0 \quad \cdot \quad 0 \right]. \tag{8.15}$$

Hence, $h_0, h_1, h_2, ..., h_L$ can be blindly identified from the autocorrelation function $R_{\hat{X}_k}(1)$ as

$$\begin{aligned} \hat{h}_0 &= \{\frac{1}{\sigma_x^2}[R_{\hat{X}_k}(1,1) - \sigma_n^2]\}^{\frac{1}{2}} \\ \hat{h}_i &= \frac{1}{\sigma_x^2 \hat{h}_0} R_{\hat{X}_k}(1,i),\ 1 \le i \le L \\ &= \frac{1}{\sigma_x^2 \hat{h}_0} \frac{1}{M} \sum_{m=1}^{M} \hat{x}(mN)\hat{x}(mN+i) \end{aligned} \tag{8.16}$$

where $SNR_{in} = \frac{\sigma_x^2}{\sigma_n^2}$ is the signal to noise ratio. Assume that the transmitted signal variance is normalized, $\sigma_x^2 = 1$, and SNR_{in} is estimated. Then, all of the channel coefficients can be blindly identified. The second part of Eq. (8.16) is the same form as presented in Ref. [62].

8.4 Optimal MMSE Linear Blind Equalization

As we saw in the previous section, the channel parameters can be blindly identified by the proposed nonmaximally decimated filterbank based precoder structure. After identifying the channel coefficients, the ISI distorted received symbols can be equalized in order to recover the transmitted signal. The nonmaximally decimated filterbank decoder structure is displayed in Figure 8.5. The ploy phase matrices of nonmaximally decimated multirate analysis and synthesis filterbank is defined as $\tilde{F}(z)$ and $\tilde{G}(z)$, respectively. Let's assume that a $(K \times N)$ decoder (equalizer) matrix W_{decode} is used. The decoded or reconstructed symbol $\overline{X}_k$ is therefore derived as

$$\begin{aligned} \overline{X}_k(z) &= \tilde{G}(z) W_{decode}(z) \tilde{F}(z) \hat{X}_k(z) \\ &= \tilde{G}(z) W_{decode}(z) \tilde{F}(z) H(z) F(z) [G(z); 0_{(N-K)\times K}]^T X_k(z) \\ &\quad + \tilde{G}(z) W_{decode}(z) \tilde{F}(z) V_k(z) \end{aligned} \tag{8.17}$$

To simplify the reconstruction process, we set the ploy phase matrices $\tilde{F}(z)$ and $\tilde{G}(z)$ to be identity matrices with sizes of N and K, respectively. In this case, Eq.

(8.17) becomes

$$\begin{aligned} \overline{X}_k(z) &= W_{decode}(z)H(z)F(z)[G(z); 0_{(N-K)\times K}]^T X_k(z) \\ &\quad + W_{decode}(z)V_k(z) \end{aligned} \tag{8.18}$$

Let's denote E_k as the reconstruction error vector which is defined as the difference between the reconstructed data vector and the transmitted information data vector; $E_k(i) = x(i) - \hat{x}(i)$ for $1 \leq i \leq K$. Then,

$$\begin{aligned} E_k(z) &= X_k(z) - \overline{X}_k(z) \\ &= [W_{decode}(z)H(z)F(z)[G(z); 0_{(N-K)\times K}]^T - I_{(K\times K)}]X_k(z) \\ &\quad + W_{decode}(z)V_k(z) \end{aligned} \tag{8.19}$$

where $I_{(K\times K)}$ is an identity matrix of size K. From Eq. (8.19), it is easy to observe that the first part is due to the intersymbol interference while the second part is caused by the AWGN noise enhancement. The perfect reconstruction condition implies that there is no ISI such that

$$W_{decode}(z)H(z)F(z)[G(z); 0_{(N-K)\times K}]^T = I_{(K\times K)} \tag{8.20}$$

In Ref. [61], $G(z)$ is set to $I_{(K\times K)}$. A methodology to find a $(K \times N)$ polynomial matrix $W_{decode}(z)$ to obtain perfectly reconstructed $\overline{x}(n)$ was suggested. It was shown that the $(K \times N)$ polynomial matrix can be derived using the Smith form operations. This solution is indeed a zero-forcing decoder or post-equalizer. The noise enhancement problem of a post-equalizer which is the second part of Eq. (8.19) was not considered in that work. Although one can get the $(K \times N)$ PR FIR polynomial matrix through the computationally involved Smith form operation, the SNR_{out} degradation of the system can be very significant.

One should mention that there are many solutions for each (K, N) pair using zero-forcing PR Smith form operation.

The equalization scheme of Ref. [62] could not suppress any noise enhancement either. It is a zero-forcing PR post-equalization method. Additionally, in [62], $G(z)$ matrix is set to be an identity matrix of size K. The precoder structures at the transmitter are indeed the same in both Ref. [61] and Ref. [62].

Due to the interpretation of Eq. (8.19), we attempt to obtain the optimal MMSE based one tap ($K \times N$) constant matrix solution to improve SNR_{out}. This MMSE based nonmaximally decimated filter bank decoder attempts to cancel ISI while not enhancing the noise such that the maximum value of SNR_{out} after the post-equalizer is achieved. It is quite similar to the conventional MMSE linear equalizer solution.

Let's assume that $G(z)$ is set to be a $K \times K$ identity matrix as in Ref. [61] and Ref. [62]. This is necessary for the proposed blind identification algorithm. Then, Eq. (8.19) is expressed as

$$\begin{aligned} E_k(z) &= X_k(z) - \overline{X}_k(z) \\ &= [W_{decode}(z)H(z)[I_{(K\times K)}; 0_{(N-K)\times K}]^T - I_{(K\times K)}]X_k(z) \\ &\quad + W_{decode}(z)V_k(z) \\ &= [W_{decode}(z)H_{part}(z) - I_{(K\times K)}]X_k(z) \\ &\quad + W_{decode}(z)V_k(z) \end{aligned} \tag{8.21}$$

The equation above is valid for any integer values of (K, N) in a multirate filterbank structure (analysis / synthesis filterbank configuration). It is a polynomial relationship in z. As we select (K, N) satisfying the conditions of Eq. (8.9), Eq. (8.21) becomes a constant matrix relationship.

Denote $W_{decode} = [W_1, W_2, ..., W_K]^T_{K\times N}$, each raw $W_i = [W_{i,1}, W_{i,2}, ..., W_{i,N}]$; $H_{part} = [H_1, H_2, ..., H_K]$. Then, the total ISI plus noise energy is written as

$$\begin{aligned} E_{error} &= \mathbf{E}[X_k^T(W_{decode}H_{part} - I_{(K\times K)})^T(W_{decode}H_{part} - I_{(K\times K)})X_k] + \\ &\quad \mathbf{E}[V_k^T W_{decode}^T W_{decode} V_k] \end{aligned}$$

$$= \sum_{i=1}^{K} E_{error}(i)$$
$$= \sum_{i=1}^{K} \sigma_x^2 \sum_{j=1}^{K} (W_i H_j - \delta_{i-j})^2 + \sigma_n^2 \sum_{i=1}^{K} W_i W_i^T \quad (8.22)$$

Now, we want to obtain an optimal $W_{decode}(i,j)$ such that ISI plus noise is minimized to get a maximum SNR_{out}. Since $E_{error} = \sum_{i=1}^{K} E_{error}(i)$, and $E_{error}(i)$ is a function of weight vector W_i only, we can derive optimal weight vector to get minimum $E_{error}(i)$ as

$$E_{error}(i) = \sigma_x^2 \sum_{j=1}^{K} (W_i H_j - \delta_{i-j})^2 + \sigma_n^2 W_i W_i^T \quad (8.23)$$

To minimize $E_{error}(i)$, we take a derivative of equation above. After some algebraic operations, the optimal weight vector W_i is written as

$$W_i^{opt} = \left[(\sum_{j=1}^{K} H_j H_j^T) + \frac{\sigma_n^2}{\sigma_x^2} I_{N \times N} \right]^{-1} H_i \quad (8.24)$$

Then, the maximum SNR_{out} is expressed as

$$SNR_{out}^{opt} = \frac{K}{\sum_{i=1}^{K} W_i (\sum_{j=1}^{K} H_j H_j^T) W_i^T - 2 \sum_{i=1}^{K} W_i H_i + K + \frac{\sigma_n^2}{\sigma_x^2} \sum_{i=1}^{K} W_i W_i^T} \quad (8.25)$$

where W_i, $1 \leq i \leq K$, are the optimal weight vectors. The optimal MMSE based nonmaximally decimated filterbank post-equalizer maximizes the SNR_{out} at the output of decoder/equalizer. It is shown that it outperforms the zero-forcing PR equalizer based system used in Ref. [61] and Ref. [62]. This improvement makes the filterbank based precoder structure perform successfully for blind identification and equalization of unknown channels.

8.5 Simulations and Performance Comparisons

In this section, we simulate channel identification and equalization using the proposed algorithm for a few unknown channel. The performance studies show the robustness of the proposed channel identification and optimal MMSE based multirate filterbank post-equalizer.

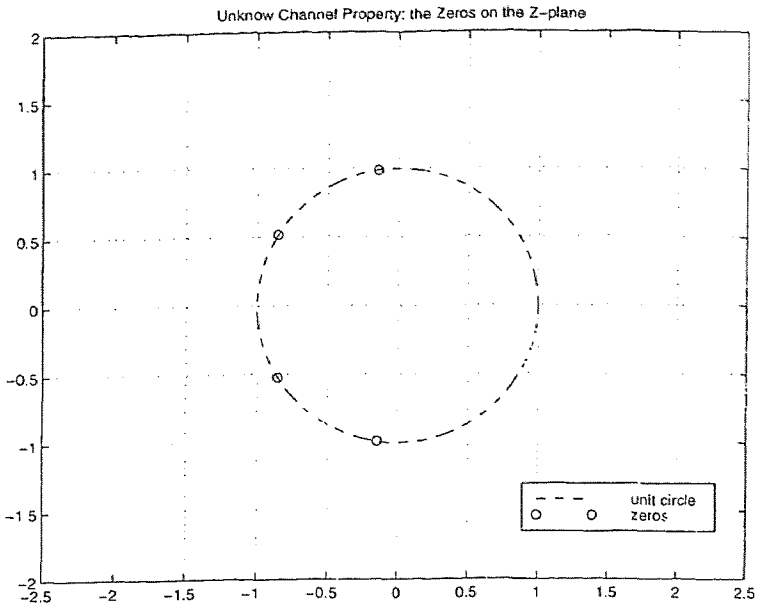

Figure 8.6 The zeros locations of the unknown transmission channel in Ref.[61] on the z plane.

The unknown linear time invariant channels which are going to be investigated are

(i) The channel $h = [0.1111, 0.2222, 0.2778, 0.2222, 0.1111]$ with four zeros on the unit circle as used in [61]. The locations of these four zeros are $-0.1464 \pm j * 0.9892$ and $-0.8536 \pm j * 0.5210$. Figure 8.6 shows the zeros location of the unknown transmission channel on the z plane. The spectrum of this ISI channel is displayed in Figure 8.7.

It is known that this channel is not identifiable by using the methods which rely on fractional spaced sampling.

500 BPSK symbols, $\{x(n)\}$ are generated and transmitted through the unknown channel. In this case, the order of unknown channel is 4. We select the critical values of $K = 5$, $N = K + L = 9$. This is just for illustration purposes. The pseudo-circular transform matrix $H(z)$ for this channel is written as

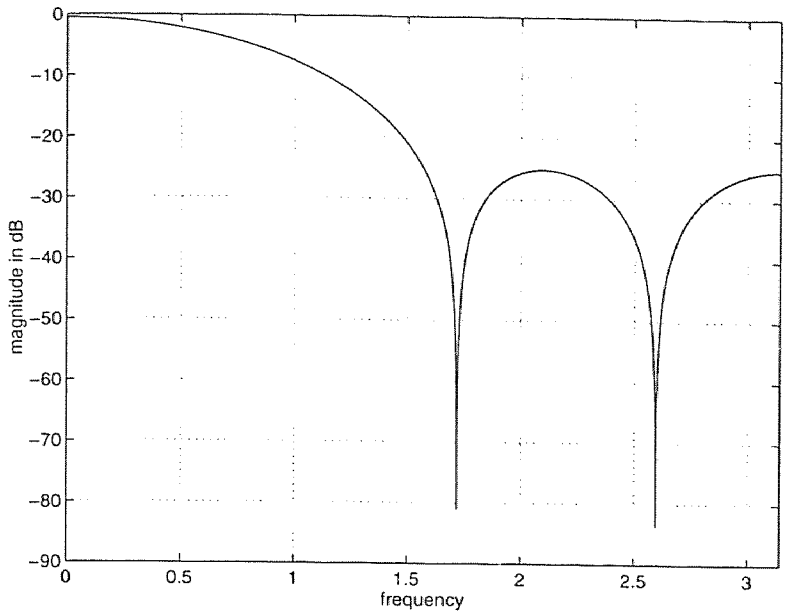

Figure 8.7 Spectrum of transmission channel with four zeros on the unit circle in Ref.[61].

$$H(z)_{(N\times N)} = \frac{1}{9}\begin{bmatrix} 1 & 0 & 0 & 0 & 0 & 1z^{-1} & 2z^{-1} & 2.5z^{-1} & 2z^{-1} \\ 2 & 1 & 0 & 0 & 0 & 0 & 1z^{-1} & 2z^{-1} & 2.5z^{-1} \\ 2.5 & 2 & 1 & 0 & 0 & 0 & 0 & 1z^{-1} & 2z^{-1} \\ 2 & 2.5 & 2 & 1 & 0 & 0 & 0 & 0 & 1z^{-1} \\ 1 & 2 & 2.5 & 2 & 1 & 0 & 0 & 0 & 0 \\ 0 & 1 & 2 & 2.5 & 2 & 1 & 0 & 0 & 0 \\ 0 & 0 & 1 & 2 & 2.5 & 2 & 1 & 0 & 0 \\ 0 & 0 & 0 & 1 & 2 & 2.5 & 2 & 1 & 0 \\ 0 & 0 & 0 & 0 & 1 & 2 & 2.5 & 2 & 1 \end{bmatrix}$$

and $H_{part}(z)$ becomes a constant matrix as

$$H_{part}(z)_{(N\times K)} = \frac{1}{9}\begin{bmatrix} 1 & 0 & 0 & 0 & 0 \\ 2 & 1 & 0 & 0 & 0 \\ 2.5 & 2 & 1 & 0 & 0 \\ 2 & 2.5 & 2 & 1 & 0 \\ 1 & 2 & 2.5 & 2 & 1 \\ 0 & 1 & 2 & 2.5 & 2 \\ 0 & 0 & 1 & 2 & 2.5 \\ 0 & 0 & 0 & 1 & 2 \\ 0 & 0 & 0 & 0 & 1 \end{bmatrix}$$

Using the proposed blind channel identification algorithm, 100, 500 and 1000 Monte Carlo simulation runs are performed in an SNR_{in} of 20 dB environment. The mean value of estimated channel coefficients, $\hat{h}$, are listed in the Table 8.1.

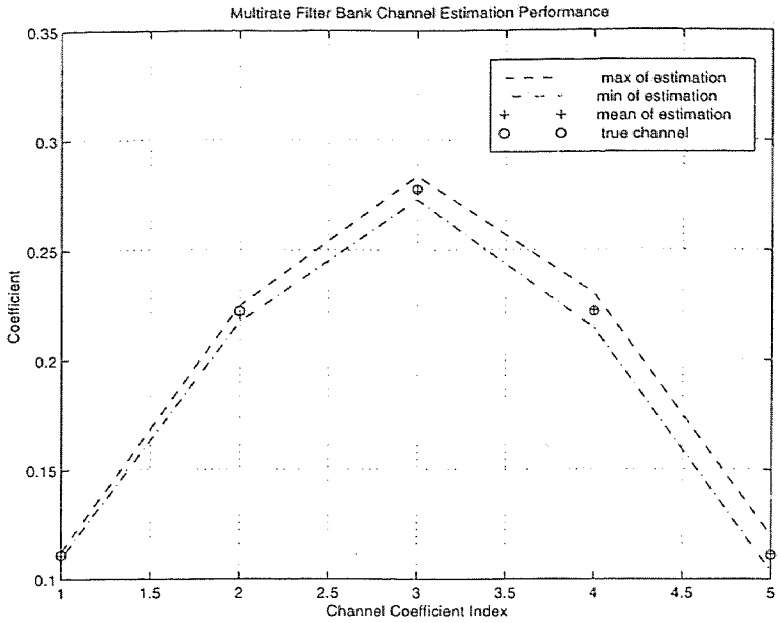

Figure 8.8 The nonmaximally decimated filterbank channel estimation peformance for the unknown transmission channel with two zeros on the unit circle of z plane.

Figure 8.8 displays the estimated channel coefficient in 10 simulations with 100 Monte Carlo runs. The mean, minimum and maximum value of coefficients are ploted. It is observed that the blind identification is performed well. The coefficient h_0 is estimated directly which is not the case in Ref. [62].

After a successful channel identification step, the channel equalization is performed. In this unknown channel case, it is not possible to get an ideal FIR zero-forcing linear postequalizer in a conventional way. Our channel equalization is performed using an optimal MMSE based linear FIR combiner. Figure 8.9 displays the constellation of recovered symbols using the optimal MMSE based equalizer. Similarly, Figure 8.10 shows the constellation for the equalizer used in Ref. [62]. Figure 8.11 and Figure 8.12 show the QAM constellation if QAM signal is transmitted. The SNR_{in} of these two figures are of 40 dB. The overall reconstruction

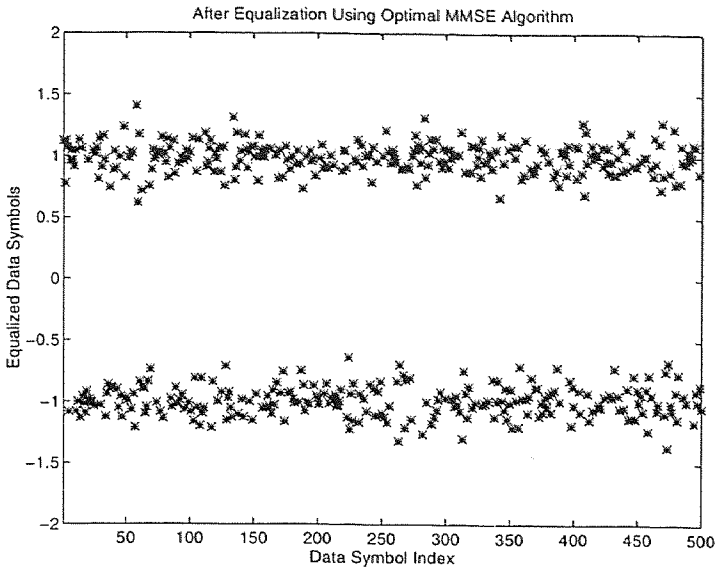

Figure 8.9 BPSK constellation, using the proposed optimal MMSE based equalizer, at the equalizer output. SNRin = 40 dB. (5,9) case of transmission channel in Ref.[61].

signal to noise ratio after post-equalization is displayed in Figure 8.13. It is shown that the optimal MMSE based FIR equalizer outperforms zero-forcing equalizer. It is much more robust when SNR is low.

(ii) The channel with 7 zeros at $0.2; \pm 1.5; \pm 0.5j; 0, 2783 \pm j * 0.3488$,

$h = [1, -0.7566, -1.6896, 1.4734, -1.1834, 0.5052, -0.1746, 0.0224]$ in Ref. [62]. Figure 8.14 shows the zero locations of this unkown channel. Notice that, it is a nonminimum phase channel.

We could select any integer $K \geq 8; N \geq K + 7$. For a simple demonstration, we pick $(K, N) = (8, 15)$. In this case, $H_{part}(z)$ becomes a constant matrix. 500 and 1000 Monte Carlo simulations are run to blindly estimate the unknown channel. Assume that the SNR_{in} is 20 dB, the mean value of estimated channel coefficients, $\hat{h}$, are listed in the Table 8.2.

Figure 8.15 displays the estimated channel coefficients in 10 simulations with 100 Monte Carlo runs. The mean, minimum and maximum value of coefficients

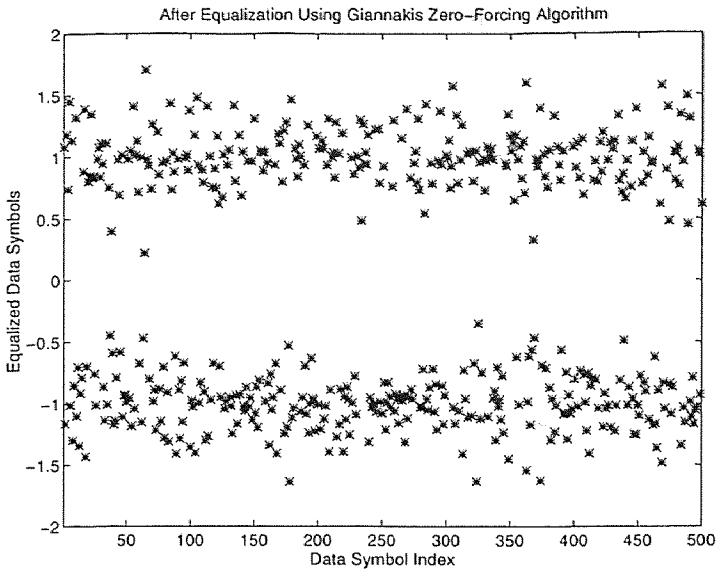

Figure 8.10 BPSK constellation for zero-forcing equalizer used in Ref.[62] at the equalizer output. SNRin = 40 dB. (5,9) case of transmission channel in Ref.[61].

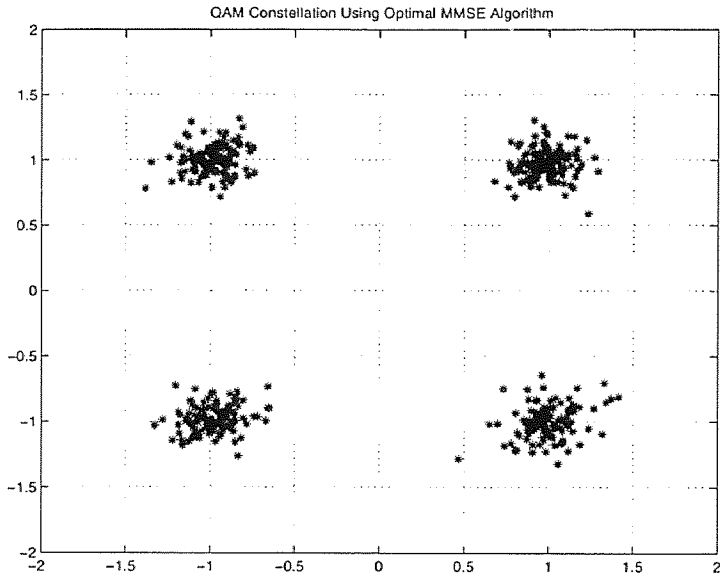

Figure 8.11 QAM constellation for zero-forcing equalizer used in Ref.[62] at the equalizer output. SNRin = 40 dB. (5,9) case of transmission channel in Ref.[61].

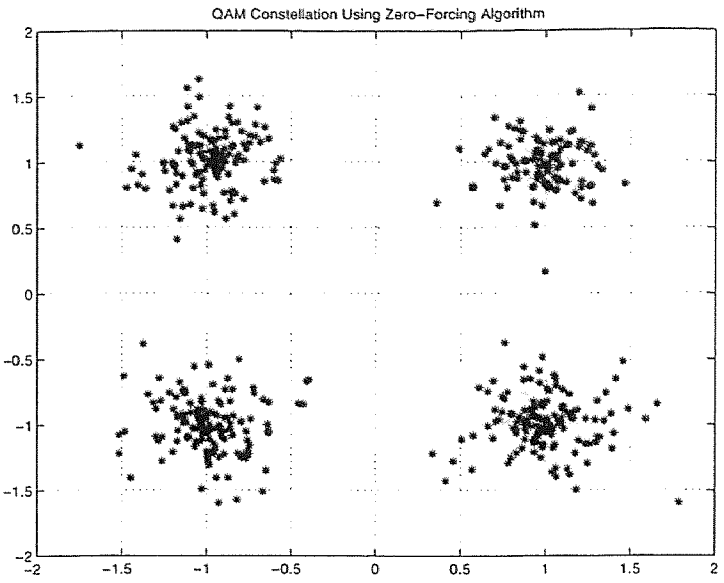

Figure 8.12 QAM constellation for zero-forcing equalizer used in Ref.[62] at the equalizer output. SNRin = 40 dB. (5,9) case of transmission channel in Ref.[61].

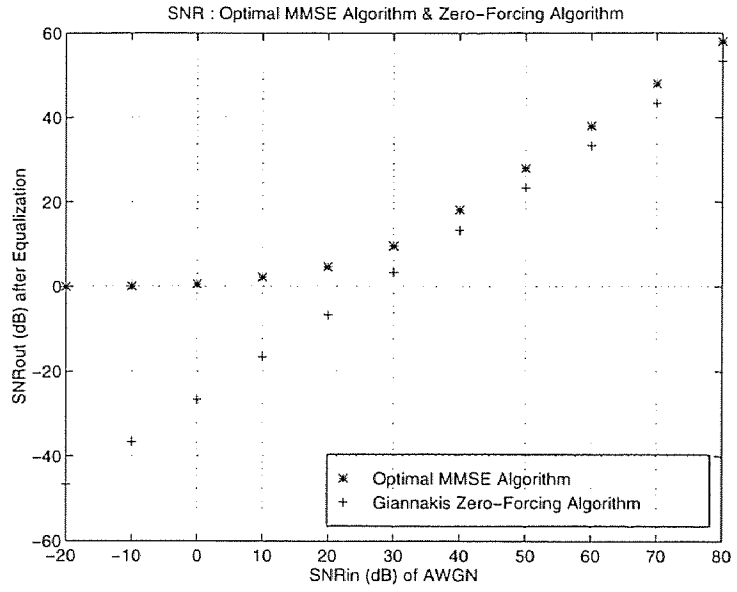

Figure 8.13 SNR performance of optimal MMSE based multirate filterbank post-equalizer and zero-forcing equalizer used in Ref. [62] at the equalizer output verses SNR_{in}. (5,9) case of transmission channel in Ref.[61].

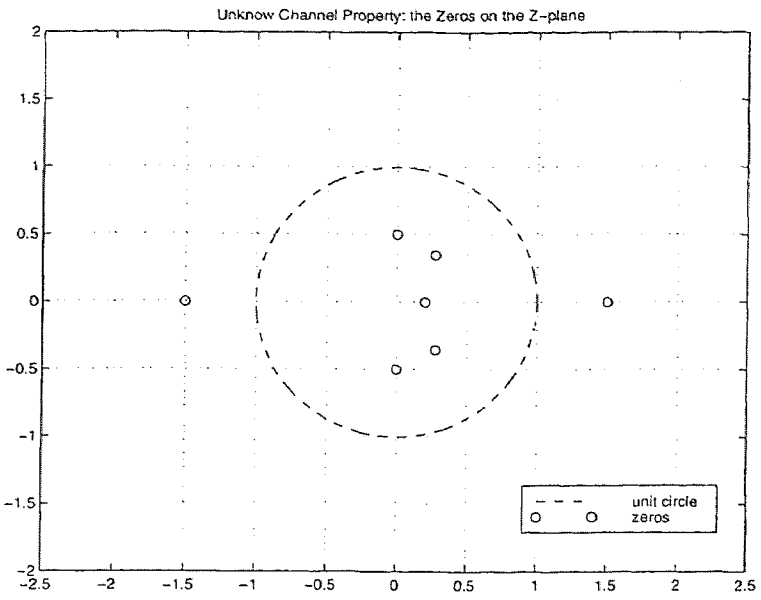

Figure 8.14 The zeros locations of the unknown transmission channel in Ref.[62] on the z plane.

are ploted. It is observed that the blind identification is performed well. The coefficient h_0 is estimated directly which is not the case in Ref. [62]. We can see that the blind identification is performed well. As reported in [62], second-order fractional oversampling blind identification technique does not work for this mixed phase channel. The proposed technique is much more robust.

Using the identified channel coefficients, the optimum MMSE based FIR equalization is performed. Figure 8.16 displays the constellation of reconstructed symbols using optimal MMSE equalizer. Figure 8.17 displays the correponding constellation for zero-forcing equalizer proposed in [62]. Figure 8.18 and Figure 8.19 show the QAM constellation if QAM signal is transmitted. The overall reconstruction SNR_{out} is displayed in Figure 8.20. It is seen that the proposed optimal MMSE based post-equalizer is much more robust than zero-forcing equalizer.

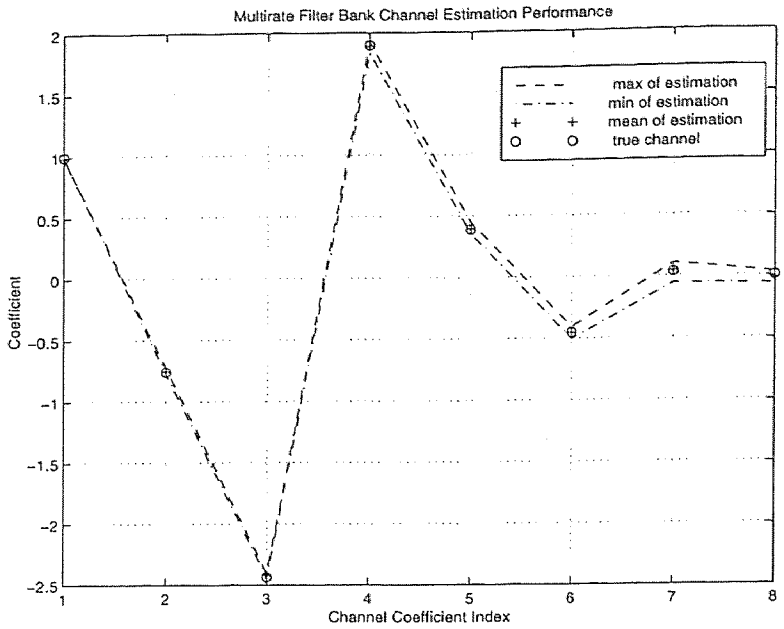

Figure 8.15 The nonmaximally decimated filterbank channel estimation peformance for the unknown transmission channel with nonminimum phase (zeros inside and outside the unit circle of z plane).

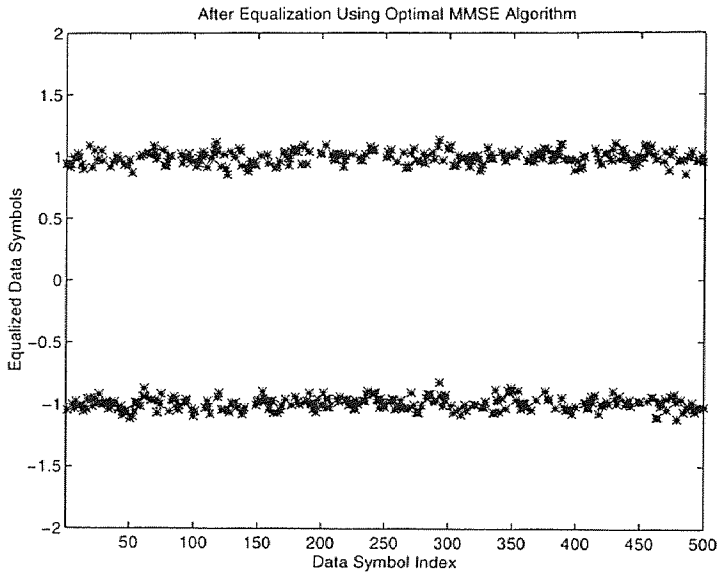

Figure 8.16 BPSK constellation, using proposed optimal MMSE based equalizer at the equalizer output. SNRin = 20 dB, (8,15) case of transmission channel in Ref. [62].

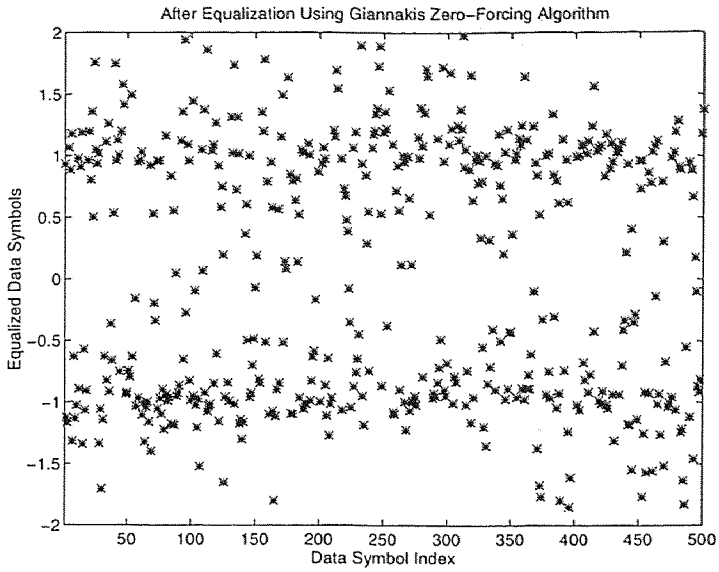

Figure 8.17 BPSK constellation using zero-forcing equalizer at the equalizer output. SNRin = 20 dB. (8,15) case of transmission channel in Ref. [62].

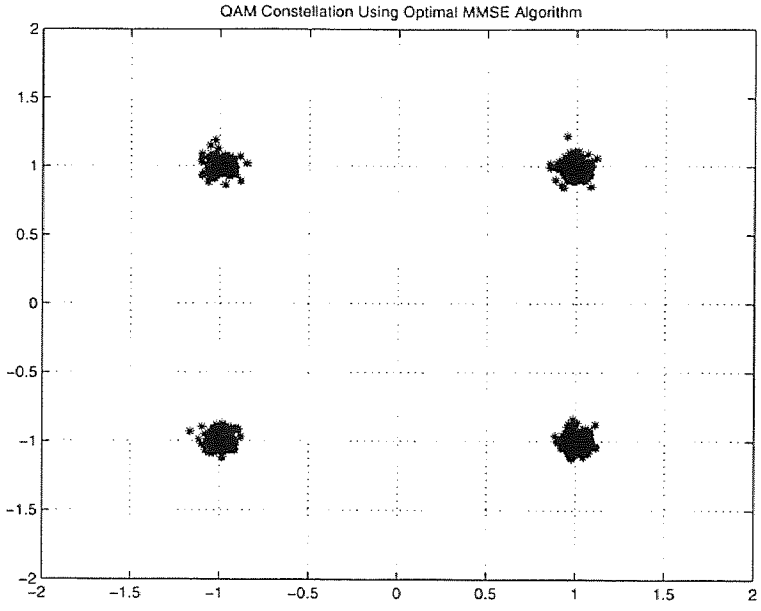

Figure 8.18 QAM constellation, using proposed optimal MMSE based equalizer at the equalizer output. SNRin = 20 dB, (8,15) case of transmission channel in Ref. [62].

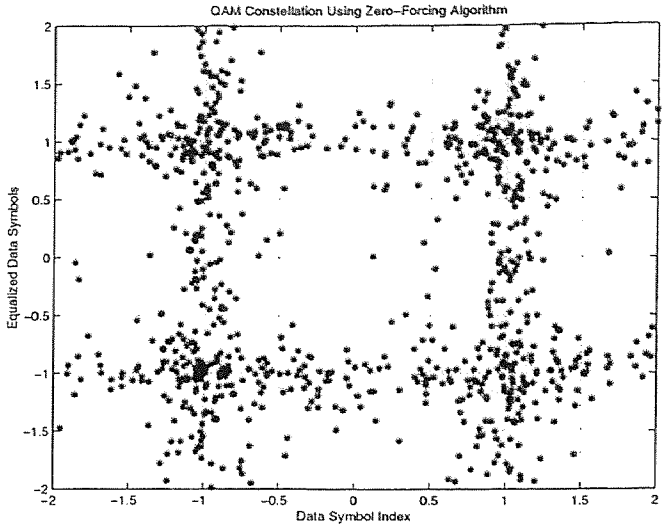

Figure 8.19 QAM constellation using zero-forcing equalizer at the equalizer output. SNRin = 20 dB. (8,15) case of transmission channel in Ref. [62].

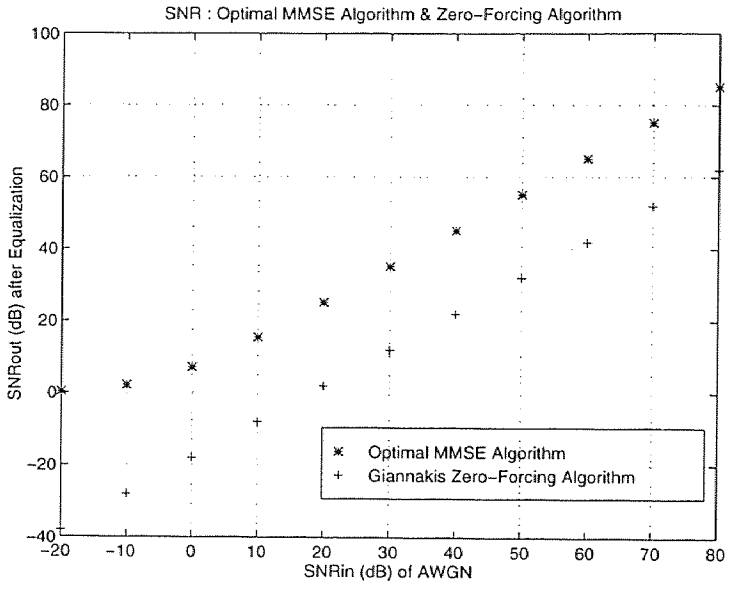

Figure 8.20 SNR performance of optimal MMSE based multirate filterbank post-equalizer and zero-forcing equalizer at the equalizer output verses SNR. (8,15) case of transmission channel in Ref. [62].

8.6 Discussions

In this chapter, an efficient nonmaximally decimated multirate filterbank structure is proposed for blind identification of unknown transmission channels. This structure is shown to be very similar to a form proposed earlier in the literature. The blind channel identification algorithm is not sensitive to the characteristics of the transmission channel. The zeros of unknown channel can be everywhere including on the unit circle. In constrast, it is not possible to use high-order statistics to do blind identification when the channel is a mixed phase channel or when the zeros are on the unit circle. The blind channel identification structure along with an optimum minimum mean square error based linear equalization algorithm are proposed. It outperforms other zero-forcing based equalization algorithms proposed earlier in the literature. It can cancel the intersymbol interference (ISI) and simultaneously suppress the noise enhancement term. The reconstructed signal to noise ratio is maximized. Simulation results show that the performance and robustness of the proposed blind identification and equalization scheme are superior to the others.

Table 8.1 Unknown channel identification, 100, 500 and 1000 Monte Carlo simulation for the channel with two zeros on the unit circle.

	h_0	h_1	h_2	h_3	h_4
ture	0.1111	0.2222	0.2778	0.2222	0.1111
100	0.1111	0.2254	0.2766	0.2219	0.1025
500	0.1108	0.2227	0.2773	0.2210	0.1095
1000	0.1117	0.2227	0.2778	0.2228	0.1132

Table 8.2 Unknown channel identification, 500 and 1000 Monte Carlo simulation for the channel with mixed phase, (zeros inside and outside the unit circle of z plane).

	h_0	h_1	h_2	h_3	h_4	h_5	h_6	h_7
ture	1	-0.7566	-1.6896	1.4734	-1.1834	0.5052	-0.1746	0.0224
500	0.9993	-0.7537	-1.6913	1.4539	-1.1701	0.5201	-0.1889	0.0447
1000	0.9995	-0.7541	-1.6909	1.4679	-1.1853	0.5080	-0.1755	0.0213

CHAPTER 9
DISCUSSIONS, CONCLUSIONS AND FUTURE RESEARCH

An orthogonal transmultiplexer which unifies multirate filter bank theory and communications theory is investigated in this dissertation.

Single Carrier based transceiver systems such as Quadrature Amplitude Modulation and Carrierless Amplitude and Phase modulation scheme, Multicarrier based transceiver systems such as Orthogonal Frequency Division Multiplexing (OFDM) or Discrete MultiTone and Discrete Subband (Wavelet) Multicarrier transceiver techniques are investigated. The research presented in this thesis shows that the theoretical performance bounds of single carrier modulation transceiver systems and multicarrier modulation transceiver systems are the same under the same conditions.

The performance of DMT and DSBMT based transceiver systems for narrow band interference are also investigated. It is shown that DMT based transceiver system performance is very sensitive to the location and strength of single tone (narrow band) interference. It is shown that an adaptive interference exciser can alleviate the sensitivity problem when the interference is strong. The improved spectral properties of DSBMT technique reduces the performance sensitivity for narrow band interference environment.

Optimal orthogonal basis functions design using cosine modulated multirate filter bank is discussed. The adaptive linear combiner at the output of analysis filter bank is implemented to eliminate the intersymbol and interchannel interference. DSBMT is the most suitable technique for narrow band interference environment.

A blind channel identification and Optimal MMSE based equalization using nonmaximally decimated filter bank precoder / postequalizer structure is presented. The performance of blind channel identification scheme is not sensitive to the characteristics of the unknown channel. The performance of the proposed optimal MMSE

equalization is shown to be superior to the Zero-forcing equalization scheme exist in literature.

The future research includes performance analysis of practical implementation issues such as

- The feasibility of short length optimal basis design to improve the computational complexity.
- The performance analysis for shorter basis.
- The practical considerations for a full duplex DSBMT transceiver system design to increase the throughput of telecommunication system. In this case, the practical echo cancellation problem in DSBMT technique might also be addressed.

The emerging digital subscriber line techniques will greatly increase the transmission speed using the existing un-shield twisted pair telephone line. The dramatic evolution of these technologies will be changing our daily life. We will greatly appreciate the impact of new services generated around these high speed digital communication technologies.

REFERENCES

1. J. W. Lechleider, "High Bit Rate Digital Subscriber Lines: A Review of HDSL Progress," *IEEE JSAC* , Vol. 9, No. 6. August 1991.

2. J. M. Cioffi, "A Multicarrier Primer," *Amati Comm. Corp. and Stanford Univ.*, Tutorial.

3. J. J. Werner, "Tutorial on Carrierless AM/PM," *AT&T Contribution to ANSI X3T9.5 TP/PMD working group*, June 1992.

4. J. S. Chow, J. C. Tu and J. M. Cioffi,"A Discrete Multitone Transceiver System for HDSL Applications," *IEEE Journal on Selected Areas in Communications*, pp. 895-908, August 1991.

5. I. Kalet, "The Multitone Channel," *IEEE Transactions on Communications*, Vol. 37, No. 2, pp. 119-124, February 1989.

6. J. J. Werner, " The HDSL Environment," *IEEE JSAC*, Vol. 9, No. 6. August 1991.

7. J. M. Cioffi, G. P. Dudevoir, M. V. Eyuboglu, G. D. Forney, "MMSE Decision-Feedback Equalizers and Coding, Part-I,II." *IEEE Transactions on Communications*, Vol. 43, No. 10, October 1995.

8. I. Kalet, " Multitone Modulation", *Subband and Wavelet Transforms: Design and Applications.* (Eds. A.N. Akansu and M.J.T. Smith), Kluwer Academic, Norwell, MA, 1996.

9. Committee T1 - Telecommunications, "A Technical Report on High Bit Rate Digital Subscriber Lines (HDSL)," *Contribution T1E1.4/96-006, Working Draft*, April 22, 1996.

10. ETSI Transmission and Multiplexing (TM), "High Bit Rate Digital Subscriber Line (HDSL) Transmission System on Metallic Local Lines", *RTR/TM-03036, Version 4*, March 1996.

11. American National Standard for Telecommunications - "Network and Customer Installation Interfaces - Asymmetric Digital Subscriber Line (ADSL) Metallic Interface," *ANSI T1.413* 1995.

12. X. Lin, M. Sorbara, A. N. Akansu, "A Performance Analysis of Single Carrier and OFDM Modulation Techniques for Digital Subscriber Line Application," *Proc. of 5th NJIT Symposium of Wavelet, Subband and Block Transforms in Communications*, Newark, NJ, March, 1997.

13. AT&T Paradyne et.al. "Draft Interface Specification for a CAP Based RADSL System," *Contribution T1E1.44/96-170*, July 22, 1996.

14. S. D. Sandberg and M. A. Tzannes, " Overlapped Discrete Multitone Modulation for High Speed Copper Wire Communication." *IEEE Journal on Sel. Areas in Commun. (JSAC)*, Vol, SAC-13, no.9, December 1995.

15. M.J.T. Smith, and T. P. Barnwell, "A Procedure for Designing Exact Reconstruction Filter Banks for Tree-Structured Subband Coders," *Proc. ICASSP*, pp. 27.1.1-27.1.4, March 1984.

16. H. Sheuermann and H. Gockler, "A Comparative Survey of Digital Transmultiplexing Methods," *Proc. IEEE*, Vol. 69, No. 11, pp. 1419-1450, Nov. 1981.

17. M. Vetterli, "Perfect Transmultiplexers," *Proc. IEEE ICASSP*, pp. 2567-2570, April 1986.

18. M. Vetterli," Filter Banks Allowing Perfect Reconstruction," *IEEE Signal Processing*, pp. 219-244, April 1986.

19. R. D. Koilpillai, T. Q. Nguyen and P. P. Vaidyanathan, "Some Results in Theory of Crosstalk-Free Transmultiplexers," *IEEE Trans. on Signal Processing*, Vol. 39, pp. 2174-2183, Oct. 1991.

20. A. Papoulis, *Signal Analysis.* McGraw-Hill, New York, NY, 1977.

21. R. A. Haddad, A. N. Akansu and A. Benyassine, "Time-Frequency Localization in M-Band Filter Banks and Wavelets: A Critical Review". *Journal of Optical Engineering*; Vol. 32, No. 7,pp. 1411-1429, July 1993.

22. R. Coifman and Y. Meyer, "Orthonormal Wave Packet Bases," *Dept. of Math., Yale University*, Preprint.

23. A. Cohen and E. Sere, "Time-frequency Localization with Non-stationary Wavelets,"*Subband and Wavelet Transforms: Design and Applications.* (Eds. by A.N. Akansu and M.J.T. Smith), Kluwer Academic, Norwell, MA, 1995.

24. A. N. Akansu, M. V. Tazebay and R. A. Haddad, "A New Look at Digital Orthogonal Transmultiplexers for CDMA Communications," *IEEE Trans. on Signal Processing*, pp. 263-267, January 1997.

25. R. Gold, "Optimal Binary Sequences for Spread Spectrum Multiplexing," *IEEE Trans. on Information Theory*, October 1967.

26. M. K. Tsatsanis and G. B. Giannakis, "Multirate Filter Banks for Code-Division Multiple Access Systems," *Proc. IEEE ICASSP*, Vol. II, pp. 1484-1487, May 1995.

27. R. W. Chang, "High-speed Multichannel Data Transmission with Bandlimited Orthogonal Signals," *Bell Sys. Tech. J.*, Vol. 45, pp. 1775-1796, December 1966.

28. A. Peled and A. Ruiz, "Frequency Domain Transmission Using Reduced Computational Complexity Algorithms," *Proc.IEEE ICASSP*, pp. 964-967, 1980.

29. S. B. Weinstein and P. M. Ebert, "Data Transmission by Frequency-Division Multiplexing Using the Discrete Fourier Transform," *IEEE Trans. on Communications*, 19(5):628–634, October 1971.

30. M. Alard and R. Lassale, "Principles of Modulation and Channel Coding for Digital Broadcasting for Mobile Receivers," *European Broadcasting Union Review Technical*, 224:168–190, August 1987.

31. B. R. Saltzberg, "Performance of an Efficient Parallel Data Transmission System," *IEEE Trans. on Communications*, Vol. 15, pp. 805-811, December 1967.

32. M. G. Bellanger and J. L. Daguet, "TDM-FDM Transmultiplexer: Digital Polyphase and FFT", *IEEE Trans. on Communications*, Vol. 22, pp. 1199-1205, September 1974.

33. B. Hirosaki, "An Orthogonally-Multiplexed QAM System Using the Discrete Fourier Transform," *IEEE Trans. on Communications*, Vol. 29, pp. 982-989, July 1981.

34. A. Benyassine and A. N. Akansu, "Performance Analysis and Optimal Structuring of Subchannels for Discrete Multitone Transceivers," *Proc. IEEE ISCAS*, 1995.

35. X. Lin and A. N. Akansu, "A Distortion Analysis and Optimal Design of Orthogonal Basis for DMT Transceivers," *Proc. IEEE ICASSP*, pp. 1475-1478, 1996.

36. A. N. Akansu, P. Duhamel, X. Lin and M. de Courville, " Orthogonal Transmultiplexers In Communication: A Review," to be published on *IEEE Trans. on Signal Processing*, Special Issue on Wavelets and Filter Bank, 1998.

37. N. J. Fliege, "Orthogonal Multiple Carrier Data Transmission," *European Transactions on Telecommunications*, Vol. 3 pp. 225-253, May 1992.

38. H. S. Malvar, *Signal Processing with Lapped Transforms.* Artech House, Cambridge, MA 1992.

39. Y-P. Lin and P. P. Vaidyanathan, "Linear Phase Cosine Modulated Maximally Decimated Filter Banks with Perfect Reconstruction," *Proc. IEEE ISCAS*, 1994.

40. J. Princen and A. Bradley, "Analysis/Synthesis Filter Bank Design Based on Time Domain Aliasing Cancellation," *IEEE Trans. on ASSP*, Vol. 34, pp. 1153-1161, October 1986.

41. T. Karp and N. J. Fliege, "MDFT Filter Banks with Perfect Reconstruction," *Proc. IEEE ISCAS*, May 1995.

42. R. Hleiss and P. Duhamel, "Oversampled Filter Banks Applied to Orthogonal Frequency Division Multiplex Systems," *International Conference on DSP*, Santorini, Greece, July, 1997, to appear.

43. M. de Courville, P. Duhamel, P. Madec and J. Palicot, "Blind Equalization of OFDM Systems Based on the Minimization of a Quadratic Criterion," *Proc. IEEE ICC*, pp. 1318-1321, June 1996.

44. K. Kwok and R. A. Haddad, "A New Family of Orthonormal Transforms with Time Localizability Based on the DFT," *Proc. SPIE Visual Comm. and Image Processing*, September 1994.

45. K. Kwok and R. A. Haddad, "Time-Frequency Analysis of Time Localizable Linear Transforms Based on the DFT," *Proc. 28th ASILOMAR Conference on Signals, Systems, and Computers*, November 1994.

46. F. Daneshgaran and M. Mondin, "Coded Modulation and Coherent Frequency-Hopped CDMA with Wavelets," *Proc. IEEE MILCOM*, November 1995.

47. K. Hetling, G. Saulnier, and P. Das, "PR - QMF Based Codes for Multipath/Multiuser Communications," *Proc. IEEE Globecom*, Oct. 1995.

48. K. Hetling, G. Saulnier, and P. Das, "Spreading Codes for Wireless Spread Spectrum Communications." H. Szu, Ed., *SPIE Proceedings - Wavelet Applications III*, Vol. 2762, April 1996.

49. A. R. Lindsey and J. Dill, "Wavelet Packet Modulation: A Generalized Method for Orthogonally Multiplexed Communications," *Proc. 27th Southeastern Symposium on System Theory*, Starkville, MS, March 1995.

50. J. Linfner, " MC - CDMA and its Relation to General Multiuser / Multi-subchannel Transmission Systems", *Proc. International Symposium on Spread Spectrum Techniques & Appli cations*, Mainz, Germany, Sept. 1996.

51. H. Rohling, K. Brueninghaus and T. Mueller, "Performances of Coherent OFDM-CDMA for Broadband Mobile Communications," Proc. RACE Mobile Telecommunications Summit, pp. 263-269, Cascais, Portugal, Nov. 1995.

52. M.J.T. Smith, and T. P. Barnwell, "A New Filter Bank Theory for Time-Frequency Representation," *IEEE Trans. ASSP*, vol. ASSP-35,no.3, pp. 314-327, March, 1987.

53. J. G. Proakis, *Digital Communications*, McGraw-Hill, New York, NY, 1995.

54. R. E. Ziemer and R. L. Peterson, *Digital Communications and Spread Spectrum Systems*, Macmillan Publishing Company, New York, New York, 1985.

55. S. Haykin, *Communication Systems*, John Wiley & Sons, New York, New York, second ed., 1983.

56. Z. Ding, "Characteristics of Band-Limited Channels Unidentifiable from Second-Order Cyclostationary Statistics," *IEEE Signal Processing Letters*, pp. 150-152, May 1996.

57. L. Tong, G. Xu, and T. Kailath,"Blind Identification and Equalization Based on Second-Order Statistics: A Time Domain Approach," *IEEE Trans. on Information Theory*, pp. 340-349, 1994.

58. L. Tong, G. Xu, B. Hassibi and T. Kailath,"Blind Channel Identification Based on Second-Order Statistics: A Frequency Domain Approach," *IEEE Trans. on Information Theory*, vol. 41, pp. 329-334, January 1995.

59. G. B. Giannakis and S. Halford, " Blind Fractionally Spaced Equalization of Noisy FIR Channels: Adaptive and Optimal Solutions," *Proceedings of ICASSP'95*, Detriot,MI, May, 1995.

60. M. K. Tsatsanis and G. B. Giannakis, " Cyclostationarity in Partial Response Signaling: A Novel Framework for Blind Equalization. " *IEEE ICASSP'97*, pp. 3597-3600. Munich, Germany, April, 1997.

61. X. G. Xia, " Intersymbol Interference Cancellation Using Nonmaximally Decimated Multirate Filterbanks," *Proc. 5th NJIT Symp. on Wavelet, Subband and Block Transforms in Communications*, March 1997.

62. G. B. Giannakis, " Filterbanks for Blind Channel Identification and Equalization," *Proc. 5th NJIT Symp. on Wavelet, Subband and Block Transforms in Communications*, March 1997.

63. X. Lin and A. N. Akansu, "An Optimal Channel Deconvolver / Equalizer Method Using A Nonmaximally Decimated Multirate Filterbank." Preprint, May 1997.

64. Special Issue on *Multi-Carrier Communications. Wireless Personal Communications.* Kluwer Academic, Vol.2, No. 1&2, Norwell, MA, 1995.

65. G. Wornell," Spread-Signature CDMA: Efficient Multiuser Communication in the Presence of Fading," IEEE Trans. Information Theory, pp.1418-1438,1995.

66. ETSI Normalization Committee,"Radio Broadcasting Systems, Digital Audio Broadcasting (DAB) to Mobile, Portable and Fixed Receivers", European Telecommunications Standards Institute, Norme ETSI, document ETS 300 401, Sophia-Antipolis, Valbonne, France, 1995.

67. A. N. Akansu and Y. Liu, "On Signal Decomposition Techniques," *Optical Engineering*, vol. 30, pp. 912–920, July 1991.

68. A. N. Akansu, "Wavelet Transforms and Relations to Filter Banks," in *IEEE ISCAS: A Tutorial*, pp. 167–177, May 1995.

69. A. N. Akansu and R. A. Haddad, *Multiresolution Signal Decomposition, Transforms, Subbands, Wavelets*, Academic Press, San Diego, California, 1992.

70. A. N. Akansu and H. Caglar, "A Measure of Aliasing Energy in Multiresolution Signal Decomposition," in *IEEE International Conference on Acoustics, Speech, and Signal Processing*, vol. IV, pp. 621–624, 1992.

71. H. Caglar, Y. Liu, and A. N. Akansu, "Statistically Optimized PR-QMF Design," in *SPIE Visual Communication and Image Processing*, pp. 86–94, November 1991.

72. A. Croisier, D. Esteban, and C. Galand, "Perfect Channel Splitting by use of Interpolation/Decimation Tree Decomposition," in *Int'l Conf. on Information Sciences and Systems*, Patras, Greece, 1976.

73. I. Daubechies, "Orthonormal Bases of Compactly Supported Wavelets," *Comm. in Pure and Applied Math.*, vol. 41, pp. 909–996, 1988.

74. N. Fliege, *Multirate Digital Signal Processing*, John Wiley & Sons, UK, 1994.

75. R. A. Haddad, "A Class of Orthogonal Nonrecursive Binomial Filters," *IEEE Transactions on Audio and Electroacoustics*, pp. 296–304, December 1971.

76. R. Iltis and L. Milstein, "Performance Analysis of Narrow-Band Interference Rejection Techniques in DS Spread-Spectrum Systems," *IEEE Trans. Communications*, vol. COM-32, pp. 1169–1177, November 1984.

77. W. Jones and K. Jones, "Narrowband Interference Suppression Using Filter Bank Analysis/Synthesis Techniques," in *IEEE MILCOM*, pp. 38.1.1–38.1.5, 1992.

78. K. Nayebi, T. P. Barnwell and M.J. Smith, "Analysis-Synthesis Systems with Time-Varying Filter Bank Structures," in *IEEE International Conference on Acoustics, Speech, and Signal Processing*, vol. IV, San Fransisco, CA, pp. 617–620, 1992.

79. J. Ketchum and J. Proakis, "Adaptive Algorithms for Estimating and Suppressing Narrow-Band Interference in PN Spread-Spectrum Systems," *IEEE Trans. Communications*, vol. COM-30, pp. 913–924, May 1982.

80. M. Medley, G. J. Saulnier, and P. Das, "Applications of the Wavelet Transform in Spread Spectrum Communications Systems," in 3^{rd} *NJIT Symposium on Applications of Subbands and Wavelets*, March 1994.

81. L. Milstein, "Interference Rejection Techniques in Spread Spectrum Communications," *Proc. IEEE*, vol. 76, no. 6, pp. 657–671, June 1988.

82. M. V. Tazebay and A. N. Akansu, "Adaptive Subband Transforms in Time-Frequency Excisers for DSSS Communications Systems," *IEEE Transactions on Signal Processing*, vol. 43, pp. 1776–1782, November 1995.

83. L. Milstein and P. Das, "An Analysis of a Real-Time Transform Domain Filtering Digital Communication System: Part I: Narrow-Band Interference Rejection," *IEEE Trans. Communications*, vol. COM-28, pp. 816–824, June 1980.

84. A. Oppenheim and R. Schafer, *Discrete-Time Signal Processing*, Prentice-Hall, Inc., Englewood Cliffs, New Jersey, 1989.

85. M. Smith and T. Barnwell, "A Procedure for Designing Exact Reconstruction Filter Banks for Tree-Structured Sub-band Coders," in *IEEE International Conference on Acoustics, Speech, and Signal Processing*, pp. 27.1.1–27.1.4, March 1984.

86. M. Smith and T. Barnwell, "Exact Reconstruction Techniques for Tree-Structured Subband Coders," *IEEE Trans. on ASSP*, pp. 434–441, August 1986.

87. M. V. Tazebay, " On Optimal Design and Applications of Linear Transforms ," Ph.D. Dissertation, Dept. of Electrical and Computer Engineering, New Jersey Institute of Technology, Newark, NJ, January 1996.

88. M. V. Tazebay and A. N. Akansu, "Progressive Optimality in Hierarchical Subband Trees," in *IEEE International Conference on Image Processing*, Austin,TX, pp. 825–829, November 1994.

89. P. P. Vaidyanathan, *Multirate Systems and Filter Banks*, Prentice-Hall, Inc., Englewood Cliffs, New Jersey, 1993.

90. P. P. Vaidyanathan, "Quadrature Mirror Filter Bank, M-band Extensions and Perfect Reconstruction Techniques," *IEEE ASSP Magazine*, pp. 4–20, July 1987.

91. P. P. Vaidyanathan, "Theory and Design of M-channel Maximally Decimated Quadrature Mirror Filters with Arbitrary M, Having the Perfect Reconstruction Property," *IEEE Trans. on ASSP*, pp. 476–492, April 1987.

92. P. P. Vaidyanathan, "Multirate Digital Filters, Filter Banks, Polyphase Networks and Applications: A Tutorial," *Proc. of IEEE*, vol. 78, pp. 56–93, 1990.

93. K. W. Martin, "Small Side-Lobe Channel-Bank Suitable for Multi-Tone Data-Communication Applications," Submission to *IEEE Trans. on Signal Processing*, 1996.

94. T. Q. Nguyen, "Near-Perfect-Reconstruction Pseudo-QMF Banks," *IEEE Trans. on Signal Processing*, Vol. 42, No. 1, pp. 65–75, January, 1994.

95. M. A. Tzannes, M. C. Tzannes, J. Proakis, and P. N. Heller, "DMT Systems, DWMT Systems and Digital Filter Banks," *IEEE International Conference on Communications*, pp. 311-315, 1994.

96. M. Vetterli, "A Theory of Multirate Filter Banks," *IEEE Trans. ASSP*, vol. 35, pp. 356–372, 1987.

97. E. Viscito and J. Allebach, "The Design of Tree-structured M-channel Filter Banks Using Perfect Reconstruction Filter Blocks," in *IEEE International Conference on Acoustics, Speech, and Signal Processing*, pp. 1475–1478, 1988.